TYPE SYNTHESIS AND INSTANTANEOUS MOBILITY ANALYSIS OF 3-UPU PARALLEL MANIPULATORS

A Thesis Submitted to the
Graduate School of Engineering and Sciences of
İzmir Institute of Technology
in Partial Fulfillment of the Requirements for the Degree of

MASTER OF SCIENCE

in Mechanical Engineering

By
Sercan BOZTAŞ

December 2017
İZMİR

We approve the thesis of **Sercan BOZTAŞ**

Examining Committee Members:

Assoc. Prof. Dr. Gökhan KİPER
Department of Mechanical Engineering, İzmir Institute of Technology

Assoc. Prof. Dr. Mehmet İsmet Can DEDE
Department of Mechanical Engineering, İzmir Institute of Technology

Assist. Prof. Dr. Erkin GEZGİN
Department of Mechatronics Engineering, İzmir Katip Çelebi University

29 December 2017

Assoc. Prof. Dr. Gökhan KİPER
Supervisor,
Department of Mechanical Engineering,
İzmir Institute of Technology

Prof. Dr. Metin TANOĞLU
Head of the Department of
Mechanical Engineering

Prof. Dr. Aysun SOFUOĞLU
Dean of the Graduate School of
Engineering and Sciences

ACKNOWLEDGMENTS

I would like to thank all of my professors. Without their help this thesis would not have been possible. Especially my supervisor Dr. Gökhan KİPER, for providing guidance throughout my graduate studies. I also would love to thank my family for being such supportive with my studies and my life. Without their support, long study hours wouldn't be productive and bearable.

ABSTRACT

TYPE SYNTHESIS AND INSTANTANEOUS MOBILITY ANALYSIS OF 3-UPU PARALLEL MANIPULATORS

In this study, the literature was examined and known derivatives of the 3-UPU parallel manipulator were investigated to reveal the mobility characteristics of the 3-UPU parallel manipulator. For a 3-UPU parallel manipulator, U represents the universal joint, while P represents the prismatic joint. It is a very well-known manipulator that can provide the platform with three degrees of freedom of pure translation, pure rotation or mixed translation and rotation with respect to the base, according to the relative directions of revolute joint axes. For this reason, in this study, alternative joint axis orientations on the platforms and the limbs are examined. The generated joint layouts for the platforms were matched with each other to generate and classify alternative manipulator architectures based on some assumptions. The topological structures of thus obtained parallel manipulators are examined and limb types were determined. These limb types were then analyzed with the help of screw theory. Reciprocal screw sets were analyzed by singular value decomposition method and the instantaneous degrees of freedom of the manipulators and the motion characteristics of the moving platforms are tabulated. The finite mobility analysis of one the parallel manipulators is performed using Solidworks Motion as an example. Among several different 3-UPU parallel manipulator architectures, especially 118 novel 3-UPU parallel manipulators with non-parasitic three degrees-of-freedom are significantly important. The classified 3-UPU parallel manipulators with determined motion characteristics can be used by researchers as a design alternative for a specific design task.

ÖZET

3-UPU PARALEL MANİPÜLATÖRLERİN TİP SENTEZİ VE ANLIK MOBİLİTE ANALİZİ

Bu çalışmada, 3-UPU paralel manipülatörlerin hareket özelliklerini araştırmak için literatür incelendi ve manipülatörün bilinen türevleri araştırıldı. 3-UPU paralel manipülatörlerde U, üniversal mafsalı, P ise kayar mafsalı temsil eder. Üniversal mafsaldaki döner mafsal eksenlerinin göreli yönlerine göre 3-UPU paralel manipülatörün hareketli platformu saf öteleme, saf dönme veya karışık öteleme ve dönme hareketlerini üç serbestlik derecesi yapabilmektedir. Bu sebeple, bu çalışmada, öncelikle platform ve bacaklarda farklı mafsal yerleşimleri araştırıldı. Platformlar için oluşturulan mafsal yerleşimlerine sahip kaide ve hareketli platformlar birbirleri ile eşlenerek bazı kabullere göre alternatif manipülatör mimarileri sınıflandırıldı. Bu şekilde elde edilen paralel manipülatörlerin topolojik yapıları incelendi ve bu manipülatörlere ait bacak tipleri belirlendi. Daha sonra bu bacak tipleri vida cebiri yardımı ile analiz edildi. Bacakların ters vidalarının oluşturduğu platform kısıt uzayı tekil değer ayrışımı kullanılarak incelendi ve hareketli platformların anlık serbestlik dereceleri ve hareket kabiliyetleri listelendi. Solidworks Motion yazılımı kullanılarak bir paralel manipülatörün sonlu hareket analizi örnek olarak sunulmuştur. Bulunan pek çok 3-UPU paralel manipülatör mimarisi arasında özellikle üç serbestlik dereceli parazitik olmayan harekete sahip 118 adet 3-UPU paralel manipülatör önem arz etmektedir. Hareket kabiliyetleri ile birlikte sınıflandırılan 3-UPU paralel manipülatörler araştırmacılarca belirli tasarım gereksinimleri için tasarım alternatifi olarak kullanılabilirler.

TABLE OF CONTENTS

LIST OF FIGURES

LIST OF TABLES

Table **Page**

CHAPTER 1

INTRODUCTION

Over the past century, various machines have been invented according to the needs of the industry. Some of them are robots invented to be used in dangerous and repetitive missions. According to the definition of the *American Heritage College Dictionary* (Houghton Mifflin Company, 2004), a robot is "a mechanical device that can perform a variety of tasks on command or by being programmed in advance". Robotics is the study or science related to the design, production, theory and applications of robots. Robots can be divided into various subgroups such as manipulators, humanoid robots, walking robots. However, the most commonly used robot-type in the industry are manipulators that are used for manufacturing, assembling, holding or moving objects.

1.1. Kinematic Structures of Robot Manipulators

Manipulators can be divided into three different groups according to their kinematic structures (Tsai, 1999). The first group is serial manipulators. These manipulators have an open kinematic chain structure like the human arm. Industrial robots such as painting robots, welding robots and pick and place robots usually have this kind of kinematic structure. A welding robot is shown in Figure 1.1.

Figure 1.1. A welding robot
(Source: ABB Robotics, 2017)

The second group is called parallel manipulators. The kinematic structures of the robots in this group have closed kinematic structure as formed in our arms when we combine our hands. A parallel manipulator is shown in Figure 1.2.

Figure 1.2. Stewart platforms
(Source: Wikipedia, 2017)

The last group is hybrid manipulators. The manipulators in this group are composed of both serial and parallel sub-assemblies. A hybrid manipulator is shown in Figure 1.3.

Figure 1.3. Hybrid manipulator
(Source: 3D printer list, 2017)

The advantages of serial manipulators over other types of manipulators can be listed as simplicity in structure; ease of control; large workspace. On the other hand serial manipulators also have some drawbacks such as low stiffness; lower payload capacity and accumulation of errors.

Parallel manipulators have a lot of advantages over their conventional serial counterparts. For example parallel manipulators compared to the conventional industrial serial manipulators have higher payload capacity; better accuracy; higher stiffness; high speed and acceleration. On the other hand they also have some disadvantages such as smaller and complex workspace.

1.2. Degrees of Freedom

Degree of freedom (DoF) is the number of independent parameters used to describe all the configurations of the system in a mechanical system (Tsai, 1999). As shown in Figure 1.4, any unconstrained rigid body has three translational and three rotational DoF in the space. If the end-effector of a spatial parallel manipulator has less than six DoF, such manipulators are called lower mobility manipulators (Di Gregorio, 2006). If the DoF of the manipulator is greater than the DoF required by the task to be performed, it is called a redundant manipulator. If the DoF of the manipulator is equal to the DoF required by the task to be performed, it is called a non-redundant manipulator. If the DoF of the manipulator is less than the DoF required by the task to be performed, it is called a lower mobility manipulator (Gallardo-Alvarado, 2016).

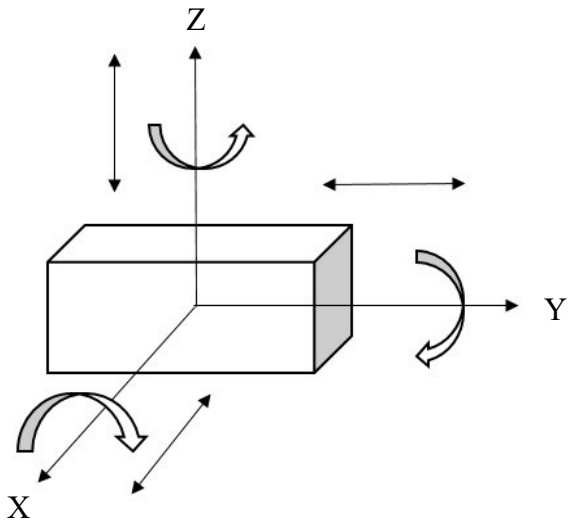

Figure 1.4. Degrees of freedom of a rigid body in space

1.3. Lower Mobility Manipulators

In the past decades, parallel manipulators have attracted intense interest from researchers and industrial communities. The parallel manipulators are being used in a wide variety of applications such as motion simulators, manufacturing and assembly

robots. In recent years, researchers have developed several lower mobility parallel mechanisms such as the Delta manipulator (Clavel, 1988). The main reason is that every task does not require six DoF. The use of lower-DoF manipulators in such tasks provides many advantages. First of all, lower-DoF manipulators are simpler in structure and cheaper in cost.

3-UPU Parallel Manipulators (PM) with lower mobility was introduced for the first time by Tsai in 1996 (Tsai L. , 1996). The mechanism is shown in Figure 1.5, which consists of a fixed base platform and a moving platform connected by three serial chains – called limbs – with each limb having a Universal (U) - Prismatic (P) – Universal (U) joint constructed in sequence. The U joints are passive and the three P joints are actuated. There are several different architectures of 3-UPU PMs, details of which are presented in Chapter 2.

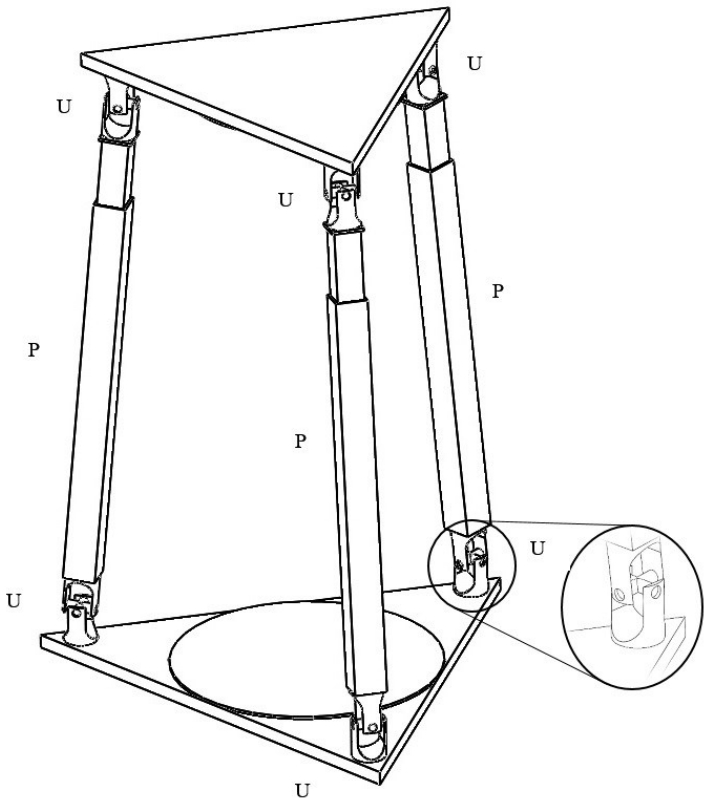

Figure 1.5. Tsai 3- UPU PM

1.4. Aim of the study

The aim of this work is to classify and design new 3-UPU PM architectures and to examine the mobility characteristics of these manipulators.

1.5. Outline of the Thesis

In Chapter 2, PMs with the same kinematic structure as the 3-UPU PM were investigated and the properties of the PMs were introduced. On the obtained results, in chapter 3, joint layouts were created for 3-UPU PMs, and these joint layouts were mapped to each other to obtain new manipulators. When these obtained PMs were examined, it was determined that they had common limb types. Then, in chapter 4 these limb types were investigated by using screw theory. In Chapter 5, analyzes of novel PMs were made.

CHAPTER 2

LITERATURE REVIEW

Different 3-UPU PM architectures can be obtained by altering the U joint axis arrangements on the base and/or moving platform. Many such different architectures have been presented and analyzed in terms of mobility, kinematic, singularity, dynamics, stiffness, workspace and positioning errors in the literature. Event though, a 3-UPU PM generically has 3-DoF, it has been demonstrated that some 3-UPU PM architectures possess more than 3-DoFs. Also, some 3-UPU PMs are kinematotropic mechanisms (Wohlhart, 1996), that is the mechanism has different DoF in different assembly modes. In this Chapter, the 3-UPU PM architectures presented in the literature are summarized.

2.1. Survey on 3-UPU PMs

The following sections present the classification of 3-UPU PMs in terms of their joints layouts, DoFs and motion characteristics.

2.1.1. Tsai's 3-UPU Parallel Manipulator

The first 3-UPU PM was presented by Lung-Wen Tsai. This PM generically has three DoFs and is designed to make pure translational motion. Such PMs are called translational PMs (TPMs). The PM consists of three extensible limbs connecting a fixed base platform to a moving platform. Each limb of the PM comprises a P joint that moves between a pair of U joints which are connected to the platforms. Totally there are six U joints and three P joints in the 3-UPU PM as presented in Figure 2.1 (Tsai L. , 1996). Later on, this new PM was further designed and optimized by Tsai. The forward and inverse kinematics of the PM and the translational motion conditions of the PM are described by Tsai. In addition, the Jacobian and singularity analysis of the PM are worked

out (Tsai & Joshi, 1999). The workspace and stiffness characteristics of the PM are compared to other types of lower mobility PMs in (Tsai & Joshi, 2001) and (Joshi & Tsai, 2003). In another study, the 3-UPU PM was used to demonstrate a new Jacobian analysis method for lower mobility PMs (Joshi & Tsai, 2002).

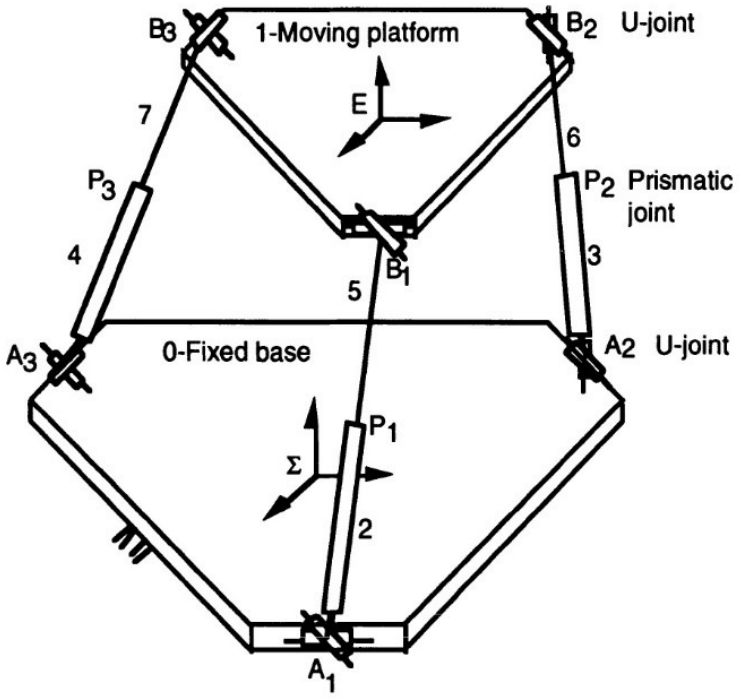

Figure 2.1. Tsai 3- UPU PM
(Source: Tsai, 1996)

Di Gregorio et al. (2000) have made static analysis of the PM and presented the most appropriate design criteria for a workspace free from singularities. In another study, they have performed extensive mobility analysis of the PM (Di Gregorio & Parenti-Castelli, 2002). They also suggest a new method of finding the kinematic and static properties of the PM (Di Gregorio & Parenti-Castelli, 2006b).

Zhao et al. have used the Tsai 3-UPU PM to identify the PM's reciprocal screws and to show a new method to do singularity analysis. In this new method, the reciprocal screws of the kinematic chains of the limbs of the PMs are determined, and different PM architectures which result in singularities are found (Zhao et al., 2005). Zhao et al. also developed a programmable method to calculate the configuration DoF of the 3-UPU PMs using reciprocal screw theory (Zhao et al., 2006). The details of the method of Zhao is presented in Chapter 4.

The workspace optimization of the Tsai 3-UPU PM was performed by Badescu and Mavroidis (2004). Various design parameters have been used to determine the optimal design for limited and unrestricted workspace of the 3-UPU PM.

Guan et al. conducted a mobility analysis of the PM based on screw theory. In this work, the PM describes three types of singularity states (Guan et al., 2004). The necessary features for a 3-UPU PM for machining applications have been determined and presented by Yi. Analyzes made using a computer aided geometric approach have shown that the PM has advantages in terms of accuracy and repeatability (Yi, 2005).

Kanaan et al. worked on the Tsai 3-UPU PM, ensuring that the PM singularities were geometrically characterized. In doing this, the geometric conditions are associated with the rows of the inverse Jacobian matrix and the dependence of the screw coordinates (Kanaan et al., 2008). In a later work, they also describe the singularities in the limbs that applied actuation forces with the same method (Kanaan et al., 2009).

Yang and O'Brien has proposed a geometric approach for detecting singularity free workspaces. They used the Tsai 3-UPU PM to create mathematical model (Yang & O'Brien, 2009). In another study, they presented a design strategy that clearly specifies the singularity free workspace for the Tsai 3-UPU PM (Yang & O'Brien, 2010).

Chebbi et al. have developed an analytical predictive model by examining the positional errors and singularities caused by the joint clearance on the Tsai 3-UPU PM (Chebbi et al., 2009).

Qi et al. designed a walking robot for people with disabilities using the Tsai 3-UPU PM. The advantages of four-legged walking robots compared to their two-legged counterparts were specified and workspaces were investigated (Qi et al., 2009).

Li et al. designed an fMRI device that uses the Tsai 3-UPU PM to examine the functioning of the human brain. The kinematic, mechanical and workspace analyzes of the device were performed. In addition, finite element model was constructed to increase the mechanical stiffness of the PM (Li et al., 2010). In a later work, they presented a new method for gravity compensation of the PM where the base platform plane is positions perpendicular to the ground (Dehkordi et al., 2012).

Bi and Wen used 3-UPU PM to investigate the loss of accuracy of the moving platform due to manufacturing errors or geometric constraints using screw theory (Bi & Wen, 2010).

Walter and Husty have developed a method to predict what kind of motions happen if the 3-UPU PM is not properly constructed for translational movement. The

motion of the PM has been studied in detail using algebraic geometry (Walter & Husty, 2011).

Wang et al. have reviewed the positional errors of the 3-UPU PM, which can be attributed to motion characteristics and manufacturing errors. Kinematic model of the PM was constructed and the results were investigated by probability methods (Wang et al., 2011).

Bhutani and Dwarakanath presented a 3-UPU PM with enhanced accuracy. Sensitivity analysis was performed to determine the results and limb ranges. The precision of the PM has been demonstrated by producing a prototype (Bhutani & Dwarakanath, 2014).

Guohua et al. made use of particle swarm optimization to optimize the workspace and stiffness of the 3-UPU PM (Guohua et al., 2013). Shuhua Sun has investigated the effect of the change of the structure size of the PMs, the change of the posture of the PM, and the lengths of the limbs (Sun, 2013).

J. Bałchanowski performed the topological and kinematic analyzes of the 3-UPU PM. The singularities of the PM are determined and shown by examples (Bałchanowski, 2014).

Aboulissane and El Bakkali performed the inverse kinematic analysis of 3-UPU PM. Then Jacobian matrix was computed and singularity analysis of the PM was made. The effect of changing the size of the base moving platform to the workspace is examined (Aboulissane & El Bakkali, 2015).

Laribi et al. compared the 3-UPU PM with the other lower mobility PMs in terms of dexterity and workspace characteristics (Laribi et al., 2015). Wei et al. studied the static stiffness properties of the 3-UPU PM. Then the structural optimization parameters required for the PM are presented (Wei et al., 2015).

All these studies about the Tsai 3-UPU PMs are summarized in Table 2.1.

Table 2. 1. Comparisons of Tsai 3-UPU studies

	Tsai 3-UPU PM							
	Mobility Analysis	Kinematic Analysis	Singularity Analysis	Dynamic Analysis	Stiffness Analysis	Workspace Analysis	Error Analysis	Application
Tsai 1996	+	+						
Tsai and Joshi 2000		+				+		
Tsai and Joshi 2001					+	+		
Tsai and Joshi 2003		+			+	+		
Joshi and Tsai 2002			+					
Di Gregorio and Castelli 1998	+	+	+					
Castelli et al. 2000			+					
Di Gregorio and Castelli 2002	+							
Di Gregorio and Castelli 2006		+	+					
Zhao et al. 2004	+		+					
Zhao et al. 2006	+							
Badescu and Mavroidis 2004						+		
Guan et al. 2004	+		+					
Lu Yi 2004								+
Kanaan et al. 2008			+					
Kanaan et al. 2009			+					
Hu and Lu 2008		+			+	+		
O'Brien and Yang 2009			+					
O'Brien and Yang 2010		+	+					
Chebbi et al. 2009						+	+	
Qi et al. 2009	+					+		+
Frisoli et al. 2010	+				+	+		+
Frisoli et al. 2012						+		+
Bi and Wen 2010							+	
Sekhar et al. 2011	+	+						
Walter and Husty 2011		+	+					
Wang et al. 2011		+					+	
Bhutani and Dwarakanath 2013		+						
Guohua et al. 2013					+	+		
Sun 2013		+						
Bałchanowski 2014		+	+					
Aboulissane and El Bakkali 2015	+	+	+			+		
Laribi et al. 2015		+				+		
Wei et al. 2015		+				+		

2.1.2. SNU 3-UPU Parallel Manipulator

After 3-UPU PM is presented by Tsai, Han et al. from Seoul National University (SNU) offered a new 3-UPU type PM with a different kind of joint layout. When mobility analysis of the SNU PM is theoretically computed, it is seen that the PM has three translational DoF. However, when the physical model of the PM was constructed (see

Figure 2.2), it was observed that the PM moved even when all the actuators are locked. Even the kinematic singularity analysis of the PM has not solved this problem. Later, researchers tried to explain this phenomenon by analyzing the kinematic sensitivity of the PM (Han et al., 2002).

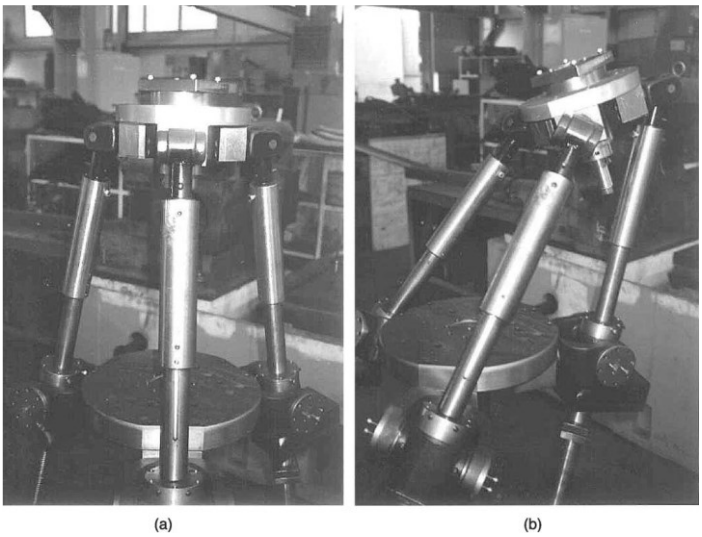

Figure 2.2. SNU 3-UPU PM a) Initial configuration b) Redundant self-motion (Source: Han et al., 2002)

After SNU 3-UPU PM was presented, many researchers have presented a number of solutions to solve this new mobility problem. Bonev and Zlatanov (2001) showed that the unexpected motions of the SNU 3-UPU PM are due to infinitesimal kinematic singularities which they call “constraint singularities”. The work done shows that in practice the PM has two rotational DoF due to singularities in addition to the three translational DoF. According to another study, constraint singularities can be or cannot be controlled by actuators. PMs should be checked for constraint singularities before analyzing input and output velocities (Zlatanov et al., 2002).

Wolf et al. (2002) studied the self-motion status of the 3-UPU using line geometry and screw theory. The work done shows that the PM's DoF is increased by two instantaneous rotational DoF. In a later work, they used line geometry and screw theory to examine the instantaneous behavior of PMs at a given position (Wolf & Shoham, 2003). To optimize the geometry and position parameters of the PM, a method has been proposed that uses reciprocal screws that come from the instantaneous wrenches of the PM’s limbs (Wolf & Shoham, 2006).

Liu et al. (2003) developed an approach to analyze the singularities of the SNU 3-UPU PM. The instantaneous kinematics of the PM were studied by Li and Huang (Li & Huang, 2005) using reciprocal screw theory. Walter et al. (2008) found all assembly modes of the SNU 3-UPU PM using algebraic geometry. The sections where the working space of the PM showed different kinematic properties were determined.

Gogu (2008) presented a new mobility formula to detect constraint singularities of PMs without the need for Jacobian analysis. Qu et al. (2012) found the infinitesimal rotational DoF of the PM by analyzing the SNU 3-UPU PM's terminal constraint system and the contour atlas of the rotational motions of the PM's platform is presented.

Chen et al. (2015) investigated the mobility of a PM derived from the SNU 3-UPU PM using screw theory. When the base and the moving platform are not parallel to each other, the PM shows two rotational and one translational movement characteristics.

All these studies about SNU 3-UPU PMs are summarized in Table 2.2.

Table 2.2. Comparisons of SNU 3-UPU studies

	SNU 3-UPU PM							
	Mobility Analysis	Kinematic Analysis	Singularity Analysis	Dynamic Analysis	Stiffness Analysis	Workspace Analysis	Error Analysis	Application
Park et al. 2001			+					
Bonev and Zlatanov 2001	+		+					
Wolf et al. 2002	+		+					
Wolf and Shoham 2003			+					
Wolf and Shoham 2005		+						
Zlatanov et al. 2002	+		+					
Liu et al. 2003			+					
Li and Huang 2005	+	+	+					
Walter et al. 2008		+	+					
Gogu 2008			+					
Qu et al. 2012			+					
Chen et al. 2015	+	+						

2.1.3. Spherical 3-UPU Parallel Manipulator

Karouia and Hervé (2000) designed a 3-UPU PM with a rotational platform. For the rotational motion of the PM, it is necessary that the revolute (R) joint axes associated with the base and the moving platform intersect at a single point at all times of the motion of the PM. In Figure 2.3 the schematic representation of this spherical 3-UPU PM is given.

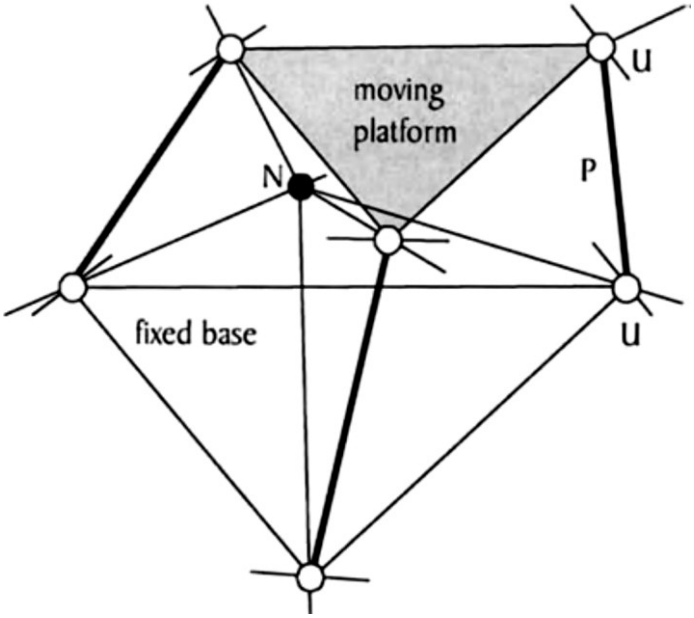

Figure 2.3. Spherical 3-UPU PM
(Source: Karouia & Hervé, 2000)

After Karouia and Hervé presented the spherical 3-UPU PM, many researchers studied on this new PM. Di Gregorio (2003) has shown that the end effector has spherical motions when the Spherical 3-UPU PM is provided properly manufactured and assembled. However, according to the work done, the PM has translational singularities. In a later work Di Gregorio PM (2004) has performed the static analysis and singularity analysis of the PM, and introduced a formula find the singularities of the PM.

Xiangzhou et al. (2006) studied the kinematic equations of 3-UPU PM. The study provided the angular velocity and acceleration values of the end effector. Using the D'Alembert principle, the inverse dynamic equations of the PM were given (Xiangzhou

et al., 2007).

Paganelli (2007) proposed a method that would allow to determine a singularity-free path in order to prevent damage that may occur if the end effector of a PM is in a singular configuration. The method was applied on the Spherical 3-UPU PM. Chebbi et al. (2013) presented the forward geometric analytical model of the Spherical 3-UPU PM. The study shows that the Spherical 3-UPU PM has a singularity-free workspace. Pramanik and Ghosal (2015) offered a solar tracking system using the Spherical 3-UPU PM. The kinematic equations are numerically formulated to determine the path for the PM to follow the sun.

All these studies about Spherical 3-UPU PMs are summarized in Table 2.3.

Table 2.3. Comparisons of Spherical 3-UPU studies

	Spherical 3-UPU PM							
	Mobility Analysis	Kinematic Analysis	Singularity Analysis	Dynamic Analysis	Stiffness Analysis	Workspace Analysis	Error Analysis	Application
Karouia and Herve 2000	+							
Di Gregorio 2002	+	+	+					
Di Gregorio 2004			+					
Xiangzhou et al. 2006		+		+				
Xiangzhou et al. 2007		+		+				
Paganelli 2007			+					
Chebbi et al. 2013b		+	+					
Pramanik and Ghosal 2015		+	+					+

2.1.4. Other Types of 3-UPU Parallel Manipulators

The 3-UPU PMs presented in the literature show that the PMs possess different kinematic properties as the R joint axis orientations of the U joints are altered on the base or moving platform. Several new 3-UPU PM architectures were created by changing the layout of U joints.

Huang and Li (2002) are the first researchers to design the U joint axes of the base or moving platform to be perpendicular to the base or moving platform planes (Figure 2.4). The first analysis shows that this new PM generically has 4 DoF with three translational and one rotational DoF. Kiper and Söylemez (2011) worked on the forward kinematic analysis of this PM using exponential rotation matrices. The work done shows that when the base and the moving platform of the PM are identical, the PM has 4-DoF and furthermore, it has a finite singularity mode with 5-DoFs when the limb lengths are the same. Guo et al. (2011) has investigated the position and orientation errors using probability distribution theory.

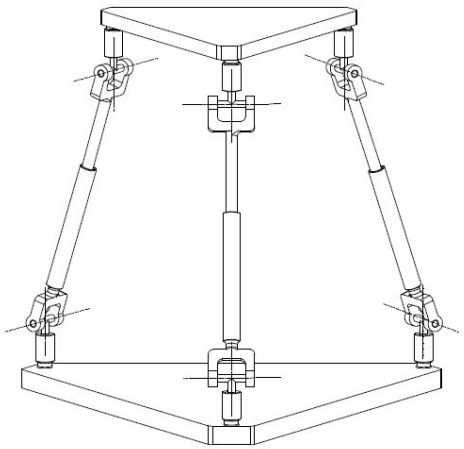

Figure 2.4. 3-UPU PM with vertical R joint axes on the platforms
(Source: Guo et al., 2011)

Huang et al. (2004) presented a new type of 3-UPU PM platforms of which are in the form of a pyramid (Figure 2.5). The PM was analyzed using the reciprocal screws to show that the PM had three translational DoF.

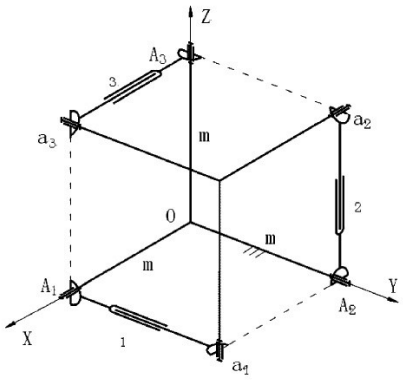

Figure 2.5. 3-UPU PM with pyramid platforms
(Source: Huang et al., 2004)

Yu et al. (2009) proposed a 3-UPU PM architecture in which the R joint axes of the U joints of the base or moving platform are positioned parallel to each other in the platform planes (Figure 2.6). Peng Binbin et al. (2011) studied the singularities of these Parallel 3-UPU PMs. Miao et al. (2013) developed a rolling mechanism using a Parallel 3-UPU PM, where the mobility, gait and stability analyzes of the PM were done.

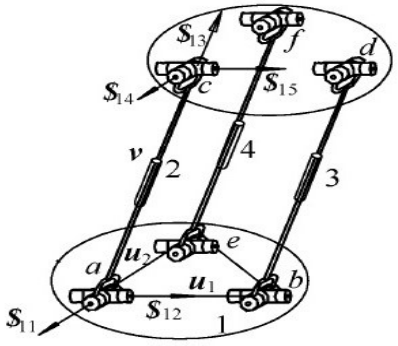

Figure 2.6. Parallel 3-UPU PM
(Source: Yu et al., 2009)

Several other 3-UPU PM architectures have been derived by changing the location of the joints on the base and moving platform of the PM. Zhao et al. (2005) proposed a new PM with SNU 3-UPU type U joints on the base, and vertical type U joints on the moving platform as represented in Figure 2.7. The PM possesses one translational and two rotational DoF.

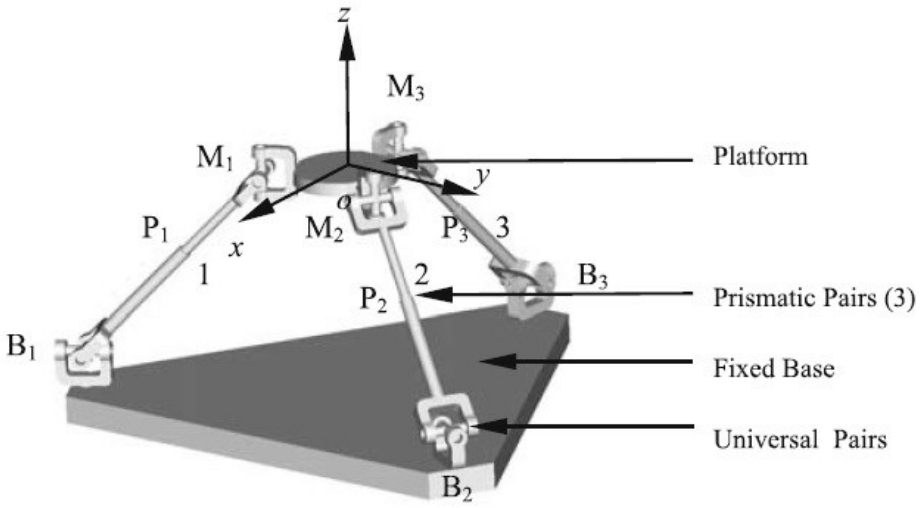

Figure 2.7. 2R1T 3-UPU PM
(Source: Zhao et al., 2005)

Lu and Hu (2006) presented a new type of 3-UPU PM with an asymmetric joint set-up (Figure 2.8).

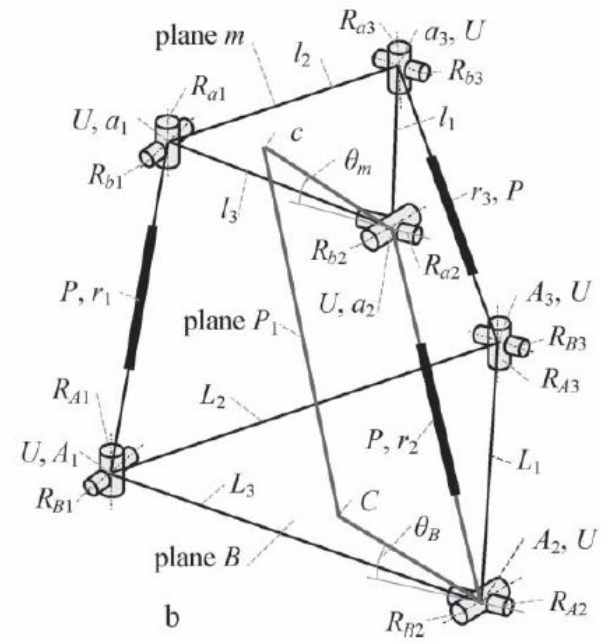

Figure 2.8. Asymmetric 3-UPU PM
(Source: Lu & Hu, 2006)

Lu et al. (2008) presented PMs with SNU type and Vertical type U joints on either base or moving platform (Figure 2.9). In a later study, a stiffness analysis of one of these new type of PMs was performed (Hu & Lu, 2011).

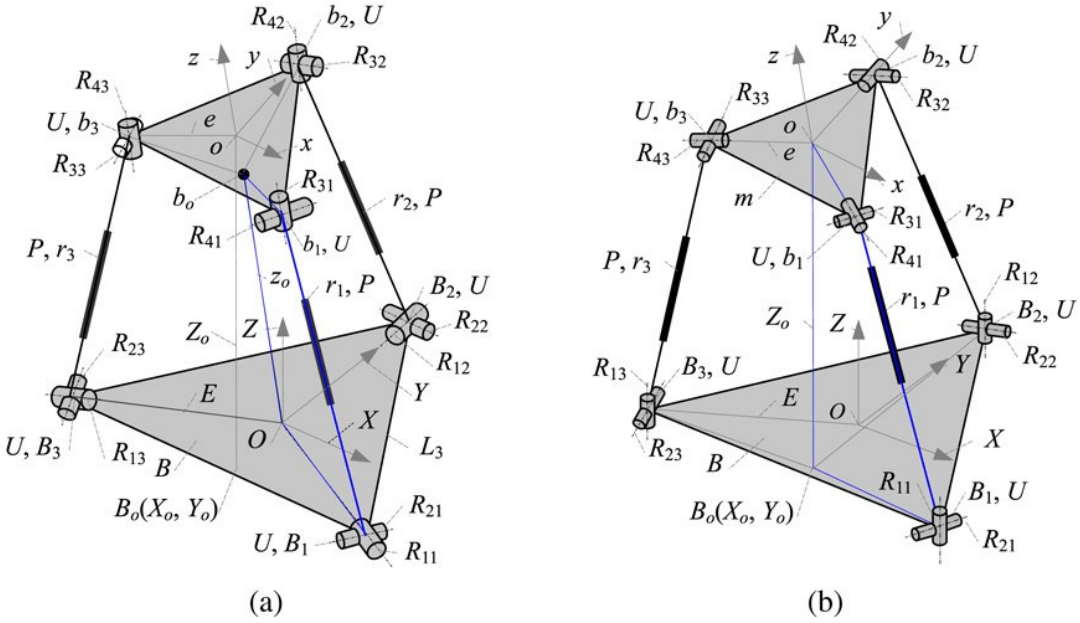

Figure 2.9. 3-UPU PMs with SNU type and Vertical type U joints on base or moving platform (Source: Lu et al., 2008)

Chebbi and Parenti-Castelli (2010) presented a study with various types of 3-UPU PMs, where the singularities of the PMs were studied and their potentials were interpreted. Wang and Ceccarelli (2013) designed a robotic leg for 3-DoF translational motion using a 3-UPU PM. All these studies about different types of 3-UPU PMs are summarized in Table 2.4.

Table 2.4. Comparisons of Different Types of 3-UPU studies

	Different Types of 3-UPU PM							
	Mobility Analysis	Kinematic Analysis	Singularity Analysis	Dynamic Analysis	Stiffness Analysis	Workspace Analysis	Error Analysis	Application
Huang and Li 2002	+	+						
Kiper and Söylemez 2011	+	+						
Guo et al. 2011		+					+	
Huang et al. 2004		+						
Zhang et al. 2009		+			+			+
Yu et al. 2009	+							
Binbin et al. 2011	+	+	+					
Miao et al. 2013	+	+						+
Zhao et al. 2005	+	+						
Lu and Hu 2006		+						
Lu et al. 2007		+				+		
Hu and Lu 2011		+			+			
Chebbi and Parenti-Castelli 2013a			+					
Wang and Ceccarelli 2013		+						+

CHAPTER 3

3-UPU PM ARCHITECTURES

Presented studies show that the 3-UPU PMs have different mobility, singularity and workspace characteristics with the change of orientations of U joints. For this reason, this study aims to classify different 3-UPU PM architectures with different the R joint axis orientations on the platforms.

3.1. 3-UPU PM Types According to Joint Layouts

In this section, 3-UPU PMs presented in the literature were investigated and the joint layouts of the R joint axes on the platforms are examined. Based on the joint layouts of these 3-UPU PMs, new 3-UPU PM architectures can be constructed.

3.1.1. Joint Layouts of Tsai 3-UPU PM

The R joint axes on the platforms of Tsai's 3-UPU PM are coplanar and form a triangle (Figure 3.1). These axes are tangent to the circumcircle of the triangle formed by the U joint centers. For this reason, this kind of joint layout of the platform is denoted as U^T, where T stands for tangent. The three U joint centers on the base platform define the base platform plane, whereas the three U joint centers on the moving platform define the moving platform plane.

As can be seen in Figure 3.1, the Global Coordinate System (GCS) is positioned at the center of the circumcircle of the U joint centers of the base of the PM. The X-axis of the GCS is oriented towards one of the U joint centers on a limb. The Y-axis of the GCS lies on the base platform plane whereas the Z-axis is perpendicular to the plane. The limb which comprises the U joint center on the X-axis is numerated as limb 1 and the other two limbs are numerated as limb 2 and limb 3 by proceeding in counter-clockwise direction about the X-axis. Three Local Coordinate Systems (LCS) for each limb are

positioned at the U joint centers of the base. The axes of LCS1 are set to be parallel to the axes of the GCS. The axis orientations of LCS2 and LCS3 differ according to the 3-UPU architecture. For the Tsai 3-UPU PM, LCS2 and LCS3 are obtained by rotating LCS1 around the Z-axis by 120° and 240°, respectively. In other words for the Tsai 3-UPU PM, the x-axes of the LCSs are normal and the y-axes are tangent to the circumcircle.

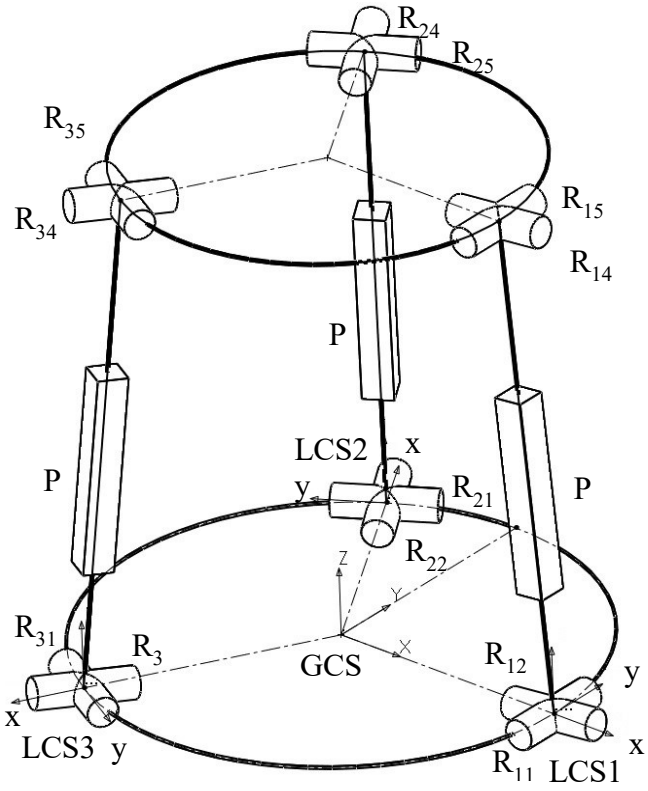

Figure 3.1. Joint Layouts of Tsai 3-UPU PM

Considering the Tsai 3-UPU PM given in Figure 3.1 as an example, in this study, the first and second R joint axes of a U joint on the base are the first joint axis (R_{i1}) and second joint axis (R_{i2}) of each limb i (i = 1, 2, 3), a P joint is the third joint of each limb, and the next two R joint axes of the U joint on the moving platform are called the fourth joint axis (R_{i4}) and the fifth joint axis (R_{i5}) of each limb.

For the Tsai 3-UPU PM, R_{i1} are positioned on the y-axis of the LCSs and R_{i2} rotate about the y-axis and hence lie on the xz-plane of the LCSs. R_{i2} and R_{i4} are parallel axes. The joint layout of the moving platform is the same as the base platform, i.e. R_{i5} are tangent to the circumcircle on the moving platform plane. Hence the Tsai 3-UPU PM architecture is denoted as U^T-U^T.

3.1.2. Joint Layouts of SNU 3-UPU PM

In the SNU 3-UPU PM, the R axes (R_{i1} or R_{i5}) on a platform (base or moving) lie on the platform plane and intersect in the circumcircle center of the triangle formed by the U-joint centers and hence are normal to the circumcircle (Figure 3.2). This kind of joint layout of the platform is denoted as U^N, where N stands for normal (see in Figure 3.8). For the SNU 3-UPU PM R_{i1} are positioned on the x-axis of the LCSs. The base and moving platforms have the same joint layout. R_{i2} and R_{i4} are parallel axes. The SNU 3-UPU PM architecture is denoted as U^N-U^N.

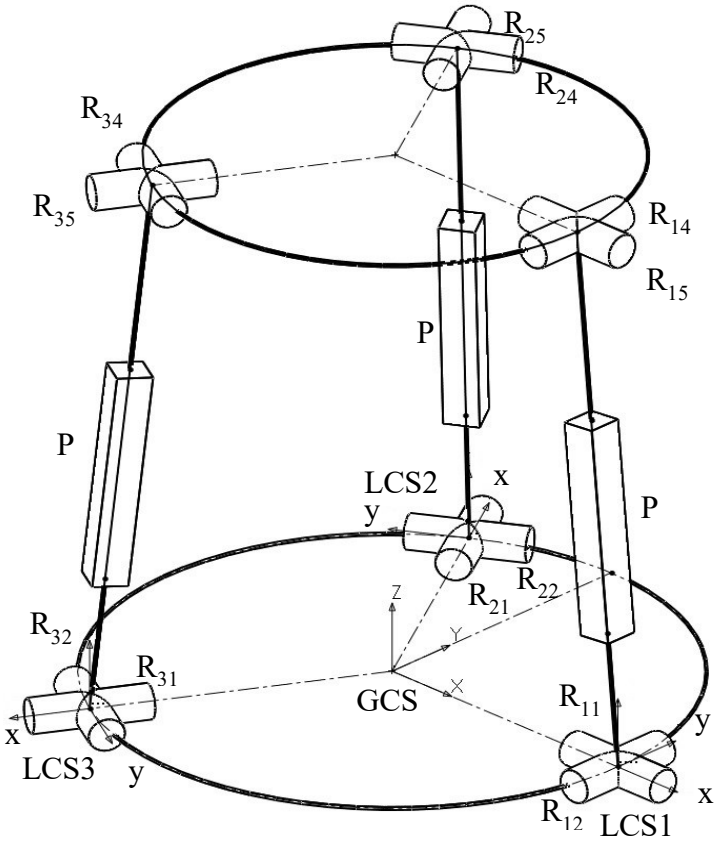

Figure 3.2. Kinematic schematic of SNU 3-UPU PM

3.1.3. Joint Layouts of Parallel 3-UPU PM

When the first axes on a platform lie on the platform plane and are all parallel to the X- or Y-axis of the global coordinate system, the joint layout of the platform is denoted as U^X or U^Y (see in Figure 3.8). The LCS axes of all three limbs are parallel to the axes of the GCS axes as shown in Figure 3.3. Depending on which R joint axes are attached to the platforms the architecture of the PM in Figure 3.3 may be U^X-U^X or U^Y-U^Y or U^X-U^Y or U^Y-U^X. R_{i2} and R_{i4} are either parallel or perpendicular to each other.

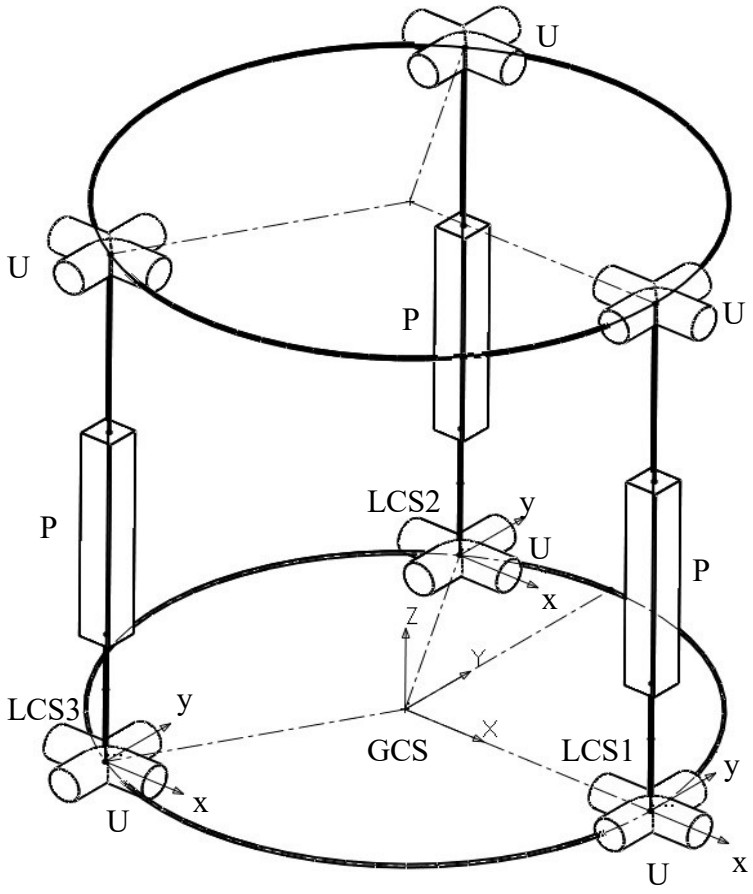

Figure 3.3. Kinematic schematic of Parallel 3-UPU PM

3.1.4. Joint Layouts of Vertical 3-UPU PM

When the first R axes on a platform are perpendicular to the platform plane, the joint layout of the platform is denoted as U^V. There are several possibilities for the relative positions of the R_{i2} and R_{i4} axes. In order to distinguish between different R_{i2} and R_{i4} axes configurations, an initial configuration of the PM is considered. For the PMs comprising platforms with U^V type, the initial configuration of the PM, according to the orientation of the second axes the U joint (R_{i2} or R_{i4}) may be denoted as U^{VT}, U^{VN}, U^{VX} or U^{VY}.

The locations of the LCSs for Vertical 3-UPU PM is the same as the Tsai 3-UPU PM. R_{i1} are positioned on the z-axes of the LCSs. For the U^{VT}, R_{i2} are on the y-axes (Figure 3.4). For U^{VN}, R_{i2} are on the x-axes of the LCSs (see in Figure 3.9). For U^{VX} and U^{VY}, R_{i2} is on either x- or y-axes of the LCSs (see in Figure 3.10).

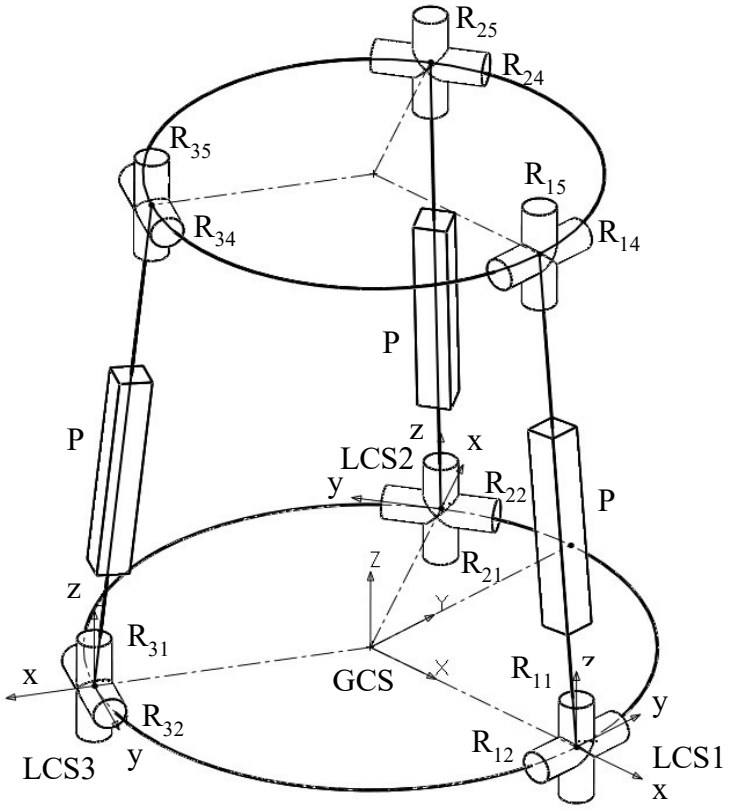

Figure 3.4. Kinematic schematic of Vertical 3-UPU PM

Based on the joint layouts of all these presented 3-UPU PMs, new joint layouts are derived and a classification of 3-UPU PMs is presented in the next section.

3.2. Sub-Joint Layouts For 3-UPU PMs

In general, a U-joint mounted on a platform can have ∞^2 possible configurations, which depends on the orientation of the R joint axis attached to the platform. So, in general for a platform comprising 3 U-joints, there are ∞^6 possible joint layouts. Also the relative locations of R_{i2} and R_{i4} axes on each limb should be considered for a 3-UPU PM. This can be taken into account by defining the R_{i2} and R_{i4} axes in an initial configuration, which is specifying the angle between R_{i2} and R_{i4}. Therefore, in general, there are ∞^{15} possible 3-UPU architectures. Among these abundantly many possible architectures, not all are practical. Therefore, based on the available architectures in the literature some ground rules are established in order to narrow down the list to a reasonable finitely many possible architectures.

In the literature, it is seen that generally the distances between the U-joint centers of a platform are taken to be equivalent, i.e. base and moving platforms are in equilateral triangle form. Therefore, in this thesis, only the 3-UPU PMs with equilateral base and moving platforms are considered. However, the base and the moving platforms need not be identical. In order to be able to perform the mobility analysis of different 3-UPU PM architectures, an initial configuration is set such that the moving platform plane is parallel to the base platform plane, the center of the moving platform is on the Z-axis of the GCS and all three limbs make a prescribed angle with the base platform plane. The relative positions of the joint axes are then defined based on this initial configuration.

Due to the particular shape of the U joint, it is known that the position of the R_{i2} and R_{i4} axes can be predicted by looking at the R_{i1} and R_{i5} axes of the U joints. As shown in Figure 3.5, if R_{i1} axis of a U joint is along the x-axis of a LCS, R_{i2} axis must move on the z-y plane. Similarly, if R_{i1} axis is along the y-axis, R_{i2} axis must move on the z-x plane. Same discussion goes for R_{i5} and R_{i4} axes of the moving platform as well. R_{i2} and R_{i4} axes have to be nonintersecting, i.e. parallel or skew, because of the P joint in between them. The P joint direction cannot be in the direction of the R_{i2} or R_{i4} axes, otherwise a cylindrical joint is obtained. The P joint direction has to be perpendicular to R_{i2} and R_{i4} axes. Furthermore, it is assumed that the common normal of R_{i2} and R_{i4} axes pass through the two U-joint centers on limb i. With these assumptions, the orientations of R_{i2} and R_{i4} axes in the initial configuration of the PM are determined depending on the angle between the limbs and the platform planes.

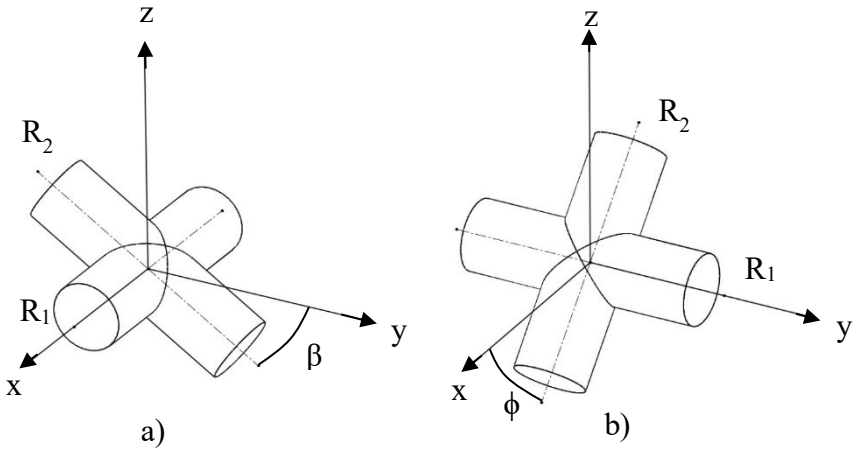

Figure 3.5. R joint axes of a U joint when R_{i1} are on a) x-axis, b) y-axis

If R_{i1} or R_{i5} axes are perpendicular to the base or moving platform planes, i.e. if R_{i1} axes are on the z-axis of the corresponding LCSs, R_{i2} and R_{i4} have to be on the platform planes, but the relative positions of R_{i2} and R_{i4} axes cannot be predicted. So, in such a case, the orientation of the R_{i2} and R_{i4} axes in the initial configuration should be specified.

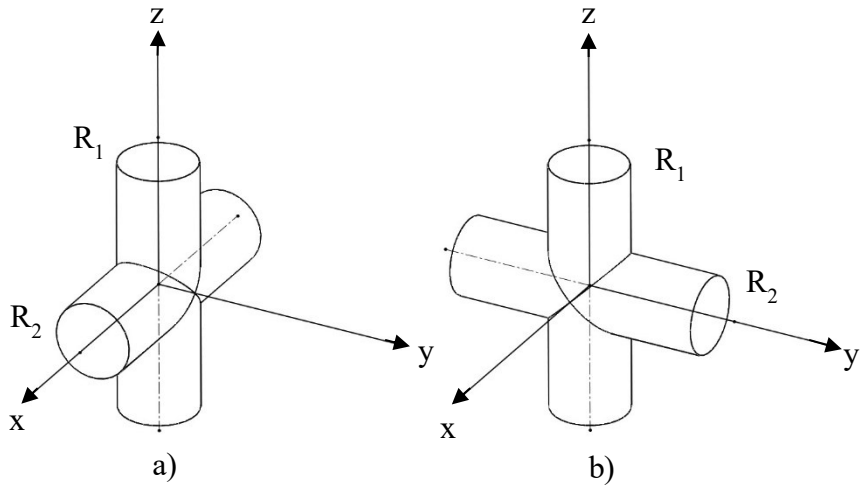

Figure 3.6. R joint axes of a U joint when R_{i1} is on the z-axis of the LCS

The case where R_{i1} and R_{i5} axes are neither on nor perpendicular to the platform planes is kept out of scope of this thesis. To sum up the previous discussions, when R_{i1}

or R_{i5} axes are on the platform plane, the orientations of R_{i2} and R_{i4} axes are determined according to the angle between the limbs and the platforms in the initial configuration of the PM, while when R_{i1} or R_{i5} axes are perpendicular to the platform plane, the orientations of R_{i2} and R_{i4} axes in the initial configuration of the PM need to be specified. By this way, it is possible to provide a proper description of the PM architecture that enables to derive new U joint layouts. As seen in Figure 3.7, the U joints are numbered in the same order as the LCSs.

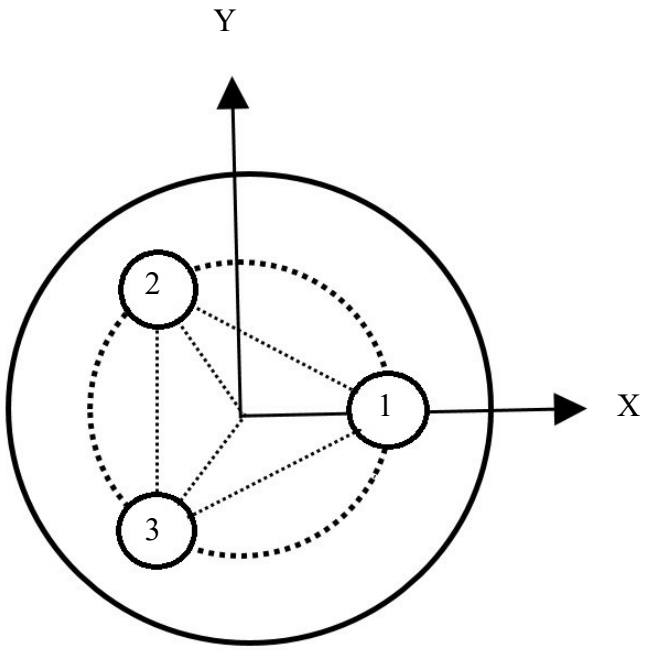

Figure 3.7. U-joint layout representation of a platform

When R_{i1} or R_{i5} axes are on a platform plane, it is assumed that either of the following four cases occur: 1) the axes are tangent to the circle passing through the U-joint centers on a platform (U^T); 2) the axes are normal to the circle passing through the U-joint centers on a platform (U^N); 3) the axes are all parallel to the X-axis of the GCS (U^X); 4) the axes are all parallel to the Y-axis of the GCS (U^Y). When R_{i1} or R_{i5} axes are perpendicular to a platform plane, the layout is shown with either U^{VT} or U^{VN} or U^{VX} or U^{VY}, depending on whether the R_{i2} or R_{i4} axes are tangent, normal or parallel to X- or Y-axis, respectively. Graphical representation of all these possible U-joint layouts are illustrated in Figure 3.8.

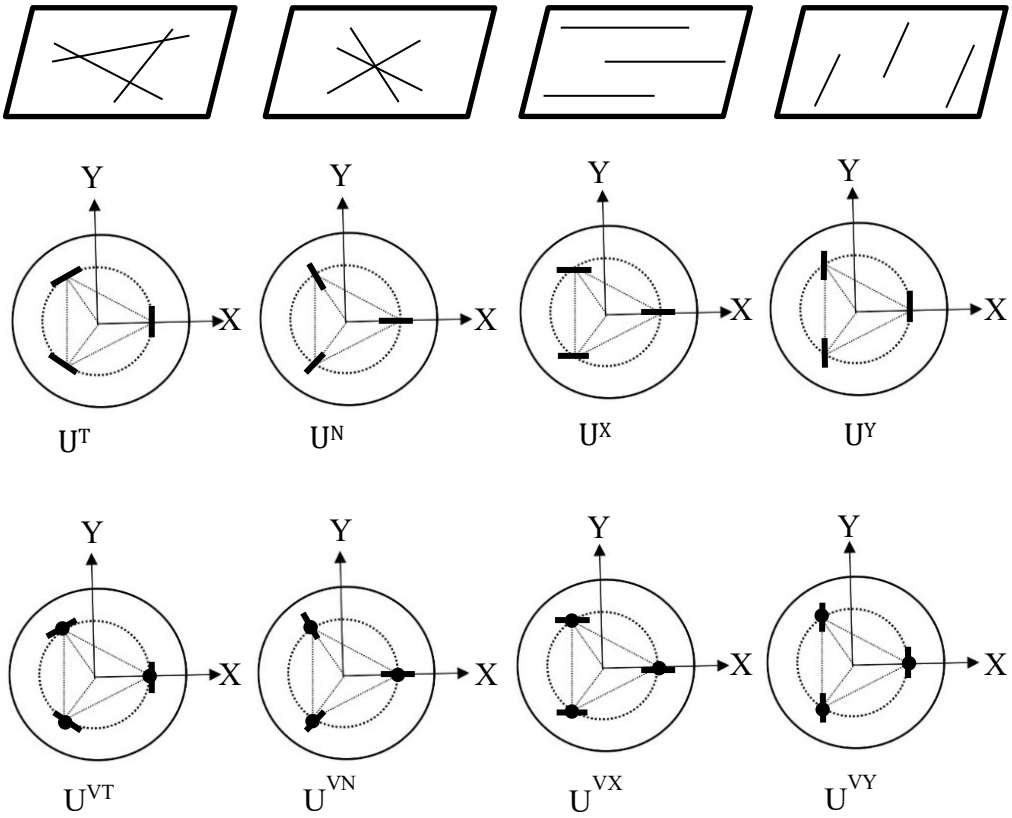

Figure 3.8. R-joint layouts of a platform

On a platform, it is also possible to have U-joint layouts where, for example two of the R_{i1} axes are tangent to the platform circle, while the remaining R_{i1} axis is normal. Such new layouts are obtained by changing the type of one of the three U-joints on a platform. The changed U-joint is assumed to be on limb 1. The case, where all three U-joints are from different layouts are kept out of scope of the thesis. In order to represent the created subgroups, the main layout associated with the two U-joints is written as a superscript, while the U-joint to be modified is written as a subscript. For example, U_N^T for a base platform represents a joint layout where the R_{11} axis is normal, while R_{21} and R_{31} are tangent to the circle passing through the U-joint centers.

Different layouts for base and moving platform are not arbitrarily selected. There are two layout subgroups among which base and moving platform layouts can be matched with each other. The two main subgroups are the ones generated from U^T, U^N, U^{VT}, U^{VN} and U^X, U^Y, U^{VX}, U^{VY}. Under these conditions, the sub-joint layouts are derived. For U^T,

U^N, U^{VT} and U^{VN} the sub-joint layouts can be seen in Figure 3.9.

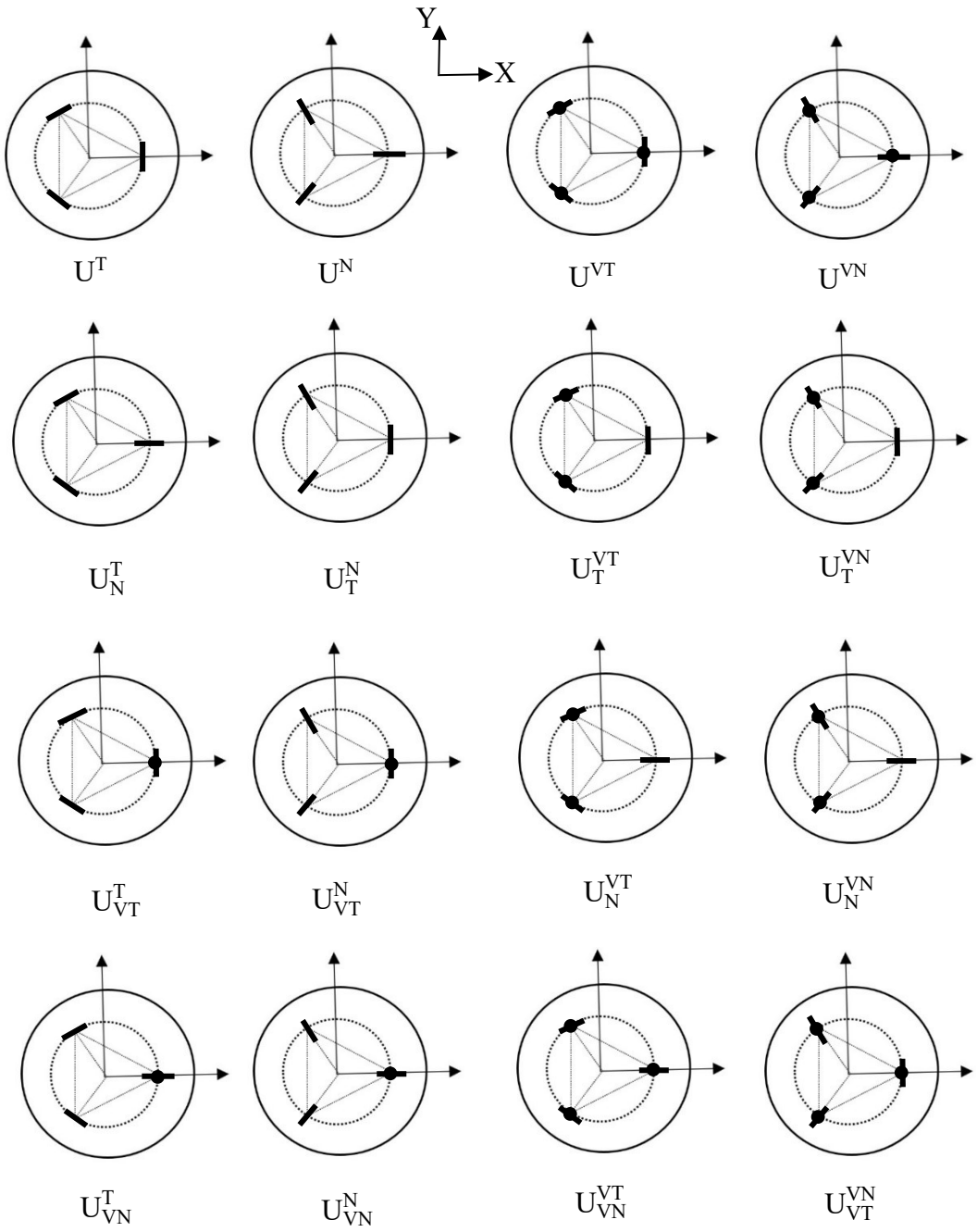

Figure 3.9. Sub-Joint Layouts for U^T, U^N, U^{VT} and U^{VN}

As shown in Figure 3.9, the sub joint layouts created for U^T are U_N^T , U_{VT}^T and U_{VN}^T. For these sub-joint layouts R_{i1} or R_{i5} axes of limbs 2 and 3 are tangent to the circumcircle whereas the R_{i1} or R_{i5} axis of the limb 1 for U_N^T is normal to the circumcenter.

For U_{VT}^{T}, the R_{i1} or R_{i5} axis of limb is perpendicular to the platform plane, while the R_{i2} or R_{i4} axis is tangent to the circumcircle in initial configuration of the PM. Similarly, the R_{i1} or R_{i5} axis of limb 1 for U_{VN}^{T} are perpendicular to the platform plane, while the R_{i2} or R_{i4} axis is normal to the circumcenter.

For the sub-joint layouts of U^{N} R_{i1} or R_{i5} axes of limbs 2 and 3 are normal to the circumcenter, whereas R_{i1} or R_{i5} axis of limb 1 for U_{T}^{N} is tangent to the circumcircle. For U_{VT}^{N} and U_{VN}^{N}, the placement of the R_{i1} or R_{i5} axis of limb 1 is like U_{VT}^{T} and U_{VN}^{T}.

For U^{VT} and its sub joint layouts, the R_{i1} or R_{i5} axes of limbs 2 and 3 are perpendicular to the platform plane while the R_{i2} or R_{i4} axes are tangent to the circumcircle in the initial configuration of the PM. For the U_{T}^{VT} and U_{N}^{VT} sub-joint layouts, the R_{i1} or R_{i5} axis of limb 1 is either tangent or normal to the circumcircle. For U_{VN}^{VT}, R_{i2} or R_{i4} axis of limb 1 is normal to the circumcenter in the initial configuration of the PM.

For U^{VN}, U_{T}^{VN}, U_{N}^{VN} and U_{VT}^{VN}, the R_{i1} or R_{i5} axes of the limbs 2 and 3 are perpendicular to the platform plane, while the R_{i2} or R_{i4} axes are normal to the circumcenter in the initial configuration of the PM. For the U_{T}^{VN} and U_{N}^{VN} sub-joint layouts, the R_{i1} or R_{i5} axis of limb 1 is either tangent or normal to the circumcircle. For U_{VT}^{VN}, R_{i1} or R_{i5} axes of the limb 1 is perpendicular to the platform plane, while R_{i2} or R_{i4} axis of limb 1 is tangent to the circumcenter in the initial configuration of the PM.

Using the same procedure, sub-joint layouts for U^{X}, U^{Y}, U^{VX} and U^{VY} joint layouts are created. As can be seen in Figure 3.10, the R_{i1} or R_{i5} axes of limbs 2 and 3 of U^{X} sub-joint layout are parallel to the X-axis of the GCS. The R_{i1} or R_{i5} axis of limb 1 for U_{Y}^{X} is parallel to the Y-axis of the GCS. The R_{i1} or R_{i5} axis of limb 1 in the U_{VX}^{X} and U_{VY}^{X} sub-joint layouts are perpendicular to the platform plane, whereas the R_{i2} or R_{i4} axis for U_{VX}^{X} are parallel to the X-axis of the GCS, while the R_{i2} or R_{i4} axis of U_{VY}^{X} is parallel to the Y-axis of the GCS in the initial configuration of the PM.

For the U^{Y} sub-joint layouts, the R_{i1} or R_{i5} axes of limbs 2 and 3 are parallel to the Y-axis of the GCS. The R_{i1} or R_{i5} axes of limb 1 for U_{X}^{Y} are parallel to the X-axis of the GCS. The placement of the R_{i1} or R_{i5} of limb 1 for U_{VX}^{Y} and U_{VY}^{Y} sub-joint layouts are the same as U_{VX}^{X} and U_{VY}^{X}.

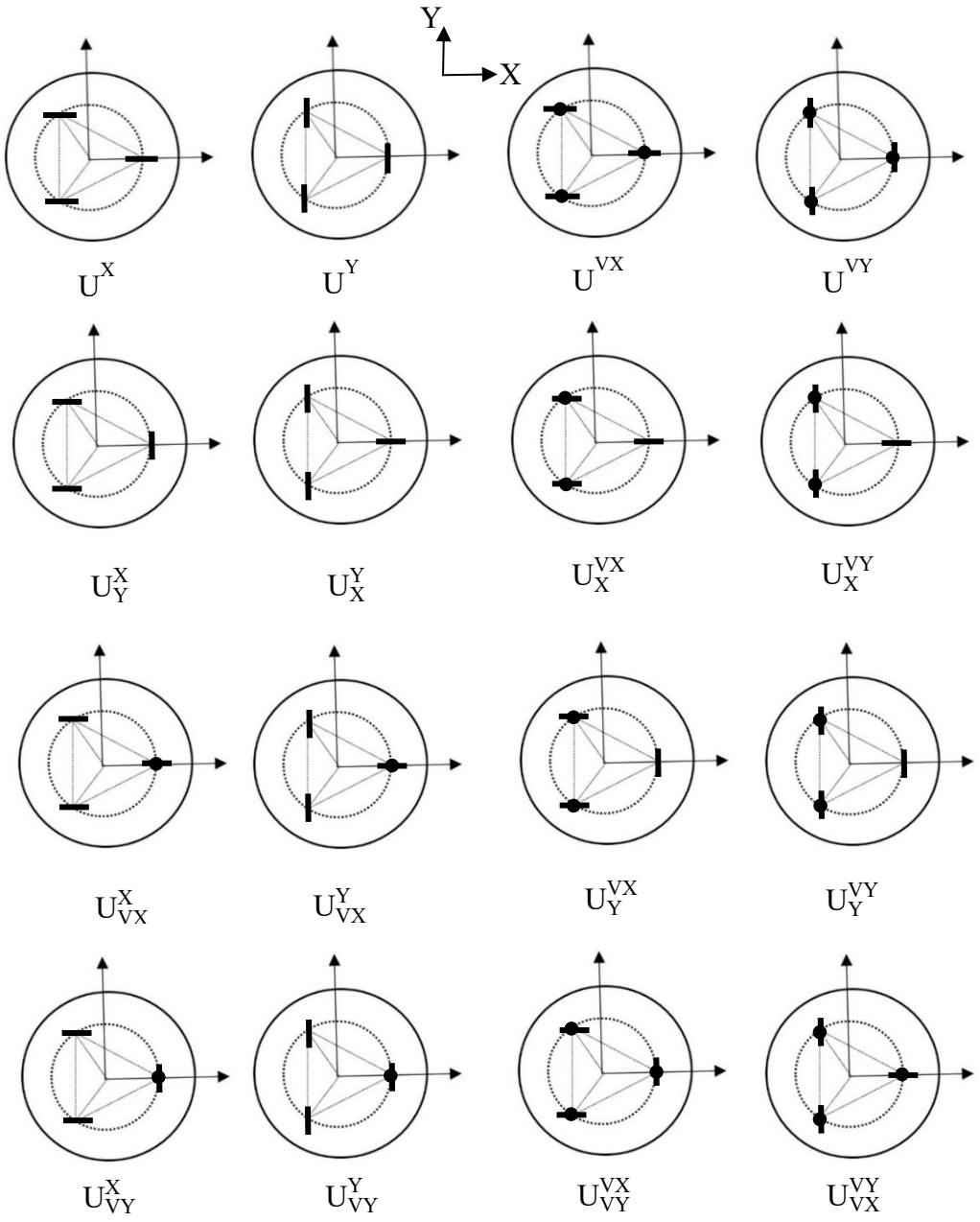

Figure 3.10. Sub-Joint Layouts for U^X, U^Y, U^{VX} and U^{VY}

The R_{i1} or R_{i5} axes of limbs 2 and 3 for the U^{VX} sub-joint layouts are perpendicular to the platform plane, while the R_{i2} or R_{i4} axes are parallel to the X-axis of the GCS. For U_X^{VX} and U_Y^{VX}, the R_{i1} or R_{i5} axis of limb 1 is parallel to the X-axis or the Y-axis of the GCS in the initial configuration of the PM. For U_{VY}^{VX} sub-joint layout, the R_{i1} or R_{i5} axis of limb 1 is perpendicular to the platform plane, while the R_{i2} or R_{i4} axis is parallel to the

Y-axis of the GCS in the initial configuration of the PM.

In the U^{VY} sub-joint layouts, the R_{i1} or R_{i5} axes of limbs 2 and 3 are perpendicular to the platform plane whereas the R_{i2} or R_{i4} axes are parallel to the Y-axis of the GCS in the initial configuration of the PM. The layouts of the R_{i1} or R_{i5} axis of limb 1 for U_X^{VY} and U_Y^{VY} are like U_X^{VX} and U_Y^{VX}. For U_{VX}^{VY}, the R_{i1} or R_{i5} axis of limb 1 is perpendicular to the layout plane, while the R_{i2} or R_{i4} axis is parallel to the X-axis of the GCS in the initial configuration of the PM.

3.3. Summary of Assumptions

The assumptions for the synthesis and analysis of the 3-UPU PMs can be summarized as follows:

- The base and the moving platform triangles are equilateral.

In order to define the relative joint locations, an initial configuration of the PM is set. At the initial configuration of the PM,

- The moving platform plane is parallel to the base platform plane.
- The center of the moving platform triangle is on the Z-axis of the GCS which is located at the center of the base platform triangle with Z-axis perpendicular to the base platform plane. Therefore, all three limbs make the same angle with the base platform plane.
- If the joint axis associated with a platform are on the platform plane, the joint axes are either tangent (denoted by T) or normal (denoted by N) to the circumcircle of the platform triangle, or else they are parallel to either X-axis (denoted by X) or Y-axis (denoted by Y) of the GCS.
- If the joint axis associated with a platform is perpendicular (V) to the platform plane, the consecutive joint axes are either tangent (denoted by VT) or normal (denoted by VN) to the circumcircle of the platform triangle, or else they are parallel to either X-axis (denoted by VX) or Y-axis (denoted by VY) of the GCS. As a consequence of this assumption, if any of the consecutive joint axes are not tangent to the circumcircle of the platform triangle, then the associated limb has to be perpendicular to the platform and hence the platforms are necessarily identical.

- A platform's sub-joint layout is obtained by only changing the joint type associated with the first limb and keeping the joint type associated with the second and third limbs.

  All analyses and results are based on these assumptions.

3.4. Novel 3-UPU PMs Consisting of Sub Joint Layouts

Created sub-joint layouts are matched with each other as base and moving platforms under two main groups: TNV group presented in Figures 3.9 and XYV group presented in Figure 3.10. Since there are 16 different sub-joint layouts in each group, a 16-by-16 table was created and 256 different PMs were derived for each group. In Chapter 4, the initial configurations of the PMs are taken into consideration while analyzing the mobility of the PM.

To proceed with the mobility analysis, limb types are classified according to the locations of the joints on the limb in the initial configuration of the PM. Accordingly, the limbs of the TNV-type PMs are located in the xz-planes of the LCSs in the initial configuration. In XYV-type manipulators, limbs are assumed to be along the z-axes of the LCSs. Therefore for a XYV-type PMs, the base and the moving platforms are assumed to be identical, because in the literature there are no XYV-type PMs with non-identical platforms and such a PM would not be a practical one. Under these assumptions, after the base and mobile platform layouts are matched to each other, it is seen that there are 16 different limb types in total. The positioning of the R joint axes in their corresponding LCSs of these limb types are presented in the following sub-sections.

3.4.1. Limb Types of PMs

The limb types are divided into four main groups according to the locations of the R_{i1} and R_{i2} axes of each limb in the LCS in the initial configuration of the PM. These groups are defined such that the R_{i1} or R_{i2} axes are along the x-, y- or z-axis of the LCS.

3.4.1.1. R_y Type Limbs

The limb types with R_{i1} axis parallel to the y-axis of the LCS are designated as R_y-. There are 4 sub-types according to the joint locations on the moving platform. As shown in Figure 3.11(a), the limb type where the R_{i5} axis is parallel to the y-axis of the LCS is designated as R_y-R_y. If the R_{i5} axis is parallel to the x-axis of the LCS, this kind of limb is denoted as R_y-R_x (Figure 3.11(b)). When R_{i5} axis is parallel to the z-axis of the LCS and R_{i4} axis is parallel to the y-axis of the LCS in the initial configuration of the PM, it is shown as R_y-R_yR_z (Figure 3.11(c)), whereas if R_{i4} axis is parallel to the x-axis of LCS in the initial configuration, it is shown as R_y-R_xR_z (Figure 3.11(d)).

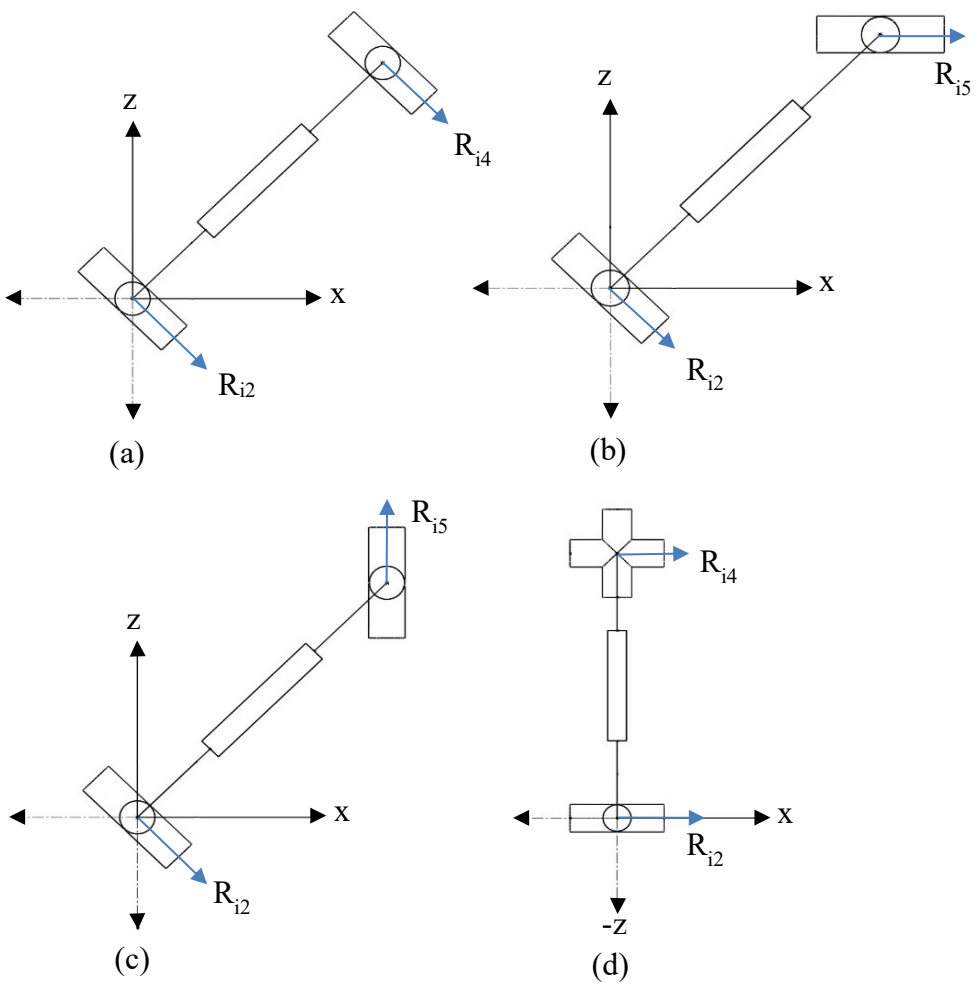

Figure 3.11. R_y Type Limbs (a) R_y-R_y, (b) R_y-R_x, (c) R_y-R_yR_z, (d) R_y-R_xR_z

3.4.1.2. R_x Type Limbs

The limb types with R_{i1} axis parallel to the x-axis of the LCS are designated as R_x-. Since the R_{i4} and R_{i5} locations are the same as R_y- type limbs, the representation of second part after the P joint is similar (Figure 3.12).

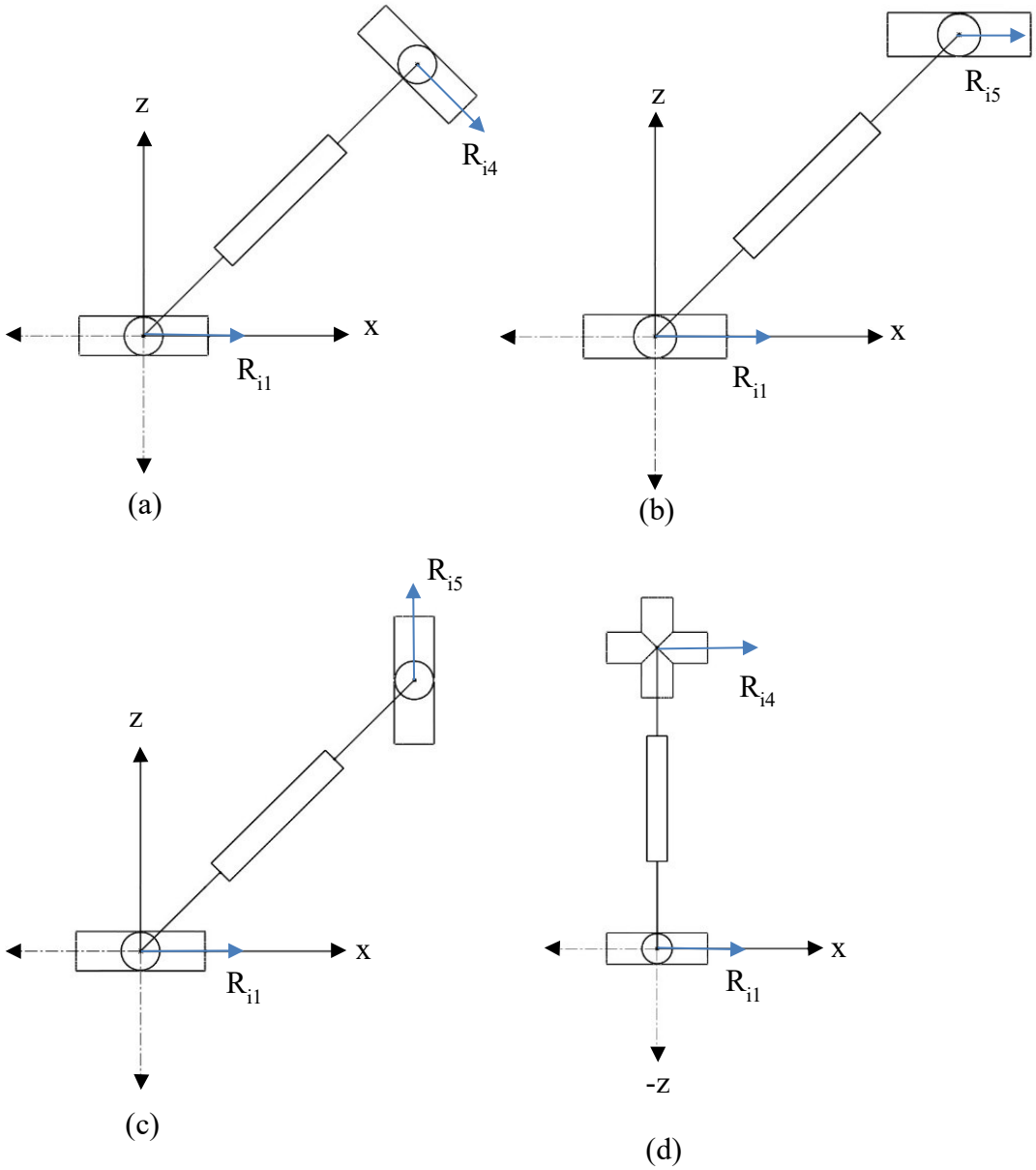

Figure 3.12. R_x Type Limbs (a) R_x-R_y, (b) R_x-R_x, (c) R_x-R_yR_z, (d) R_x-R_xR_z

3.4.1.3. R_zR_y Type Limbs

The limb types with R_{i1} axis parallel to the z-axis and R_{i2} axis parallel to the y-axis of the LCS are designated as R_zR_y-. As shown in Figure 3.13(a), the limb type with R_{i5} axis parallel to the y-axis of the LCS is designated as R_zR_y-R_y. If R_{i5} axis is parallel to the x-axis of the LCS, this kind of limb is denoted as R_zR_y-R_x (Figure 3.13(b)). When R_{i5} axis is parallel to the z-axis of the LCS and R_{i4} axis is parallel to the y-axis of the LCS in the initial configuration of the PM, it is shown as R_zR_y-R_yR_z (Figure 3.13(c)) whereas if R_{i4} axis is parallel to the x-axis of LCS, it is shown as R_zR_y-R_xR_z (Figure 3.13(d)).

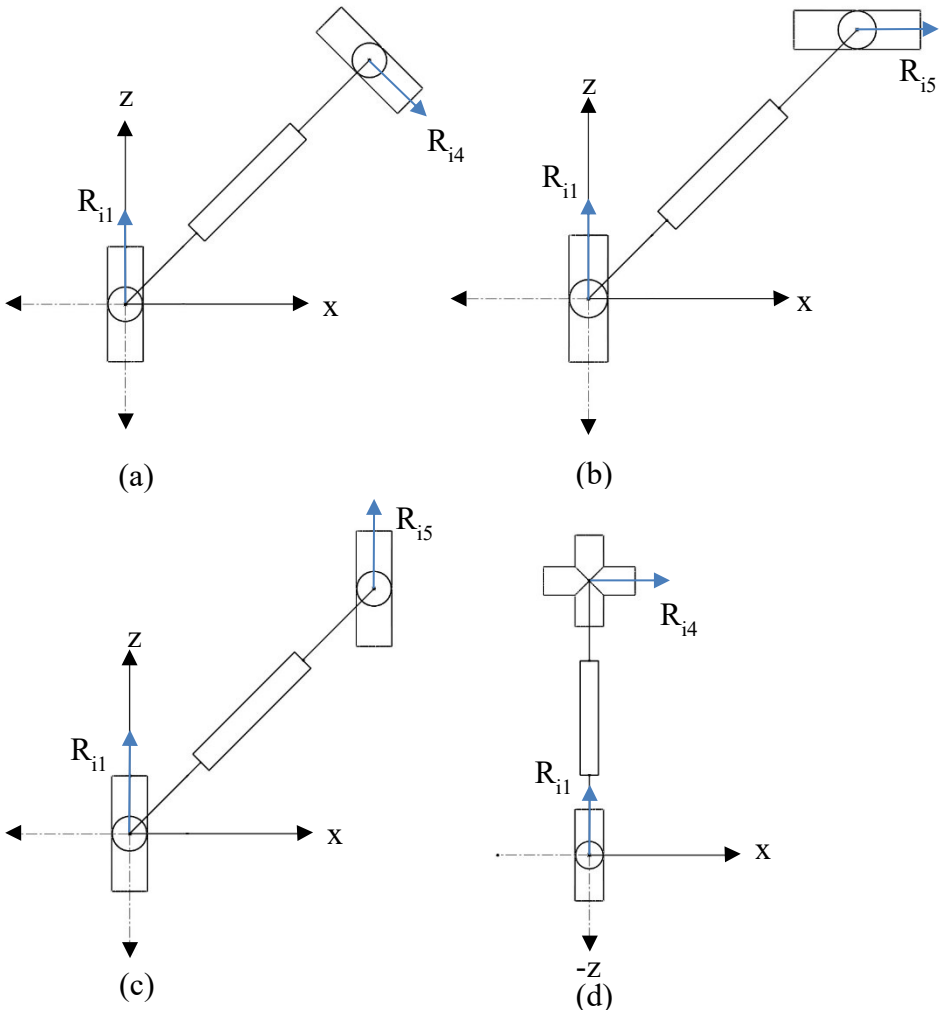

Figure 3.13. R_zR_y Type Limbs (a) R_zR_y-R_y, (b) R_zR_y-R_x, (c) R_zR_y-R_yR_z, (d) R_zR_y-R_xR_z

3.4.1.4. R_zR_x Type Limbs

The limb types with R_{i1} axis parallel to the z-axis and R_{i2} axis parallel to the x-axis of the LCS are designated as R_zR_x-. Since the R_{i4} and R_{i5} locations are the same as R_zR_y type limbs, the representation of second part after the P joint is similar (Figure 3.14).

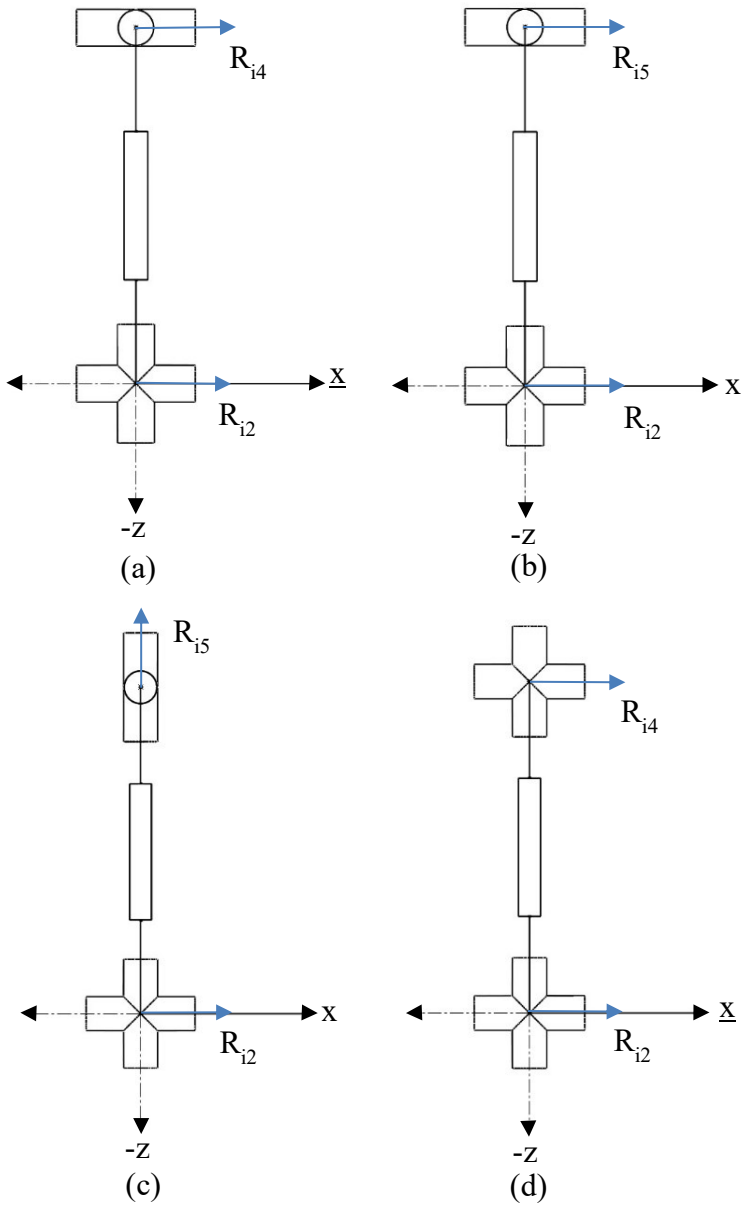

Figure 3.14. R_zR_x Type Limbs (a) R_zR_x-R_y, (b) R_zR_x-R_x, (c) R_zR_x-R_yR_z, (d) R_zR_x-R_xR_z

3.4.1.5. Limb Types Summarized

There are totally 16 limb types described in the previous sub-sections. For brevity, these limb types are designated with k_i for i = 1, …, 16 as given in Table 3.1.

Table 3.1. Symbolic equivalents of limb types

k_1	R_y - R_y	k_9	$R_z R_y$ - R_y
k_2	R_y - R_x	k_{10}	$R_z R_y$ - R_x
k_3	R_y - $R_y R_z$	k_{11}	$R_z R_y$ - $R_y R_z$
k_4	R_y - $R_x R_z$	k_{12}	$R_z R_y$ - $R_x R_z$
k_5	R_x - R_y	k_{13}	$R_z R_x$ - R_y
k_6	R_x - R_x	k_{14}	$R_z R_x$ - R_x
k_7	R_x - $R_y R_z$	k_{15}	$R_z R_x$ - $R_y R_z$
k_8	R_x - $R_x R_z$	k_{16}	$R_z R_x$ - $R_x R_z$

3.4.2. Joint Layout Matching

When a base and a moving platform of given joint layout are matched with each other, the limps types will be one of the 16 types given in Table 3.1. As it is assumed that one limbs 2 and 3 need to be identical while limb 1 can be different, the limbs of the TNV-type and XYV-type platforms can be classified as given in Tables 3.2-3.5. As an example, when a U_T^{VT} base and a U_N^T moving platform are matched, limb 1 type is k_2 (from Table 3.2) and limbs 2&3 type is k_9 (from Table 3.3). By this way, it can be seen that there are 256 TNV-type PMs (each element of Table 3.2 or 3.3) and 256 XYV-type PMs (each element of Table 3.4 or 3.5). The mobility analysis of all PMs are performed in Chapter 5 based on the theory presented in Chapter 4.

Table 3.2. Limb types of first limbs of TNV-type PMs

Limb-1		MOVING PLATFORM															
		U^{T}	U^{N}	U^{VT}	U^{VN}	U_{N}^{T}	U_{T}^{N}	U_{T}^{VT}	U_{T}^{VN}	U_{N}^{VT}	U_{N}^{VN}	U_{VT}^{T}	U_{VN}^{T}	U_{VT}^{N}	U_{VN}^{N}	U_{VN}^{VT}	U_{VT}^{VN}
BASE	U^{T}	k_1	k_2	k_3	k_4	k_2	k_1	k_1	k_1	k_2	k_2	k_3	k_4	k_3	k_4	k_4	k_3
	U^{N}	k_5	k_6	k_7	k_8	k_6	k_5	k_5	k_5	k_6	k_6	k_7	k_8	k_7	k_8	k_8	k_7
	U^{VT}	k_9	k_1	k_{11}	k_{12}	k_1	k_9	k_9	k_9	k_{10}	k_{10}	k_{11}	k_{12}	k_{11}	k_{12}	k_{12}	k_{11}
	U^{VN}	k_1	k_1	k_{15}	k_{16}	k_1	k_1	k_{13}	k_{13}	k_{14}	k_{14}	k_{15}	k_{16}	k_{15}	k_{16}	k_{16}	k_{15}
	U_{N}^{T}	k_5	k_6	k_7	k_8	k_6	k_5	k_5	k_5	k_6	k_6	k_7	k_8	k_7	k_8	k_8	k_7
	U_{T}^{N}	k_1	k_2	k_3	k_4	k_2	k_1	k_1	k_1	k_2	k_2	k_3	k_4	k_3	k_4	k_4	k_3
	U_{T}^{VT}	k_1	k_2	k_3	k_4	k_2	k_1	k_1	k_1	k_2	k_2	k_3	k_4	k_3	k_4	k_4	k_3
	U_{T}^{VN}	k_1	k_2	k_3	k_4	k_2	k_1	k_1	k_1	k_2	k_2	k_3	k_4	k_3	k_4	k_4	k_3
	U_{N}^{VT}	k_5	k_6	k_7	k_8	k_6	k_5	k_5	k_5	k_6	k_6	k_7	k_8	k_7	k_8	k_8	k_7
	U_{N}^{VN}	k_5	k_6	k_7	k_8	k_6	k_5	k_5	k_5	k_6	k_6	k_7	k_8	k_7	k_8	k_8	k_7
	U_{VT}^{T}	k_9	k_1	k_{11}	k_{12}	k_1	k_9	k_9	k_9	k_{10}	k_{10}	k_{11}	k_{12}	k_{11}	k_{12}	k_{12}	k_{11}
	U_{VN}^{T}	k_1	k_1	k_{15}	k_{16}	k_1	k_1	k_{13}	k_{13}	k_{14}	k_{14}	k_{15}	k_{16}	k_{15}	k_{16}	k_{16}	k_{15}
	U_{VT}^{N}	k_9	k_1	k_{11}	k_{12}	k_1	k_9	k_9	k_9	k_{10}	k_{10}	k_{11}	k_{12}	k_{11}	k_{12}	k_{12}	k_{11}
	U_{VN}^{N}	k_1	k_1	k_{15}	k_{16}	k_1	k_1	k_{13}	k_{13}	k_{14}	k_{14}	k_{15}	k_{16}	k_{15}	k_{16}	k_{16}	k_{15}
	U_{VN}^{VT}	k_1	k_1	k_{15}	k_{16}	k_1	k_1	k_{13}	k_{13}	k_{14}	k_{14}	k_{15}	k_{16}	k_{15}	k_{16}	k_{16}	k_{15}
	U_{VT}^{VN}	k_9	k_1	k_{11}	k_{12}	k_1	k_9	k_9	k_9	k_{10}	k_{10}	k_{11}	k_{12}	k_{11}	k_{12}	k_{12}	k_{11}

Table 3.3. Limb types of second and third limbs of TNV-type PMs

Limbs 2&3		MOVING PLATFORM															
		U^{T}	U^{N}	U^{VT}	U^{VN}	U_{N}^{T}	U_{T}^{N}	U_{T}^{VT}	U_{T}^{VN}	U_{N}^{VT}	U_{N}^{VN}	U_{VT}^{T}	U_{VN}^{T}	U_{VT}^{N}	U_{VN}^{N}	U_{VN}^{VT}	U_{VT}^{VN}
BASE	U^{T}	k_1	k_2	k_3	k_4	k_1	k_2	k_3	k_4	k_3	k_4	k_1	k_1	k_2	k_2	k_3	k_4
	U^{N}	k_5	k_6	k_7	k_8	k_5	k_6	k_7	k_8	k_7	k_8	k_5	k_5	k_6	k_6	k_7	k_8
	U^{VT}	k_9	k_1	k_{11}	k_{12}	k_9	k_1	k_{11}	k_{12}	k_{11}	k_{12}	k_9	k_9	k_{10}	k_{10}	k_{11}	k_{12}
	U^{VN}	k_1	k_1	k_{15}	k_{16}	k_1	k_1	k_{15}	k_{16}	k_{15}	k_{16}	k_{13}	k_{13}	k_{14}	k_{14}	k_{15}	k_{16}
	U_{N}^{T}	k_1	k_2	k_3	k_4	k_1	k_2	k_3	k_4	k_3	k_4	k_1	k_1	k_2	k_2	k_3	k_4
	U_{T}^{N}	k_5	k_6	k_7	k_8	k_5	k_6	k_7	k_8	k_7	k_8	k_5	k_5	k_6	k_6	k_7	k_8
	U_{T}^{VT}	k_9	k_1	k_{11}	k_{12}	k_9	k_1	k_{11}	k_{12}	k_{11}	k_{12}	k_9	k_9	k_{10}	k_{10}	k_{11}	k_{12}
	U_{T}^{VN}	k_1	k_1	k_{15}	k_{16}	k_1	k_1	k_{15}	k_{16}	k_{15}	k_{16}	k_{13}	k_{13}	k_{14}	k_{14}	k_{15}	k_{16}
	U_{N}^{VT}	k_9	k_1	k_{11}	k_{12}	k_9	k_1	k_{11}	k_{12}	k_{11}	k_{12}	k_9	k_9	k_{10}	k_{10}	k_{11}	k_{12}
	U_{N}^{VN}	k_1	k_1	k_{15}	k_{16}	k_1	k_1	k_{15}	k_{16}	k_{15}	k_{16}	k_{13}	k_{13}	k_{14}	k_{14}	k_{15}	k_{16}
	U_{VT}^{T}	k_1	k_2	k_3	k_4	k_1	k_2	k_3	k_4	k_3	k_4	k_1	k_1	k_2	k_2	k_3	k_4
	U_{VN}^{T}	k_1	k_2	k_3	k_4	k_1	k_2	k_3	k_4	k_3	k_4	k_1	k_1	k_2	k_2	k_3	k_4
	U_{VT}^{N}	k_5	k_6	k_7	k_8	k_5	k_6	k_7	k_8	k_7	k_8	k_5	k_5	k_6	k_6	k_7	k_8
	U_{VN}^{N}	k_5	k_6	k_7	k_8	k_5	k_6	k_7	k_8	k_7	k_8	k_5	k_5	k_6	k_6	k_7	k_8
	U_{VN}^{VT}	k_9	k_1	k_{11}	k_{12}	k_9	k_1	k_{11}	k_{12}	k_{11}	k_{12}	k_9	k_9	k_{10}	k_{10}	k_{11}	k_{12}
	U_{VT}^{VN}	k_1	k_1	k_{15}	k_{16}	k_1	k_1	k_{15}	k_{16}	k_{15}	k_{16}	k_{13}	k_{13}	k_{14}	k_{14}	k_{15}	k_{16}

Table 3.4. Limb types of first limbs of XYV-type PMs

Limb-1		MOVING PLATFORM															
		U^{X}	U^{Y}	U^{VX}	U^{VY}	U^{X}_{Y}	U^{Y}_{X}	U^{VX}_{X}	U^{VY}_{X}	U^{VX}_{Y}	U^{VY}_{Y}	U^{X}_{VX}	U^{X}_{VY}	U^{Y}_{VX}	U^{Y}_{VY}	U^{VX}_{VY}	U^{VY}_{VX}
BASE	U^{X}	k_6	k_5	k_8	k_7	k_5	k_6	k_6	k_6	k_8	k_7	k_8	k_7	k_5	k_5	k_7	k_8
	U^{Y}	k_2	k_1	k_4	k_3	k_1	k_2	k_2	k_2	k_4	k_3	k_4	k_3	k_1	k_1	k_3	k_4
	U^{VX}	k_1	k_1	k_{16}	k_{15}	k_1	k_1	k_{14}	k_{14}	k_{16}	k_{15}	k_{16}	k_{15}	k_{13}	k_{13}	k_{15}	k_{16}
	U^{VY}	k_1	k_9	k_{12}	k_{11}	k_9	k_1	k_{10}	k_{10}	k_{12}	k_{11}	k_{12}	k_{11}	k_9	k_9	k_{11}	k_{12}
	U^{X}_{Y}	k_2	k_1	k_4	k_3	k_1	k_2	k_2	k_2	k_4	k_3	k_4	k_3	k_1	k_1	k_3	k_4
	U^{Y}_{X}	k_6	k_5	k_8	k_7	k_5	k_6	k_6	k_6	k_8	k_7	k_8	k_7	k_5	k_5	k_7	k_8
	U^{VX}_{X}	k_6	k_5	k_8	k_7	k_5	k_6	k_6	k_6	k_8	k_7	k_8	k_7	k_5	k_5	k_7	k_8
	U^{VY}_{X}	k_6	k_5	k_8	k_7	k_5	k_6	k_6	k_6	k_8	k_7	k_8	k_7	k_5	k_5	k_7	k_8
	U^{VX}_{Y}	k_1	k_1	k_{16}	k_{15}	k_1	k_1	k_{14}	k_{14}	k_{16}	k_{15}	k_{16}	k_{15}	k_{13}	k_{13}	k_{15}	k_{16}
	U^{VY}_{Y}	k_1	k_9	k_{12}	k_{11}	k_9	k_1	k_{10}	k_{10}	k_{12}	k_{11}	k_{12}	k_{11}	k_9	k_9	k_{11}	k_{12}
	U^{X}_{VX}	k_1	k_1	k_{16}	k_{15}	k_1	k_1	k_{14}	k_{14}	k_{16}	k_{15}	k_{16}	k_{15}	k_{13}	k_{13}	k_{15}	k_{16}
	U^{X}_{VY}	k_1	k_9	k_{12}	k_{11}	k_9	k_1	k_{10}	k_{10}	k_{12}	k_{11}	k_{12}	k_{11}	k_9	k_9	k_{11}	k_{12}
	U^{Y}_{VX}	k_2	k_1	k_4	k_3	k_1	k_2	k_2	k_2	k_4	k_3	k_4	k_3	k_1	k_1	k_3	k_4
	U^{Y}_{VY}	k_2	k_1	k_4	k_3	k_1	k_2	k_2	k_2	k_4	k_3	k_4	k_3	k_1	k_1	k_3	k_4
	U^{VX}_{VY}	k_1	k_9	k_{12}	k_{11}	k_9	k_1	k_{10}	k_{10}	k_{12}	k_{11}	k_{12}	k_{11}	k_9	k_9	k_{11}	k_{12}
	U^{VY}_{VX}	k_1	k_1	k_{16}	k_{15}	k_1	k_1	k_{14}	k_{14}	k_{16}	k_{15}	k_{16}	k_{15}	k_{13}	k_{13}	k_{15}	k_{16}

Table 3.5. Limb types of second and third limbs of XYV-type PMs

Limbs 2&3		MOVING PLATFORM															
		U^{X}	U^{Y}	U^{VX}	U^{VY}	U^{X}_{Y}	U^{Y}_{X}	U^{VX}_{X}	U^{VY}_{X}	U^{VX}_{Y}	U^{VY}_{Y}	U^{X}_{VX}	U^{X}_{VY}	U^{Y}_{VX}	U^{Y}_{VY}	U^{VX}_{VY}	U^{VY}_{VX}
BASE	U^{X}	k_6	k_5	k_8	k_7	k_6	k_5	k_8	k_7	k_6	k_6	k_5	k_5	k_8	k_7	k_8	k_7
	U^{Y}	k_2	k_1	k_4	k_3	k_2	k_1	k_4	k_3	k_2	k_2	k_1	k_1	k_4	k_3	k_4	k_3
	U^{VX}	k_1	k_1	k_{16}	k_{15}	k_1	k_1	k_{16}	k_{15}	k_{14}	k_{14}	k_{13}	k_{13}	k_{16}	k_{15}	k_{16}	k_{15}
	U^{VY}	k_1	k_9	k_{12}	k_{11}	k_1	k_9	k_{12}	k_{11}	k_{10}	k_{10}	k_9	k_9	k_{12}	k_{11}	k_{12}	k_{11}
	U^{X}_{Y}	k_6	k_5	k_8	k_7	k_6	k_5	k_8	k_7	k_6	k_6	k_5	k_5	k_8	k_7	k_8	k_7
	U^{Y}_{X}	k_2	k_1	k_4	k_3	k_2	k_1	k_4	k_3	k_2	k_2	k_1	k_1	k_4	k_3	k_4	k_3
	U^{VX}_{X}	k_1	k_1	k_{16}	k_{15}	k_1	k_1	k_{16}	k_{15}	k_{14}	k_{14}	k_{13}	k_{13}	k_{16}	k_{15}	k_{16}	k_{15}
	U^{VY}_{X}	k_1	k_9	k_{12}	k_{11}	k_1	k_9	k_{12}	k_{11}	k_{10}	k_{10}	k_9	k_9	k_{12}	k_{11}	k_{12}	k_{11}
	U^{VX}_{Y}	k_6	k_5	k_8	k_7	k_6	k_5	k_8	k_7	k_6	k_6	k_5	k_5	k_8	k_7	k_8	k_7
	U^{VY}_{Y}	k_6	k_5	k_8	k_7	k_6	k_5	k_8	k_7	k_6	k_6	k_5	k_5	k_8	k_7	k_8	k_7
	U^{X}_{VX}	k_2	k_1	k_4	k_3	k_2	k_1	k_4	k_3	k_2	k_2	k_1	k_1	k_4	k_3	k_4	k_3
	U^{X}_{VY}	k_2	k_1	k_4	k_3	k_2	k_1	k_4	k_3	k_2	k_2	k_1	k_1	k_4	k_3	k_4	k_3
	U^{Y}_{VX}	k_1	k_1	k_{16}	k_{15}	k_1	k_1	k_{16}	k_{15}	k_{14}	k_{14}	k_{13}	k_{13}	k_{16}	k_{15}	k_{16}	k_{15}
	U^{Y}_{VY}	k_1	k_9	k_{12}	k_{11}	k_1	k_9	k_{12}	k_{11}	k_{10}	k_{10}	k_9	k_9	k_{12}	k_{11}	k_{12}	k_{11}
	U^{VX}_{VY}	k_1	k_1	k_{16}	k_{15}	k_1	k_1	k_{16}	k_{15}	k_{14}	k_{14}	k_{13}	k_{13}	k_{16}	k_{15}	k_{16}	k_{15}
	U^{VY}_{VX}	k_1	k_9	k_{12}	k_{11}	k_1	k_9	k_{12}	k_{11}	k_{10}	k_{10}	k_9	k_9	k_{12}	k_{11}	k_{12}	k_{11}

CHAPTER 4

JOINT SCREWS OF THE LIMBS

Screw theory studies start with Chasles (1830) where he defines the simplest motion of a rigid body in between two given poses as a screw motion. Plücker (1865) then published his work on representations of lines with six coordinates. Ball (1900) discussed the kinematics and dynamics of rigid bodies under constraints by using screw theory. Among several contributors, Dimentberg (1965) formulated screw calculus using dual vectors. A major contribution to the subject is made by Hunt (1978) where he presents a complete classification of screw systems.

In this Chapter, first a brief explanation of screw theory the screw systems of the limb types found in the Chapter 3 are determined.

4.1. Screw Coordinates

The displacement of a rigid body in space is defined by six parameters. These parameters can be defined using motion screws called screws with a magnitude. Chasles (1830) states this relationship as follows: the most general rigid body displacement can be produced by a translation along a line (called its screw axis) accompanied by a rotation about that line. A screw $\$$ is geometrically described by a line in space – called the screw axis – accompanied with a pitch μ which relates the amount of rotation, say θ, about the screw axis to the amount of translation, say d, in the direction of the screw axis as $d = \mu\theta$ (Figure 4.1). One needs four independent parameters to describe a line. Together with the pitch μ and a magnitude, a screw can possess the six parameters required to describe the infinitesimal or finite displacement of a rigid body.

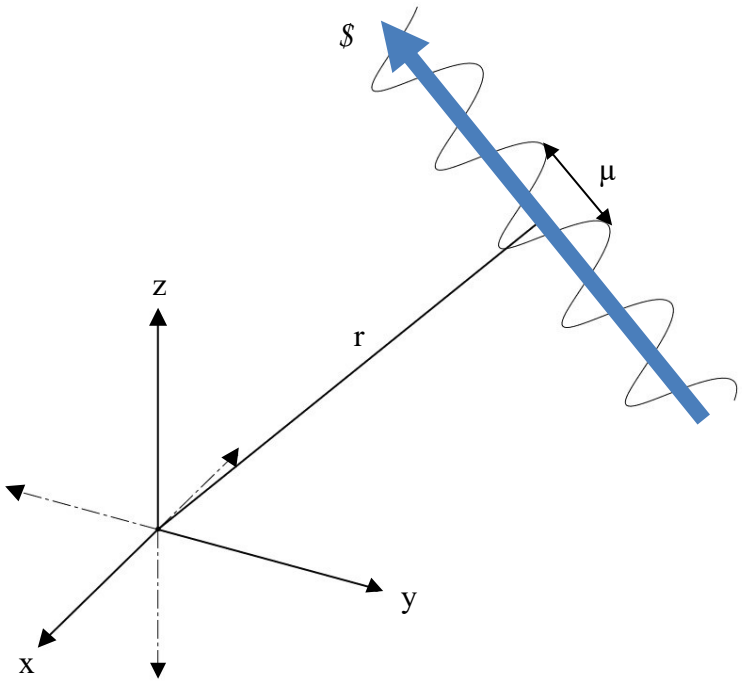

Figure 4.1. General screw motion

Analytically a screw $ can be described with two components

$$\$ = (\mathbf{s}; \mathbf{s_0}) \tag{4.1}$$

where $\mathbf{s} = (l, m, n)^T$, called the primary part of the screw, is a unit vector along the screw axis represented in a specific Cartesian frame and $s_0 = (p, q, r)^T = (\mu\mathbf{s} + \mathbf{r} \times \mathbf{s})$, called the secondary part of the screw, is composed of the summation of the moment $\mathbf{r} \times \mathbf{s}$ of $\mathbf{s}$ about the origin and a $\mu\mathbf{s}$ term along the screw axis. $\mathbf{r} = (x, y, z)^T$ is a vector from the origin to an arbitrary point on the screw axis. The relationship between $\mathbf{s}$ and $\mathbf{s_0}$ is as follows

$$\begin{pmatrix} p \\ q \\ r \end{pmatrix} = \begin{pmatrix} \mu & -z & y \\ z & \mu & -x \\ -y & x & \mu \end{pmatrix} \begin{pmatrix} l \\ m \\ n \end{pmatrix} \tag{4.2}$$

Accordingly, a screw can be written as follows

$$\$ = (l, m, n; p, q, r)^T \tag{4.3}$$

In mechanism science, revolute joints describe pure rotational motion between two links, hence they are described by zero-pitch screws:

$$\$_R = (\mathbf{s}; \mathbf{r} \times \mathbf{s}) \tag{4.4}$$

For a prismatic joint, the relative motion is pure translation, hence it described by an infinite-pitch screw:

$$\$_P = (0; s) \tag{4.5}$$

4.1.1. Screws of the 3-UPU PM Limbs

In this section, the screw system of the limb types described in Chapter 3 are presented. The locations of the joint axes and the limb axes in between the universal joint centers at the terminals of the limb in the initial configuration of the PM are considered. In the initial configuration of a TNV-type PM, the limb axes are always on the xz-plane of their respective LCSs. Meanwhile, in the initial configuration of an XYV-type PM, the limb axes are along the z-axis of their respective LCSs. The angle between the limb axis and the x-axis on the xz-plane in the initial configuration of the PM is denoted by θ (Figure 4.2). For the TNV-type PMs, typical values of θ are used for mobility analysis: 0°, 30°, 45°, 60°, 90°. These values correspond to the cases which result in PMs with extra mobility in the literature (Zhao et al., 2005).

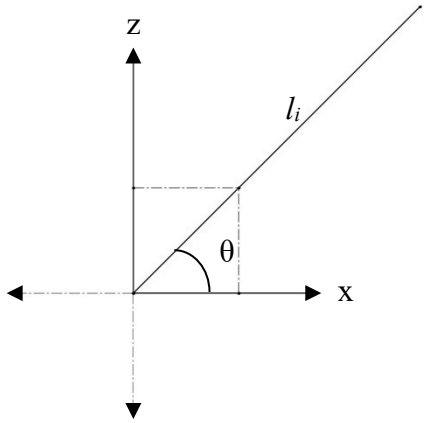

Figure 4.2. A limb with length l_i on the xz-axis, in the initial configuration of the PM

4.1.1.1. Screws of R_y Type Limbs

As seen in Figure 4.3, the R_{i1} joint axes of the R_y type limbs are along the y-axis of the LCS on the base. For this reason, as seen in Table 4.1, the primary part of the first screws of the R_y type limbs are the unit vector along the y-axis. For the second screws, R_{i2} joint axes of the R_y-R_y, R_y-R_x, and R_y-R_yR_z limbs are located on the xz-plane, whereas the R_y-R_xR_z limb has to be along the x-axis of the LCS in the initial configuration of the PM. Hence the primary part of the second screw of R_y-R_xR_z limb is the unit vector along the x-axis of the LCS. Likewise, for the third screws of R_y-R_xR_z limb, R_{i3} joint direction has to be along the z-axis of the LCS on the base, whereas R_{i3} joint directions of the rest of the limbs are on the xz-plane. The prismatic joint corresponds to infinite-pitch screws, so the secondary part of the third screw of the R_y-R_xR_z limb is unit vector along the z-axis, whereas it is on the xz-plane for the rest of the limbs.

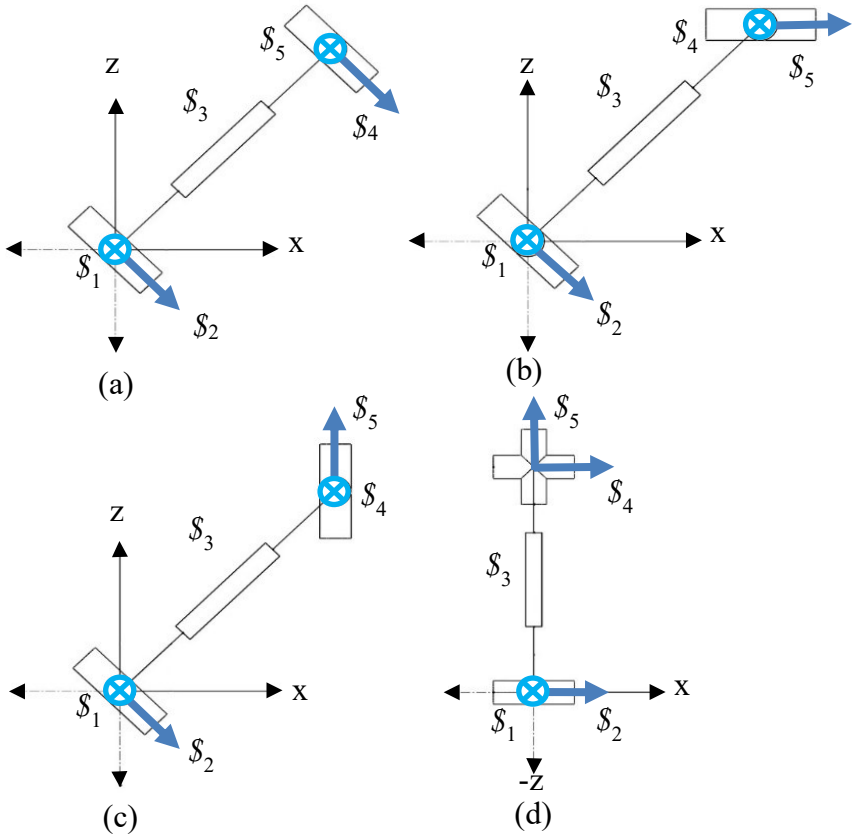

Figure 4.3. Screws of R_y Type Limbs (a) R_y-R_y, (b) R_y-R_x, (c) R_y-R_yR_z, (d) R_y-R_xR_z

For R_y-R_y limb, the primary part of the fourth screw is identical to the second screw of R_y-R_y limb. The fourth screws for R_y-R_x and R_y-R_yR_z limbs are identical to each other and the primary parts are the same as the first screws. For the R_y-R_xR_z limb the primary part of the fourth screw is unit vector along x-axis in the initial configuration of the PM. R_{i5} joint axis of R_y-R_y limb is parallel to the y-axis of the LCS and the primary part of the fifth screw of R_y-R_y limb is unit vector along the y-axis in the initial configuration of the PM. R_{i5} joint axis of R_y-R_x limb is parallel to the x-axis of the LCS and the primary part of the fifth screw of R_y-R_x limb is unit vector along the x-axis in the initial configuration of the PM. For the R_y-R_yR_z and R_y-R_xR_z limbs, the primary part of the fifth screws of R_y-R_yR_z and R_y-R_xR_z limbs are unit vectors along the z-axis. The screws of R_y type limbs are given in Table 4.1 in detail.

Table 4. 1. Screws of R_y Type Limbs (R_y-R_y, R_y-R_x, R_y-R_yR_z, R_y-R_xR_z)

	R_y-R_y	R_y-R_x	R_y-R_yR_z	R_y-R_xR_z
$\$_1$	(0, 1, 0; 0, 0, 0)	(0, 1, 0; 0, 0, 0)	(0, 1, 0; 0, 0, 0)	(0, 1, 0; 0, 0, 0)
$\$_2$	(sθ, 0, -cθ; 0, 0, 0)	(sθ, 0, -cθ; 0, 0, 0)	(sθ, 0, -cθ; 0, 0, 0)	(1, 0, 0; 0, 0, 0)
$\$_3$	(0, 0, 0; cθ, 0, sθ)	(0, 0, 0; cθ, 0, sθ)	(0, 0, 0; cθ, 0, sθ)	(0, 0, 0; 0, 0, 1)
$\$_4$	(sθ, 0, -cθ; 0, *l*, 0)	(0, 1, 0; -*l*sθ, *0*, *l*cθ)	(0, 1, 0; -*l*sθ, 0, *l*cθ)	(1, 0, 0; 0, *l*, 0)
$\$_5$	(0, 1, 0; -*l*sθ, 0, *l*cθ)	(1, 0, 0; 0, *l*sθ, 0)	(0, 0, 1; 0, -*l*cθ, 0)	(0, 0, 1; 0, 0, 0)

4.1.1.2. Screws of R_x Type Limbs

As seen in Figure 4.4, the R_{i1} joint axes of the R_x type limbs are along the x-axis of the LCS on the base. For this reason, as seen in Table 4.2, the primary parts of the first screws of the R_x type limbs are the unit vector along the x-axis. For the second screws, R_{i2} joint axes of the R_x-R_y, R_x-R_x, R_x-R_yR_z and R_x-R_xR_z limbs are along the y-axis of the LCS on the base in the initial configuration of the PM, so the primary part of screws are the unit vector along the y-axis. The third screws of the R_y type limbs are the same as the third screws of the R_x type limbs. For the R_x-R_y limb, the primary part of the fourth screw is identical to the second screw of the R_y-R_y limb. The fourth screws for R_x-R_x and R_x-R_yR_z limbs are identical to each other and the primary parts are the same as the second screws. For the R_x-R_xR_z limb, the primary part of the fourth screw is unit vector along the x-axis in the initial configuration of the PM. The primary part of the fifth screw of R_x-R_y is unit vector along the y-axis in the initial configuration of the PM. The primary part of the fifth screw of the R_y-R_x limb is unit vector along the x-axis in the initial configuration of the PM.

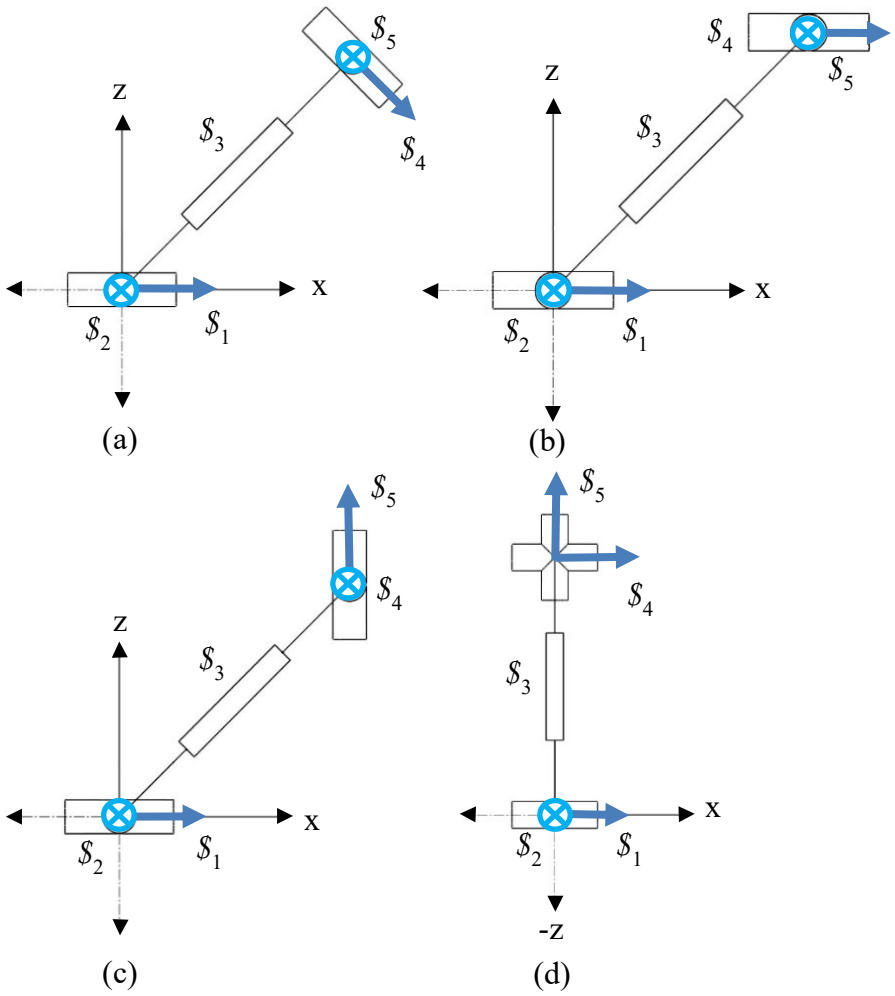

Figure 4.4. Screws of R_x Type Limbs (a) R_x-R_y, (b) R_x-R_x, (c) R_x-R_yR_z, (d) R_x-R_xR_z

For the R_x-R_yR_z and R_x-R_xR_z, R_{i5} limbs the primary part of the fifth screw are unit vector along the z-axis. The screws of R_x type limbs are given in Table 4.2 in detail.

Table 4.2. Screws of R_x Type Limbs (R_x-R_y, R_x-R_x, R_x-R_yR_z, R_x-R_xR_z)

$\$_i$	R_x-R_y	R_x-R_x	R_x-R_yR_z	R_x-R_xR_z
$\$_1$	(1, 0, 0; 0, 0, 0)	(1, 0, 0; 0, 0, 0)	(1, 0, 0; 0, 0, 0)	(1, 0, 0; 0, 0, 0)
$\$_2$	(0, 1, 0; 0, 0, 0)	(0, 1, 0; 0, 0, 0)	(0, 1, 0; 0, 0, 0)	(0, 1, 0; 0, 0, 0)
$\$_3$	(0, 0, 0; cθ, 0, sθ)	(0, 0, 0; cθ, 0, sθ)	(0, 0, 0; cθ, 0, sθ)	(0, 0, 0; 0, 0, 1)
$\$_4$	(sθ, 0, -cθ; 0, *l*, 0)	(0, 1, 0; -*l*sθ, *0*, *l*cθ)	(0, 1, 0; -*l*sθ, 0, *l*cθ)	(1, 0, 0; 0, *l*, 0)
$\$_5$	(0, 1, 0; -*l*sθ, 0, *l*cθ)	(1, 0, 0; 0, *l*sθ, 0)	(0, 0, 1; 0, -*l*cθ, 0)	(0, 0, 1; 0, 0, 0)

4.1.1.3. Screws of R_zR_y Type Limbs

As seen in Figure 4.5, the R_{i1} joint axes of the R_zR_y type limbs are along the z-axis of the LCS on the base. For this reason, as seen in Table 4.3, the first screws of the R_zR_y type limbs are the unit vector along the z-axis. For the second screws, R_{i2} joint axes of the R_zR_y-R_y, R_zR_y-R_x, R_zR_y-R_yR_z and R_zR_y-R_xR_z limbs are along the y-axis of the LCS on the base in the initial configuration of the PM and the the primary part of screws are the unit vector along the y-axis. The third screws of the R_zR_y type limbs are the same as the third screws of the R_x type limbs.

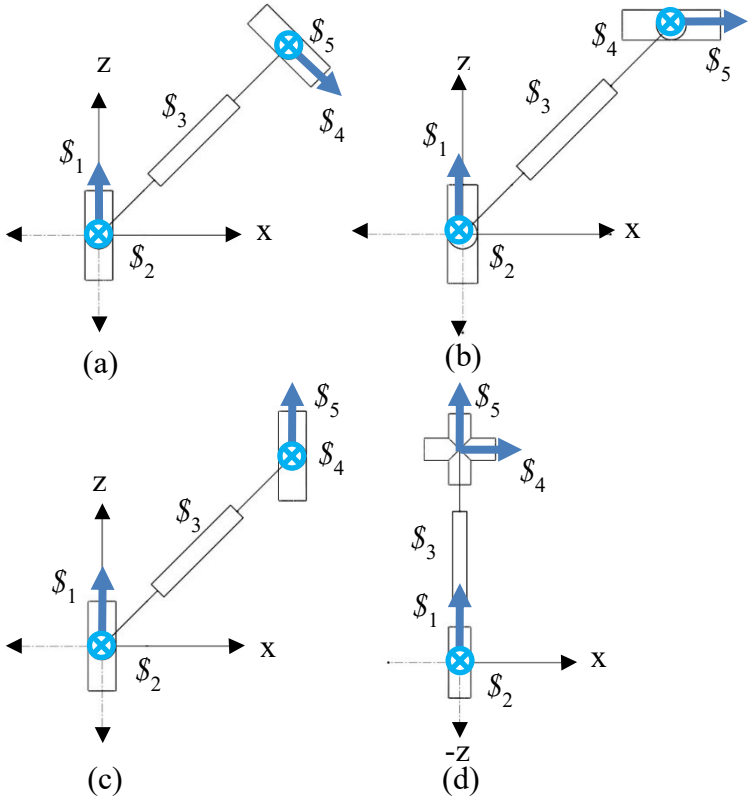

Figure 4.5. Screws of R_zR_y Type Limbs (a) R_zR_y-R_y, (b) R_zR_y-R_x, (c) R_zR_y-R_yR_z, (d) R_zR_y-R_xR_z

For R_zR_y-R_y limb, the primary part of the fourth screw is identical to the second screw of R_y-R_y limb. The fourth screws for R_zR_y-R_x and R_zR_y-R_yR_z limbs are identical to each other and the primary parts are the same as the second screws. For the R_zR_y-R_xR_z limb, the primary part of the fourth screw is unit vector along the x-axis in the initial

configuration of the PM. R_{i5} joint axis of the R_zR_y-R_y limb is parallel to the y-axis of LCS and the primary part of the fifth screw of the R_zR_y-R_y limb is unit vector along the y-axis in the initial configuration of the PM. R_{i5} joint axis of the R_zR_y-R_x limb is parallel to the x-axis of LCS and the primary part of the fifth screw of the R_zR_y-R_x limb is unit vector along the x-axis in the initial configuration of the PM. For the R_zR_y-R_yR_z and R_zR_y-R_xR_z limbs, the primary part of the fifth screw are unit vector along the z-axis. The screws of R_zR_y type limbs are given in Table 4.3 in detail.

Table 4.3. Screws of R_zR_y Type Limbs R_zR_y-R_y, R_zR_y-R_x, R_zR_y-R_yR_z, R_zR_y-R_xR_z

$\$_i$	R_zR_y-R_y	R_zR_y-R_x	R_zR_y-R_yR_z	R_zR_y-R_xR_z
$\$_1$	(0, 0, 1; 0, 0, 0)	(0, 0, 1; 0, 0, 0)	(0, 0, 1; 0, 0, 0)	(0, 0, 1; 0, 0, 0)
$\$_2$	(0, 1, 0; 0, 0, 0)	(0, 1, 0; 0, 0, 0)	(0, 1, 0; 0, 0, 0)	(0, 1, 0; 0, 0, 0)
$\$_3$	(0, 0, 0; cθ, 0, sθ)	(0, 0, 0; cθ, 0, sθ)	(0, 0, 0; cθ, 0, sθ)	(0, 0, 0; 0, 0, 1)
$\$_4$	(sθ, 0, -cθ; 0, *l*, 0)	(0, 1, 0; -*l*sθ, *0*, *l*cθ)	(0, 1, 0; -*l*sθ, 0, *l*cθ)	(1, 0, 0; 0, *l*, 0)
$\$_5$	(0, 1, 0; -*l*sθ, 0, *l*cθ)	(1, 0, 0; 0, *l*sθ, 0)	(0, 0, 1; 0, -*l*cθ, 0)	(0, 0, 1; 0, 0, 0)

4.1.1.4. Screws of R_zR_x Type Limb

As seen in Figure 4.6, the R_{i1} joint axes of the R_zR_x type limbs are along the z-axis of the LCS on the base. For this reason, as seen in Table 4.4, the first screws of the R_zR_x type limbs are the unit vector along the z-axis. For R_{i2} joint axes of the R_zR_x-R_y, R_zR_x-R_x, R_zR_x-R_yR_z and R_zR_x-R_xR_z limbs the primary part of screws are the unit vector along the x-axis. For the third screws of R_zR_x type limbs, R_{i3} joint axes has to be positioned along the z-axis of the LCS on the base in the initial configuration of the PM.

For R_zR_x-R_y and R_zR_x-R_xR_z limbs, the primary part of the fourth screw is identical to the second screw of R_zR_x type limbs. The fourth screws for R_zR_x-R_x and R_zR_x-R_yR_z limbs are identical to each other and the primary parts are the unit vector along the y-axis. The primary part of the fifth screw of R_zR_x-R_y is unit vector along the y-axis in the initial configuration of the PM. The fifth screw of R_zR_x-R_x is unit vector along the x-axis in the initial configuration of the PM.

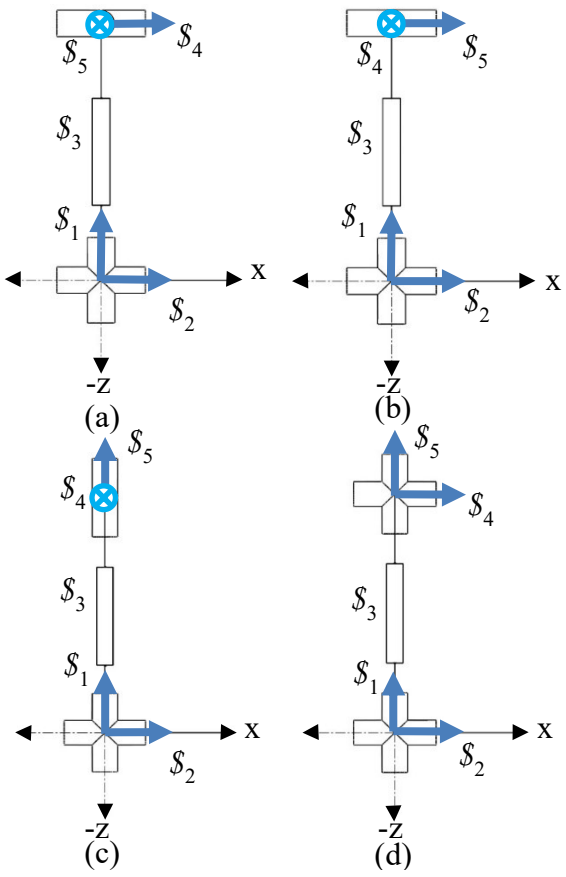

Figure 4.6. Screws of R_zR_x Type Limbs (a) R_zR_x-R_y, (b) R_zR_x-R_x, (c) R_zR_x-R_yR_z, (d) R_zR_x-R_xR_z

For the R_zR_x-R_yR_z and R_zR_x-R_xR_z limbs, the primary part of the fifth screw of R_zR_x-R_yR_z and R_zR_x-R_xR_z are unit vector along the z-axis. The screws of R_zR_x type limbs are given in Table 4.4 in detail.

Table 4.4. Screws of R_zR_x Type Limbs R_zR_x-R_y, R_zR_x-R_x, R_zR_x-R_yR_z, R_zR_x-R_xR_z

$\$_i$	R_zR_x-R_y	R_zR_x-R_x	R_zR_x-R_yR_z	R_zR_x-R_xR_z
$\$_1$	(0, 0, 1;0, 0, 0)	(0, 0, 1; 0, 0, 0)	(0, 0, 1; 0, 0, 0)	(0, 0, 1; 0, 0, 0)
$\$_2$	(1, 0, 0; 0, 0, 0)	(1, 0, 0; 0, 0, 0)	(1, 0, 0; 0, 0, 0)	(1, 0, 0; 0, 0, 0)
$\$_3$	(0, 0, 0; 0, 0, 1)	(0, 0, 0; 0, 0, 1)	(0, 0, 0; 0, 0, 1)	(0, 0, 0; 0, 0, 1)
$\$_4$	(1, 0, 0; 0, *l*, 0)	(0, 1, 0; -*l*, *0*, *0*)	(0, 1, 0; -*l*, 0, *0*)	(1, 0, 0; 0, *l*, 0)
$\$_5$	(0, 1, 0; -*l*, 0, *0*)	(1, 0, 0; 0, *l*, 0)	(0, 0, 1; 0, 0, 0)	(0, 0, 1; 0, 0, 0)

4.2. Reciprocal Screw Theory

Reciprocal screws can be obtained after the screw sets of the limbs are obtained. The mathematical relation for the reciprocal screw theory is as follows

$$\$^T \boldsymbol{\Delta}\, \$^r = \mathbf{0} \qquad (4.6)$$

where $\boldsymbol{\Delta} = \begin{pmatrix} \mathbf{0} & \mathbf{I} \\ \mathbf{I} & \mathbf{0} \end{pmatrix}$ with $\mathbf{0}$ being the 3×3 zero matrix and $\mathbf{I}$ being the 3×3 identity matrix, $\$^T$ is the transpose of the screw set and $\$^r$ is reciprocal screw of the screw set . The mathematical relation between a screw and a reciprocal screw is as follows

$$l_i \cdot p^r + m_i \cdot q^r + n_i \cdot r^r + p_i \cdot l^r + q_i \cdot m^r + r_i \cdot n^r = 0 \qquad (4.7)$$

For the 3-UPU PMs the reciprocal screw of a screw set consisting of five screws is found as follows

$$\begin{pmatrix} p_1 & q_1 & r_1 & l_1 & m_1 & n_1 \\ p_2 & q_2 & r_2 & l_2 & m_2 & n_2 \\ p_3 & q_3 & r_3 & l_3 & m_3 & n_3 \\ p_4 & q_4 & r_4 & l_4 & m_4 & n_4 \\ p_5 & q_5 & r_5 & l_5 & m_5 & n_5 \end{pmatrix} \begin{pmatrix} l^r \\ m^r \\ n^r \\ p^r \\ q^r \\ r^r \end{pmatrix} = \begin{pmatrix} 0 \\ 0 \\ 0 \\ 0 \\ 0 \\ 0 \end{pmatrix} \qquad (4.8)$$

However, this method attempts to find out five unknowns from six equations. Although it can be solved with linear algebra methods, Dai and Jones (2003) has developed a more practical equation to solve reciprocal of five screw system. With the method they have developed, researchers find the reciprocal screw that takes the determinant of the 5×5 sub-matrices of a 5×6 matrix. The sub-matrices $\mathbf{A}_i$ are determined

by removing the i^{th} column of the 5×6 matrix. By this way, the reciprocal screw is found as follows

$$\$^{r} = (|\mathbf{A}_4|, -|\mathbf{A}_5|, |\mathbf{A}_6|, -|\mathbf{A}_1|, |\mathbf{A}_2|, -|\mathbf{A}_3|) \tag{4.9}$$

In the next Chapter, instantaneous mobility analysis of the PMs is performed using the screws of limb types.

CHAPTER 5

INSTANTANEOUS MOBILITY ANALYSIS OF 3-UPU PMS

When a PM is to be designed, first the DoF of the manipulator should be determined. Several studies have been conducted for the mobility analysis of mechanisms. The most commonly used formula is the Chebychev–Grübler–Kutzbach formula (Söylemez, 2017). The formula used for spatial mechanisms is as follows

$$M = 6(n - j - 1) + \sum_{i=1}^{j} f_i \tag{5.1}$$

where n is the number of links; j is the number of joints and f_i is DoF of the i^{th} joint. Not all spatial mechanisms obey this formula and such mechanisms are called over-constraint spatial mechanisms. There are several methods developed to determine the correct DoF of over-constrained mechanisms. One of these methods make use of screw theory. Zhao et al. (2004) used screw theory to detect 3-UPU architectures with R_x-R_x limbs which result in over-constrained mechanisms by changing the inclination of the limbs in the initial configuration of the PM. With this method it is also possible to determine the motion screws of the moving platform.

5.1. Instantaneous Mobility Analysis of Generated 3-UPU PMs

In order to determine the instantaneous mobility of the PMs, the screw coordinates of each limb of the PM must first be determined. For a 3-UPU PM, each limb has a five screw system. The reciprocal screws of the screws for each limb are then defined by Eq. (4.9). In general three reciprocal screws are obtained for the 3-UPU PM. These screw sets are defined as

$$\$^{r} = \begin{pmatrix} \$_1^r \\ \$_2^r \\ \$_3^r \end{pmatrix} \tag{5.2}$$

Each of these screws represents a motion constraint on the platform. Then the set of reciprocal screws are analyzed by singular value decomposition:

$$\$^{r} = \mathbf{USV}^{T} \tag{5.3}$$

where **U** denotes an m × m orthogonal matrix, **V** denotes an n × n orthogonal matrix and **S** denotes an m × n diagonal matrix. The rows of $\mathbf{V}^T$ corresponding to the zero singular values form an orthonomal basis of the null space of $\$^r$ and the remaining rows of $\mathbf{V}^T$ form an orthonomal basis of the orthogonal complement. Therefore, the dimension of the constraint space of the PM is given by

$$d = \text{Rank}\ (\$^{r}) \tag{5.4}$$

and the DoF of the PM is given by

$$M = 6 - d \tag{5.5}$$

In the $\mathbf{V}^T$ matrix, last "M" rows provide the motion characteristics of the PM.

General steps to follow to determine the DoF are as follows:

- The limbs of the PMs are examined individually in their respective LCSs. The screws of the limbs are obtained according to the LCSs.

- The reciprocal screws of each limb are determined. Normalization is done if necessary.
- The reciprocal screws created for each limb are placed in a single matrix.
- The set of reciprocal screws are analyzed by singular value decomposition to obtain the DoF and the motion characteristics of the PM

These mobility analyses were performed for all 256 TNV type PMs and 256 XYV type PMs. The motion patterns of all PMs are listed in Appendix A. As an illustration of the procedure, the mobility analysis of a U_N^T - U_N^T PM is presented here. The base and moving platform joint layouts of the U_N^T - U_N^T PM are given in Figure 5.1. R_{i1} and R_{i5} joint axes of the first limb are parallel to the x-axis of the LCS, whereas R_{i1} and R_{i5} joint axes of the second and third limbs are parallel to the y-axis of the LCSs.

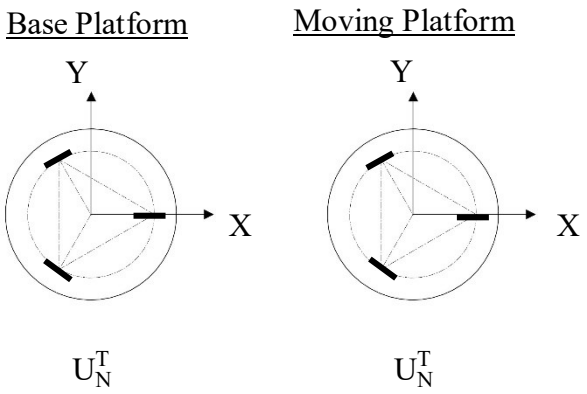

Figure 5.1. Joint Layouts of U_N^T - U_N^T

As can be seen in Tables 3.2 and 3.3, limb type k_6 is used for the first limb, whereas limb type k_1 is used for the second and third limbs. The U joint centers on the platforms are located at equal distances to form equilateral triangles. In other words, there is 120° between consequtive x-axes of the LCSs.

As seen in Figure 5.2, the first limb of the PM is the R_x-R_x type. The second and third limbs are of R_y-R_y type. Using Table 4.2, the screw set for the first limb of the manipulator is found as follows

$$
\begin{aligned}
\$_{11} &= (1, 0, 0; 0, 0, 0) \\
\$_{12} &= (0, 1, 0; 0, 0, 0) \\
\$_{13} &= (0, 0, 0; c\theta_1, 0, s\theta_1) \\
\$_{14} &= (0, 1, 0; -l_1 s\theta_1, 0, l_1 c\theta_1) \\
\$_{15} &= (1, 0, 0; 0, l_1 s\theta_1, 0)
\end{aligned} \tag{5.7}
$$

Using the reciprocal screw theory, the reciprocal screw of the screw set of the first limb of PM is found as

$$
\$_1^r = (0, 0, 0; 0, 0, s\theta_1 l_1^2) \tag{5.8}
$$

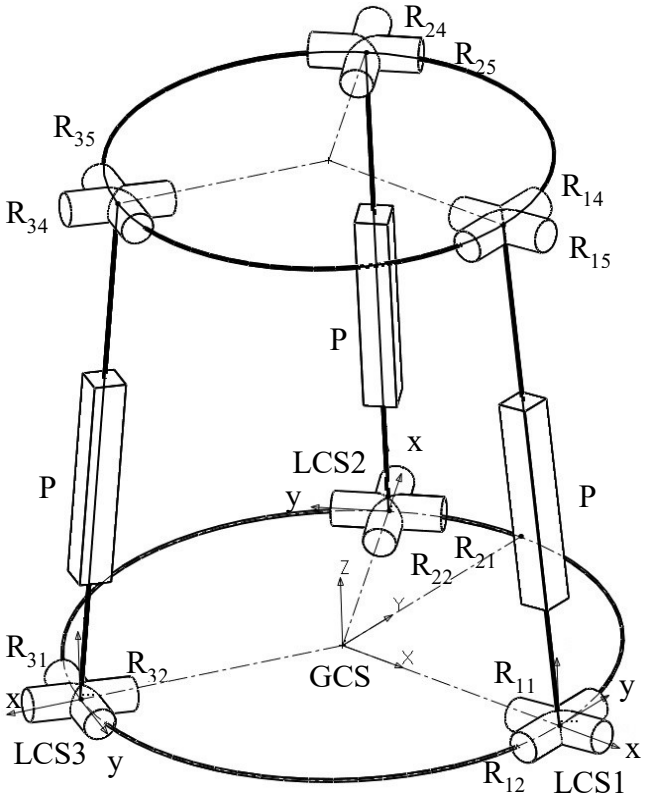

Figure 5.2. Kinematic scheme of U_N^T-U_N^T PM

Using Table 4.1, the screw set for the second and third limbs of the manipulator are found as

$$
\begin{aligned}
\$_{21} &= (0,\ 1,\ 0;\ 0,\ 0,\ 0)\\
\$_{22} &= (\ s\theta_2,\ 0,\ -\ c\theta_2;\ 0,\ 0,\ 0)\\
\$_{23} &= (0,\ 0,\ 0;\ c\theta_2,\ 0,\ s\theta_2)\\
\$_{24} &= (\ s\theta_2,\ 0,\ -\ c\theta_2;\ -0,\ l_2,\ 0)\\
\$_{25} &= (0,\ 1,\ 0;\ -l_2\, s\theta_2,\ 0,\ l_2\, c\theta_2)
\end{aligned}
\tag{5.9}
$$

$$
\begin{aligned}
\$_{31} &= (0,\ 1,\ 0;\ 0,\ 0,\ 0)\\
\$_{32} &= (\ s\theta_3,\ 0,\ -\ c\theta_3;\ 0,\ 0,\ 0)\\
\$_{33} &= (0,\ 0,\ 0;\ c\theta_3,\ 0,\ s\theta_3)\\
\$_{34} &= (\ s\theta_3,\ 0,\ -\ c\theta_3;\ 0,\ l_3,\ 0)\\
\$_{35} &= (0,\ 1,\ 0;\ -l_3\, s\theta_3,\ 0,\ l_3\, c\theta_3)
\end{aligned}
\tag{5.10}
$$

Using the reciprocal screw theory, the reciprocal screws of the screw set of the second and third limbs of PM was found as

$$\$_2^r = (0,\ 0,\ 0;\ c\theta_2\, l_2^2,\ 0,\ s\theta_2\, l_2^2) \tag{5.11}$$

$$\$_3^r = (0,\ 0,\ 0;\ c\theta_3\, l_3^2,\ 0,\ s\theta_3\, l_3^2) \tag{5.12}$$

The normalized reciprocal screws of the limbs according to the axes of the LCS are as follows.

$$\$_1^r = (0,\ 0,\ 0;\ 0,\ 0,\ 1) \tag{5.13}$$

$$\$_2^r = (0,\ 0,\ 0;\ c\theta_2,\ 0,\ s\theta_2) \tag{5.14}$$

$$\$_3^r = (0,\ 0,\ 0;\ c\theta_3,\ 0,\ s\theta_3) \tag{5.15}$$

In order to calculate the mobility of the PM, reciprocal screws calculated according to the LCS must be transformed into the GCS. For this, the transformation matrices suggested by Wang et al. (2015) are used. The formulation is as follows

$$\$^{r}_{global} = \begin{pmatrix} \mathbf{s}^{r}_{global} \\ \mathbf{s}_{0}{}^{r}_{global} \end{pmatrix} = \begin{pmatrix} \mathbf{R} & \mathbf{0} \\ \mathbf{-R.T} & \mathbf{R} \end{pmatrix} \begin{pmatrix} \mathbf{s}^{r}_{local} \\ \mathbf{s}_{0}{}^{r}_{local} \end{pmatrix} \tag{5.16}$$

where **R** is rotation matrix around z-axis of GCS:

$$\mathbf{R} = \begin{pmatrix} c\alpha_i & -s\alpha_i & 0 \\ s\alpha_i & c\alpha_i & 0 \\ 0 & 0 & 1 \end{pmatrix} \tag{5.17}$$

and **T** is translation vector:

$$\mathbf{T} = (rc\gamma_i, rs\gamma_i, 0)^T \tag{5.18}$$

α and γ angles for U_N^T - U_N^T are as follows

$$\begin{aligned} \alpha_1 &= \pi & \gamma_1 &= 0 \\ \alpha_2 &= \frac{5\pi}{3} & \gamma_2 &= \frac{2\pi}{3} \\ \alpha_3 &= -\frac{5\pi}{3} & \gamma_3 &= \frac{4\pi}{3} \end{aligned} \tag{5.19}$$

After applying the transformation procedure, the values of the reciprocal screws created for each limb according to GCS are as follows

$$\begin{aligned} \$^{r}_{G1} &= (0, 0, 0; 0, 0, 1) \\ \$^{r}_{G2} &= (0, 0, 0; \tfrac{1}{2}c\theta_2, \tfrac{-\sqrt{3}}{2}c\theta_2, s\theta_2) \\ \$^{r}_{G3} &= (0, 0, 0; \tfrac{1}{2}c\theta_3, \tfrac{\sqrt{3}}{2}c\theta_3, s\theta_3) \end{aligned} \tag{5.20}$$

Since the generated global reciprocal screws have only variables on the translational side, the singularities can be found by taking the determinant of the translational side of the matrix. The determinant of the translational side is as follows

$$\begin{vmatrix} 0 & 0 & 1 \\ \frac{1}{2}\,c\theta_2 & \frac{-\sqrt{3}}{2}\,c\theta_2 & s\theta_2 \\ \frac{1}{2}\,c\theta_3 & \frac{\sqrt{3}}{2}c\theta_3 & s\theta_3 \end{vmatrix} = \frac{\sqrt{3}}{2}\,c\theta_2\,c\theta_3 \tag{5.21}$$

The conditions that make the determinant of the K matrix zero are the singular points of the PM. The singular architectures of the PM are obtained for $\theta_2 = \theta_3 = 90°$. That is, if the limbs are inclined with 90° in the initial configuration of the PM, the DoF of the PM is more than 3. When the limb angles of the PM is between 0° and 90°, the reciprocal screw matrix has rank = 3, hence the DoF of the PM is 3. The motion characteristics of the PM are found by looking at the last 3 rows of the $\mathbf{V}^T$ matrix obtained by singular value decomposition of the matrix:

$$V_\theta^T = \begin{pmatrix} 0 & 0 & 0 & 0 & 0 & 1 \\ 0 & 0 & 0 & 0 & 1 & 0 \\ 0 & 0 & 0 & 1 & 0 & 0 \end{pmatrix} \tag{5.22}$$

As seen in Eq. 5.22, the manipulator has 3 translational DoF. The motion pattern is illustrated in Figure 5.3.

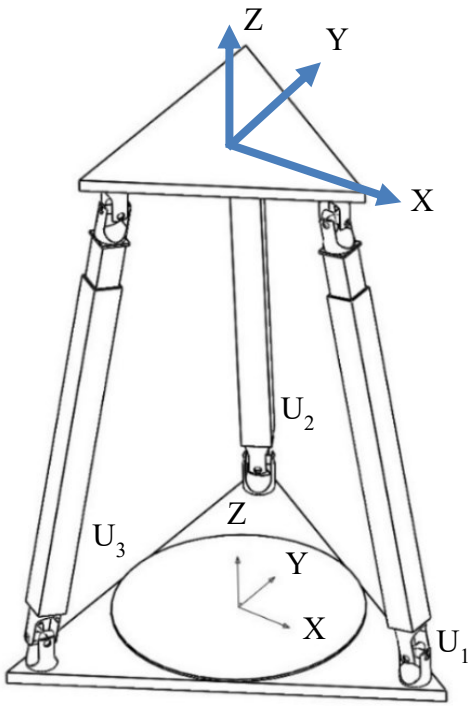

Figure 5.3. Singularity case of U_N^T-U_N^T PM when $\theta = 0°\sim90°$

All these mobility analyses formulations are implemented and computations are performed in Wolfram Mathematica. The mobility results are validated using the Motion module of Solidworks. Figure 5.4 shows the result of Solidworks Motion analysis for $\theta = 0°\sim90°$ degrees. As can be seen, the mobility analysis results are the same.

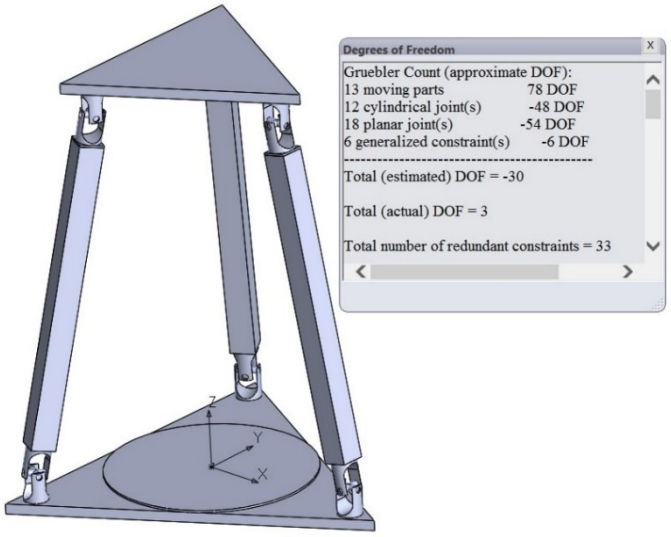

Figure 5.4. Result of Solidworks Motion analysis of U_N^T-U_N^T PM when $\theta = 0°\sim90°$

When the limbs angles of the PM is 90° in the initial configuration, the reciprocal screws are as follows

$$\begin{aligned} \$_{G1}^{r} &= (0, 0, 0; 0, 0, 1) \\ \$_{G2}^{r} &= (0, 0, 0; 0, 0, 1) \\ \$_{G3}^{r} &= (0, 0, 0; 0, 0, 1) \end{aligned} \tag{5.23}$$

Since the matrix of these three reciprocal screw set's rank is 1, there is only one constraint in the DoF of the PM. That is, the degree of freedom of PM is 5. The motion characteristics of the PM are found by looking at the last 5 rows of the $\mathbf{V}^T$ matrix obtained by singular value decomposition of the matrix which is formed by these three reciprocal

screw sets. The last 5 rows of the $\mathbf{V}^T$ matrix are as follows

$$V_{90^\circ}^T = \begin{pmatrix} 0 & 1 & 0 & 0 & 0 & 0 \\ 1 & 0 & 0 & 0 & 0 & 0 \\ 0 & 0 & 0 & 0 & 0 & 1 \\ 0 & 0 & 0 & 0 & 1 & 0 \\ 0 & 0 & 0 & 1 & 0 & 0 \end{pmatrix} \tag{5.24}$$

As seen in Eq. 5.24, the manipulator has 5 DoF and has translational motion along the X-, Y-, and Z-axes and it can rotate about the X- and Y-axes of the GCS. The motion pattern is illustrated in Figure 5.5.

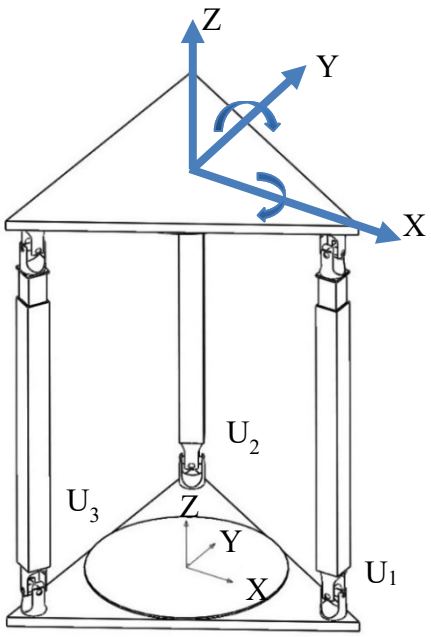

Figure 5.5. Singular architecture of U_N^T-U_N^T PM when $\theta = 90^\circ$

Figure 5.6 shows a snapshot of a Solidworks Motion analysis for an example.

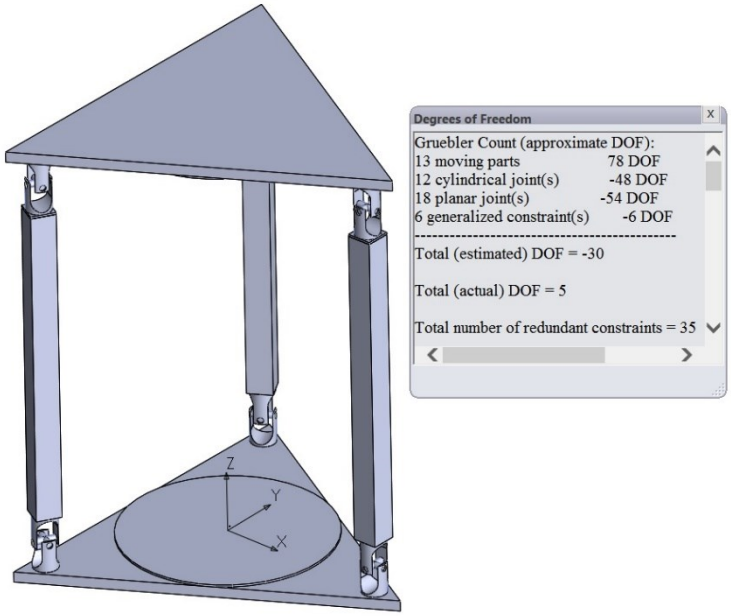

Figure 5.6. Result of Solidworks Motion analysis of U_N^T-U_N^T PM when $\theta = 90°$ in parallel mode

For the XYV type PMs, the limbs are along the z-axes of the LCSs, i.e. $\theta = 90°$, in the initial configuration of the PM. The mobility results for all classified PMs are presented in detail in Appendix A. Tables A.1-to-A10 list the PMs for which non-identical platforms are permissible. In these tables, the instantaneous mobility of the PMs may change according to whether the angles of the limbs are $\theta = 0°$ or $0° < \theta < 90°$ at the initial configuration of the PM. The rotation DoFs of the platform about the x-, y- and z-axes are respectively represented by R_x, R_y, R_z, whereas the translation DoFs are denoted by T_x, T_y, T_z. When a twist involves more than one nonzero element in its six coordinates, it means that the twist represents a single-DoF motion with multiple rotation and/or translation components about/along different axis. Such motions are termed as parasitic motions. In the tables in Appendix A, the parasitic motions are represented in parenthesis. Each pair of parenthesis represents a single-DoF twist. For example (R_zT_y) means a twist with coordinates (0 0 a; 0 b 0) with some nonzero, but coupled elements for R_z and T_y motions. The remaining tables starting from Table A.10 consist only of PMs with identical base and moving platforms, and hence $\theta = 90°$.

It should be noted that the results obtained provide the instantaneous mobility of the PMs in the initial configuration. The studies do not reflect the finite mobility

information. A more through kinematic analysis should be performed in order to reveal the finite mobility characteristics of a specific PM. Raw motion analysis can be performed to check the finite mobility characteristics of the PMs using the Motion module of Solidworks (Gezgin, 2006). As an example, for the U_N^T-U_N^T PM with $\theta = 0°\sim90°$ case with non-identical base and moving platforms, the moving platform has 3-DoF with $T_xT_yT_z$ type motion (Table A.8). When raw motion analysis is performed with random inputs for the three prismatic joints, it is seen that the orientation of the moving platform does not change (Figure 5.7). Therefore, the moving platform has 3 translational finite DoF, i.e. the PM is a TPM.

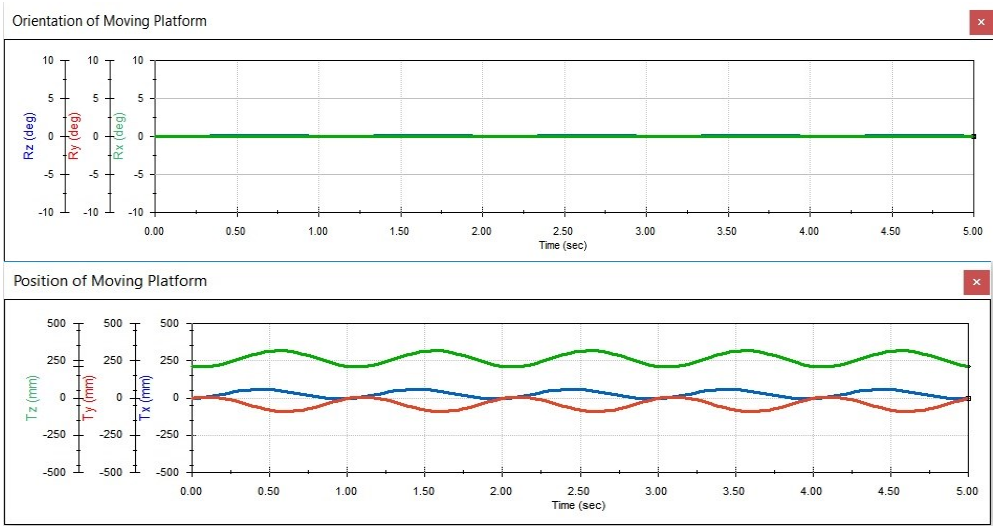

Figure 5.7. Orientation and Position of Moving Platform of U_N^T-U_N^T PM when $\theta = 0°\sim90°$

For the $\theta = 90°$ case, the instantaneous mobility of the PM in its initial configuration is found to be 5 with $R_xR_yT_xT_yT_z$ type motion in Table A.11. When the moving platform of the Solidworks model of the PM is manually moved, it is seen that as oppose to the $\theta = 0°\sim90°$ case, the PM is not a TPM anymore for the $\theta = 90°$ case. The raw motion analysis in Solidwors is started from a generic configuration where the moving platform is not parallel to the base platform (Figure 5.8). At this configuration, Solidworks evaluates the instantaneous DoF as 3 as depicted in Figure 5.8.

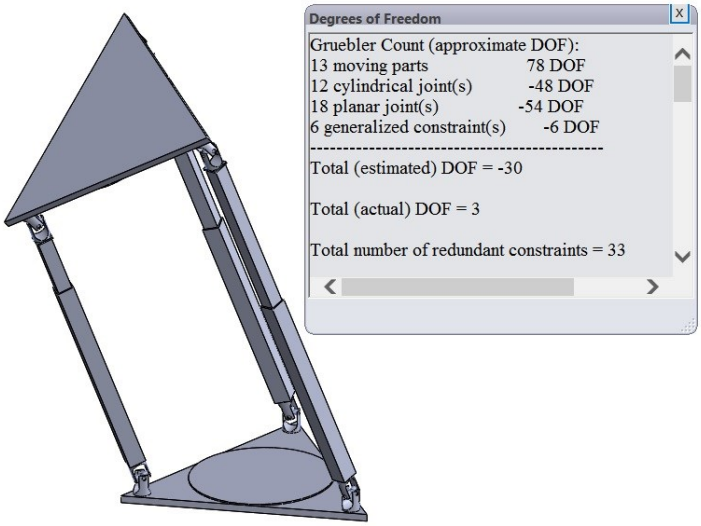

Figure 5.8. The starting configuration for the Solidworks Motion analysis of U_N^T-U_N^T PM when $\theta = 90°$

Raw motion analysis is performed in Solidworks Motion with random inputs for the three prismatic joints, it is seen that both of the orientation and position of the moving platform changes (Figure 5.9). Although the moving platform has 3 DoF, all translational and rotational motions are observed due to the parasitic motions.

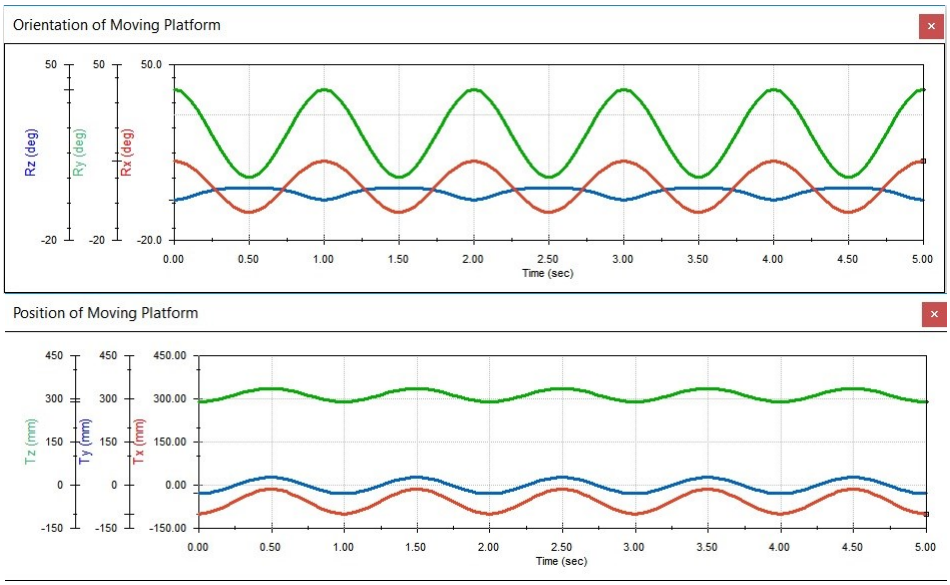

Figure 5.9. Orientation and Position of Moving Platform of U_N^T-U_N^T PM when $\theta = 90°$ in non-parallel mode

The mobility characteristics of the 3-UPU PMs existing in the literature are verified in this study. Tsai 3-UPU PM (Tsai, 1996) it the U^{T}-U^{T} PM in Table A.8, the SNU 3-UPU PM (Han et al., 2002) is the U^{N}-U^{N} PM in Table A.5, the Parallel 3-UPU PMs (Yu et al., 2009) are the U^{X}-U^{X} and U^{Y}-U^{Y} PMs in Table A.18, the Vertical 3-UPU PMs (Huang & Li, 2002) are the U^{VT}-U^{VT} in Table A.6, Zhao's (2005) 3-UPU PM is the U^{N}-U^{VT} PM in Table A.8, Lu's (2006) 3-UPU PM is the U_{N}^{VT}-U_{N}^{VT} PM in Table A.8, Hu's (2011) 3-UPU PM is the U^{VT}-U^{N} PM in Table A.10 and Chebbi's (2013) 3-UPU PMs are the U_{Y}^{X}-U_{X}^{Y} in Tables A.18 and U_{VT}^{T}-U_{VT}^{T} PMs in Tables A.8.

Among the classified 3-UPU PMs, the 3-DoF PMs with non-parasitic motion may be considered to be valuable in applications. The DoF values in the tables in the Appendix A are instantaneous DoF values, however, if the instantaneous DoF is 3, it can be deduced that the finite DoF is also 3. The same conclusion cannot be drawn for the PMs with more than 3-DoF. Also, the instantaneous DoF being 3 is a necessary, but not sufficient condition to conclude that the finite DoF is 3.

The non-parasitic TPMs are only listed in Tables A.11 and A.16 and all these PMs are TNV type PMs. Besides the Tsai 3-UPU PM (Tsai, 1996) there are 6 types of novel TPMs: U_{VT}^{T}-U_{VT}^{T}, U_{T}^{VT}-U_{T}^{VT} with $0° < \theta < 90°$, U_{N}^{T}-U_{N}^{T}, U_{N}^{VT}-U_{N}^{VT} with $0° \leq \theta < 90°$ and U_{N}^{T}-U_{N}^{VT}, U_{N}^{VT}-U_{N}^{T} with $\theta = 0°$. Non-parasitic 3-DoF PMs with 1 rotational and 2 translation DoF are listed in Table A.23 with $R_xT_yT_z$ or $R_yT_xT_z$ type motion. All such PMs are XYV type PMs and there are 46 many of them. Non-parasitic 3-DoF PMs with 2 rotational and 1 translational (2R1T) DoF are listed in Tables A.5, A.11, A.16, A.23. Among the PMs listed in these tables, the PMs with $R_xR_zT_z$ motion in Table A.5 are different from the others, because the PMs with $R_xR_zT_z$ motion has both rotational and translational DoF about the z-axis. There are 6 such novel PMs: U_{VN}^{T}- U^{VN}, U_{VN}^{T}-U_{T}^{VN}, U_{VN}^{T}-U_{N}^{VN}, U_{VN}^{N}-U^{VN}, U_{VN}^{N}-U_{T}^{VN}, U_{VN}^{N}-U_{N}^{VN} with $\theta = 90°$. The other PMs with 2R1T motion have $R_xR_yT_z$ type motion. Besides Zhao's (2005) U^{N}-U^{VT} PM there are 40 such novel PMs. Totally, 118 new 3-DoF non-parasitic 3-UPU PMs are found in this study.

CHAPTER 6

CONCLUSION

In this study, different 3-UPU parallel manipulator architectures are classified and their mobility characteristics are investigated. First, the topologies of the 3-UPU PMs available in the literature are examined and possible orientations of the U joint axes are determined. Various joint layouts are determined in accordance with the results obtained. Then, the joint layouts for the base and the moving platform are matched with each other. When these 3-UPU PM architectures are examined, it is found that they have similar limb structures. All these studies are performed based on several assumptions listed in Section 3.3. These limbs are numerated and the kinematic properties of the limbs are examined with screw theory. The reciprocal screws of the limbs are worked out in order to perform the instantaneous mobility analysis of PMs in their initial configurations. The results of the instantaneous mobility analysis are tabulated in order to give an insight into the future work of researchers. Also, the finite mobility analysis of one the PMs is performed using Solidworks Motion as an example.

Among the classified PMs, 118 many of them are novel 3-DoF non-parasitic 3-UPU PMs: 6 TPMs, 46 PMs with 1 rotational and 2 translational DoF, 6 PMs with $R_xR_zT_z$ and 40 PMs with $R_xR_yT_z$ type motion.

REFERENCES

3D printer list. (2017, March 17). Retrieved from 3D printer list WEB Site: http://sites.google.com/site/3dprinterlist/delta-3d-printers/parallel-kinetics

ABB Robotics. (2017, March 17). Retrieved from ABB Robotics WEB Site: http://new.abb.com

Aboulissane, B., & El Bakkali, l. (2015). Modeling and Simulation of Spatial Mechanism. *Xème Conférence Internationale : Conception et Production Intégrées.* Tanger, Morocco.

Badescu, M., & Mavroidis, C. (2004). Workspace Optimization of 3-Legged UPU and UPS Parallel Platforms With Joint Constraints. *ASME. J. Mech. Des., 126*(2), 291-300.

Bałchanowski, J. (2014). Some aspects of topology and kinematics of a 3DOF translational parallel mechanism. *International Journal of Applied Mechanics and Engineering, 19*(1), 5-15.

Ball, R. (1900). *Treatise on the theory of screws.* Cambridge: Cambridge University Press.

Bhutani, G., & Dwarakanath, T. (2014). Novel design solution to high precision 3 axes translational parallel mechanism. *Mechanism and Machine Theory, 75*, 118-130.

Bi, J., & Wen, R. (2010). Errors Analysis of 3-UPU Parallel Manipulator Using Screw Theory. *International Conference on Measuring Technology and Mechatronics Automation*, (pp. 137-140). Changsha City.

Binbin, P., Zengming, L., Kai, W., & Yu, S. (2011). Kinematic Characteristics of 3-UPU Parallel Manipulator in Singularity and Its Application. *International Journal of Advanced Robotic Systems, 8*(4), 54-64.

Bonev, I., & Zlatanov, D. (2001). *The Mystery of the Singular SNU Translational Parallel Robot.* Retrieved from parallemic.org: https://www.parallemic.org/Reviews/Review004.html

Chebbi, A., & Parenti-Castelli, V. (2010). Potential of the 3-UPU Translational Parallel Manipulator. In I. D. Conference (Ed.), *34th Annual Mechanisms and Robotics Conference. 2*, pp. 1089-1099. ASME.

Chebbi, A., Affi , Z., & Romdhane, L. (2013). Modelling and analysis of the 3-UPU spherical manipulator. *European Journal of Computational Mechanics, 22*(2-4), 157-169.

Chebbi, A., Affi, Z., & Romdhane, L. (2009). Prediction of the pose errors produced by joints clearance for a 3-UPU parallel robot. *Mechanism and Machine Theory, 44*(9), 1768-1783.

Chen, Z., Zhang, Y., Huang, K., Ding, H., & Huang, Z. (2015). Mobility and Motion Analysis of a Special 3-UPU Parallel Mechanism. *The 14th IFToMM World Congress.* Taipei, Taiwan.

Clavel, R. (1988). Delta, a fast robot with parallel geometry. *18th International Symposium on Industrial Robots*, (pp. 91-100).

Dai, J., & Jones, J. (2003). A Linear Algebraic Procedure in Obtaining Reciprocal Screw Systems. *J. Robotic Syst., 20*, 401–412.

Dehkordi, M., Frisoli, A., Sotgiu, E., & Bergamasco, M. (2012). Modelling and Experimental Evaluation of a Static Balancing Technique for a new Horizontally Mounted 3-UPU Parallel Mechanism. *International Journal of Advanced Robotic Systems* .

Di Gregorio, R. (2003, March). Kinematics of the 3-UPU wrist. *Mechanism and Machine Theory, 38*(3), 253-263.

Di Gregorio, R. (2004). Statics and singularity loci of the 3-UPU wrist. *IEEE Transactions on Robotics*, *20*, pp. 630-635.

Di Gregorio, R. (2006). Parallel Manipulators with Lower Mobility. In S. Cubero, *Industrial Robotics: Theory, Modelling and Control* (pp. 557-572).

Di Gregorio, R., & Parenti-Castelli, V. (2002). Mobility Analysis of the 3-UPU Parallel Mechanism Assembled for a Pure Translational Motion. *ASME. J. Mech. Des.* , 259-264.

Di Gregorio, R., & Parenti-Castelli, V. (2006b). A New Approach for the evaluation of kinematic and static performances of a family of 3-UPU translational manipulators. *Romansy 16. CISM Courses and Lectures, vol 487*, 47-54.

Dimentberg, F. (1965). *The Screw Calculus and Its Application to Mechanics.* Moscow: U.S. Department of Commerce, (N.T.I.S).

Gallardo-Alvarado, J. (2016). *Kinematic Analysis of Parallel Manipulators by Algebraic Screw Theory.* Celaya, Mexico: Springer International Publishing.

Gezgin, E. (2006). *Biokinematic Analysis Of Human Arm*. MSc thesis, İzmir Institute of Technology.

Gogu, G. (2008). Constraint Singularities and the Structural Parameters of Parallel Robots. *Advances in Robot Kinematics: Analysis and Design*, 21-28.

Guan, L.-W., Wang, J.-S., & Wang, L.-P. (2004). Mobility analysis of the 3-UPU parallel mechanism based on screw theory. *2004 International Conference on Intelligent Mechatronics and Automation* (pp. 309-314). Chengdu, China: IEEE.

Guo, S., Wang, N., Fang, Y., & Li, X. (2011). Study on error sensibility of UPU parallel manipulator based on probability distribution. *2011 IEEE International Conference on Mechatronics and Automation*, (pp. 2045-2050). Beijing.

Guohua, C., Bin, W., Nan, W., & Yanwei, Z. (2013). Stiffness, Workspace Analysis and Optimization for 3UPU Parallel Robot Mechanism. *Indonesian Journal of Electrical Engineering and Computer Science, 11*(9), 5253-5261.

Han, C., Kim, J., Kim, J., & Park, F. (2002). Kinematic sensitivity analysis of the 3-UPU parallel mechanism. *Mechanism and Machine Theory, 37*(8), 787-798.

Houghton Mifflin Company. (2004). *The American Heritage college dictionary.* Boston: Houghton Mifflin.

Hu, B., & Lu, Y. (2011). Solving stiffness and deformation of a 3-UPU parallel manipulator with one translation and two rotations. *Robotica, 29*(6), 815-822.

Huang, Z., & Li, Q. (2002). Construction and Kinematic Properties of 3-UPU Parallel Mechanisms. *International Design Engineering Technical Conferences and Computers and Information in Engineering Conference: 27th Biennial Mechanisms and Robotics Conference. 5*, pp. 1027-1033. Montreal, Quebec, Canada: ASME.

Huang, Z., Li, S., & Zuo, R. (2004). Feasible instantaneous motions and kinematic characteristics of a special 3-DOF 3-UPU parallel manipulator. *Mechanism and Machine Theory, 39*(9), 957-970.

Hunt, K. (1978). *Kinematic geometry of mechanisms.* Oxford: Oxford University Press.

Joshi, S., & Tsai, L. (2003). A comparison study of two 3-DOF parallel manipulators: one with three and the other with four supporting legs. *IEEE Transactions on Robotics and Automation, vol. 19, no. 2*, 200-209.

Joshi, S., & Tsai, L. W. (2002). Jacobian Analysis of Limited-DOF Parallel Manipulators. *ASME. J. Mech. Des.*, 254-258.

Kanaan, D., Wenger, P., & Chablat, D. (2008). Singularity Analysis of Limited-dof Parallel Manipulators using Grassmann-Cayley Algebra. *11th International Symposium on Advances in Robot Kinematics.* France: eprint arXiv.

Kanaan, D., Wenger, P., Caro, S., & Chablat, D. (2009). Singularity Analysis of Lower Mobility Parallel Manipulators Using Grassmann–Cayley Algebra. *IEEE Transactions on Robotics, 25*(5), 995-1004.

Karouia, M., & Hervé, J. (2000). A Three-dof Tripod for Generating Spherical Rotation. *Advances in Robot Kinematics*, 395-402.

Kiper, G., & Söylemez, E. (2011). Kinematic Analysis of a 3-UPU Parallel Manipulator Using Exponential Rotation Matrices. *15th National Conference on Machines and Mechanisms.* Chennai, India.

Laribi, M., Mlika, A., Romdhane, L., & Zeghloul, S. (2015). Geometric and Kinematic Performance Analysis and Comparison of Three Translational Parallel Manipulators. *The 14th IFToMM World Congress.* Taipei, Taiwan.

Li, S., & Huang, Z. (2005). Instantaneous Kinematic Characteristics of a Special 3-UPU Parallel Manipulator. *29th Mechanisms and Robotics Conference. 7*, pp. 691-697. ASME.

Li, S., Frisoli, A., Solazzi, M., & Bergamasco, M. (2010). Mechanical design and optimization of a novel fMRI compatible haptic manipulator. *19th International Symposium in Robot and Human Interactive Communication*, (pp. 1-6). Viareggio.

Liu, G., Lou, Y., & Li, Z. (2003, Aug.). Singularities of parallel manipulators: a geometric treatment. *IEEE Transactions on Robotics and Automation, 19*(4), 579-594.

Lu, Y., & Hu, B. (2006). Analysis of kinematics and solution of active/constrained forces of asymmetric 2UPU+X parallel manipulators. *Proceedings of the Institution of Mechanical Engineers, Part C: Journal of Mechanical Engineering Science, 220*(12), 1819-1830.

Lu, Y., Shi, Y., & Hu, B. (2008). Kinematic analysis of two novel 3UPU I and 3UPU II PKMs. *Robotics and Autonomous Systems, 56*(4), 296-305.

Miao, Z., Yao, Y., & Kong, X. (2013). A rolling 3-UPU parallel mechanism. *Frontiers of Mechanical Engineering*, 340-349.

Paganelli, D. (2007). Avoiding Parallel Singularities of 3UPS and 3UPU Spherical Wrists. *Proceedings 2007 IEEE International Conference on Robotics and Automation*, (pp. 1201-1206). Roma.

Parenti-Castelli, V., Gregorio, R., & Bubani, F. (2000). Workspace and Optimal Design of a Pure Translation Parallel Manipulator. *Meccanica*, 203-214.

Plücker, J. (1865). On a new geometry of space. *Philos Trans*, 725–791.

Pramanik, S., & Ghosal, A. (2015). Development of a Sun Tracking System using a 3-UPU Spherical Wrist Manipulator. *Proceedings of iNaCoMM 2015.* Kanpur, India.

Qi, Z., Wang, H., Huang, Z., & Zhang, L. (2009). Kinematics of a quadruped/biped reconfigurable walking robot with parallel leg mechanisms. *ASME/IFToMM International Conference on Reconfigurable Mechanisms and Robots*, 558-564.

Qu, H., Fang, Y., & Guo, S. (2012). Parasitic rotation evaluation and avoidance of 3-UPU parallel mechanism. *Frontiers of Mechanical Engineering, 7*(2), 210-218.

Söylemez, E. (2017, November). *http://ocw.metu.edu.tr*. Retrieved from http://ocw.metu.edu.tr/mod/resource/view.php?id=2097

Sun, S. (2013). Accuracy Analysis of 3-UPU Translational Parallel Robot Mechanism. *Advanced Materials Research*, 1617-1620.

Tsai, L. W. (1996). Kinematics of a three-dof platform with three extensible limbs. *Recent Advances in Robot Kinematics* (pp. 401-410). Kluwer Academic Publisher.

Tsai, L. W. (1999). *Robot analysis : the mechanics of serial and parallel manipulatiors.* New York: John-Wiley.

Tsai, L. W., & Joshi, S. (1999). Kinematics and Optimization of a Spatial 3-UPU Parallel Manipulator. *ASME. J. Mech Des.*, 439-446.

Tsai, L. W., & Joshi, S. (2001). Comparison Study of Architectures of Four 3 Degree-Of-Freedom Translational Parallel Manipulators. ICRA.

Walter, D., & Husty, M. (2011). Kinematic Analysis of the TSAI-3UPU Parallel Manipulator Using Algebraic Methods. *13th World Congress in Mechanism and Machine Science*, (pp. 19-25). Guanajuato, Mexico.

Walter, D., Husty, M., & Pfurner, M. (2008). The SNU 3-UPU parallel robot from a theoretical viewpoint. *Proceedings of the Second International Workshop on Fundamental Issues and Future Research Directions for Parallel Mechanisms and Manipulators.* Montpellier, France.

Wang, L., Xu, H., & Guan, L. (2015). Mobility analysis of parallel mechanisms based on screw theory and mechanism topology. *Advances in Mechanical Engineering, 7*(11).

Wang, M., & Ceccarelli, M. (2013). Design and Simulation for Kinematic Characteristics of a Tripod Mechanism for Biped Robots. *International Journal of Mechanics and Control*.

Wang, N., Guo, S., Fang, Y., & Li, X. (2011). Error sensibility analysis of 3-UPU parallel manipulator based on probability distribution. *2011 Second International Conference on Mechanic Automation and Control Engineering*, (pp. 1296-1301). Hohhot.

Wei, Y., Fan, Y., Li, Q., & Wang, Z. (2015). Structure Optimization Design of 3-UPU Parallel Mechanism Based on the Comprehensive Dexterity. *Recent Advances in Electrical & Electronic Engineering, 8*(1), 26-32.

Wikipedia. (2017, March 17). Retrieved from Wikipedia WEB Site: http://en.wikipedia.org/wiki/Stewart_platform

Wohlhart, K. (1996). Kinematotropic Linkages. *Recent Advances in Robot Kinematics* (pp. 359-368). Dordrecht: Springer.

Wolf , A., & Shoham, M. (2003). Investigation of Parallel Manipulators Using Linear Complex Approximation. *ASME. J. Mech. Des.*, 564-572.

Wolf, A., & Shoham, M. (2006). Screw theory tools for the synthesis of the geometry of a parallel robot for a given instantaneous task. *Mechanism and Machine Theory, 41*(6), 656-670.

Wolf, A., Shoham, M., & Park, F. (2002). Investigation of Singularities and Self-Motions of the 3-UPU Robot. *Advances in Robot Kinematics*, 165-174.

Xiangzhou, Z., Hongzan, B., & Yougao, L. (2006). *Kinematics of 3-UPU Parallel Manipulator with a Pure Spherical Motion Based on Quaternion Transformation.*

Xiangzhou, Z., Yougao, L., & Hongzan, B. (2007). Inverse Dynamics of 3-UPU Parallel Mechanism with Pure Rotation Based on D'Alembert Principle. *International Conference on Mechatronics and Automation*, (pp. 2842-2847). Harbin.

Yang, Y., & O'Brien, J. (2009). A geometric approach for the design of singularity-free parallel robots. *IEEE International Conference on Robotics and Automation*, (pp. 1801-1806). Kobe.

Yang, Y., & O'Brien, J. (2010). Singularity-free workspace design for the translational 3-UPU parallel robot. *IEEE International Conference on Automation Science and Engineering*, (pp. 222-227). Toronto.

Yi, L. (2005). Computer-aided geometric machining of a 3D free surface using a 3-UPU spatial parallel machine tool. *The International Journal of Advanced Manufacturing Technology, 26*(9-10), 1018-1025.

Yu, J., Dai, J., Zhao, T., Bi , S., & Zong, G. (2009). Mobility analysis of complex joints by means of screw theory. *Robotica, 27*(6), 915-927.

Zhao, J., Zhou, K., & Feng, Z. (2004). A theory of degrees of freedom for mechanisms. *Mechanism and Machine Theory, 39*(6), 621-643.

Zhao, J.-S., Feng, Z.-J., & Dong, J.-X. (2006). Computation of the configuration degree of freedom of a spatial parallel mechanism by using reciprocal screw theory. *Mechanism and Machine Theory, 41*(12), 1486-1504.

Zhao, J.-S., Feng, Z.-J., Zhou, K., & Dong, J.-X. (2005). Analysis of the singularity of spatial parallel manipulator with terminal constraints. *Mechanism and Machine Theory, 40*(3), 275-284.

Zlatanov, D., Bonev, I., & Gosselin, C. (2002). Constraint singularities of parallel mechanisms. *IEEE International Conference on Robotics and Automation*, *1*, pp. 496-502.

APPENDIX A

MOBILITY PROPERTIES OF 3-UPU PMS

Table A.1. Mobility properties of TNV Type PMs with 5-DoF when θ = 0°

5-DoF	$\mathbf{R_xR_yT_xT_yT_z}$
	U^N-U^N

Table A.2. Mobility properties of TNV Type PMs with 4-DoF when θ = 0°

4-DoF	$\mathbf{R_xR_yT_xT_z}$
	U^N-U^N_{VT}, U^N_{VT}- U^N, U^N-U^N_T, U^N_T-U^N
	$\mathbf{R_yT_xT_yT_z}$
	U^N_T-U^N_T, U^N_{VT}-U^N_{VT}, U^N_T-U^N_{VT}, U^N_{VT}-U^N_T
	$\mathbf{R_zT_xT_yT_z}$
	U^T-U^T, U^T_{VT}-U^T_{VT}, U^{VT}_T-U^{VT}_T, U^T-U^T_{VT}, U^T_{VT}-U^T, U^{VT}-U^{VT}_T, U^{VT}_T-U^{VT}, U^T-U^{VT}, U^T-U^{VT}_T, U^T_{VT}-U^{VT}_T, U^{VT}-U^T, U^{VT}_T-U^T_{VT}, U^{VT}_T-U^T, U^T_{VT}-U^{VT}, U^{VT}-U^T_{VT}, U^{VT}-U^{VT}

Table A.3. Mobility properties of TNV Type PMs with 3-DoF when θ = 0°

3-DoF	$\mathbf{T_xT_yT_z}$
	U^T_N-U^T_N, U^{VT}_N-U^{VT}_N, U^T_N-U^{VT}_N, U^{VT}_N-U^T_N
	$\mathbf{R_xR_yT_z}$
	U^N-U^T, U^N-U^T_{VT}, U^N-U^{VT}, U^N-U^{VT}_T, U^N-U^{VT}_N, U^N_T-U^T_N, U^N_{VT}-U^T_N, U^N_T-U^{VT}_N, U^N_{VT}-U^{VT}_N, U^T-U^N, U^T_N-U^T_N, U^T_N-U^N_{VT}, U^T_{VT}-U^N, U^{VT}-U^N, U^{VT}_N-U^N_{VT}, U^{VT}_T-U^N, U^{VT}_N-U^N_T, U^{VT}_N-U^N, U^N-U^T_N, U^T_N-U^N

Table A.4. Mobility properties of TNV Type PMs with 3-DoF with one parasitic mobility when $\theta = 0°$

	$\mathbf{R_yT_z(R_zT_xT_y)}$
	U_T^N-U^T, U_T^N-U_{VT}^T, U_{VT}^N-U^T, U_T^N-U^{VT}, U_T^N-U_T^{VT}, U_{VT}^N-U_T^{VT}, U_{VT}^N-U_{VT}^T, U_{VT}^N-U^{VT}
	$\mathbf{R_yT_z(R_zT_y)}$
	U^T-U_T^N, U^T-U_{VT}^N, U_{VT}^T-U_T^N, U^{VT}-U_T^N, U_T^{VT}-U_{VT}^N, U_T^{VT}-U_T^N, U_{VT}^T-U_{VT}^N, U^{VT}-U_{VT}^N
	$\mathbf{T_xT_z(R_zT_y)}$
	U^T-U_N^T, U_N^T-U^T, U_N^T-U_{VT}^T, U_{VT}^T-U_N^T, U^{VT}-U_N^{VT}, U_N^{VT}-U^{VT}, U_T^{VT}-U_N^{VT}, U_N^{VT}-U_T^{VT}, U^T-U_N^{VT}, U_N^T-U^{VT}, U_N^T-U_T^{VT}, U_{VT}^T-U_N^{VT}, U^{VT}-U_N^T, U_N^{VT}-U_{VT}^T, U_T^{VT}-U_N^T, U_N^{VT}-U^T

Table A.5. Mobility properties of TNV Type PMs with 5-DoF when $0° < \theta < 90°$

5-DoF	$\mathbf{R_xR_yT_xT_yT_z}$
	U^N-U^N

Table A.6. Mobility properties of TNV Type PMs with 4-DoF when $0° < \theta < 90°$

4-DoF	$\mathbf{R_xR_yT_xT_z}$
	U^N-U_T^N, U^N-U_{VT}^N
	$\mathbf{R_yT_xT_yT_z}$
	U_T^N-U_T^N, U_{VT}^N-U_{VT}^N
	$\mathbf{R_zT_xT_yT_z}$
	U^{VT}-U^{VT}

Table A.7. Mobility properties of TNV Type PMs with 4-DoF with one parasitic mobility when $0° < \theta < 90°$

4-DoF	$\mathbf{R_yT_xT_z(R_xT_y)}$
	U_T^N-U^N, U_T^N-U_{VT}^N, U_{VT}^N-U^N, U_{VT}^N-U_T^N

Table A.8. Mobility properties of TNV Type PMs with 3-DoF when $0° < \theta < 90°$

3-DoF	$\mathbf{T_xT_yT_z}$
	U^T-U^T, U_N^T-U_N^T, U_{VT}^T-U_{VT}^T, U_T^{VT}-U_T^{VT}, U_N^{VT}-U_N^{VT}
	$\mathbf{R_xR_yT_z}$
	U^N-U^T, U^N-U_N^T, U^N-U_{VT}^T, U^N-U^{VT}, U^N-U_T^{VT}, U^N-U_N^{VT}

Table A.9. Mobility properties of TNV Type PMs with 3-DoF with one parasitic mobility when $0° < \theta < 90°$

3-DoF	$\mathbf{R_yT_z(R_xR_zT_xT_y)}$
	U^N_T-U^T, U^N_T-U^T_N, U^N_T-U^T_{VT}, U^N_{VT}-U^T, U^N_{VT}-U^T_N, U^N_T-U^{VT}, U^N_T-U^{VT}_T, U^N_T-U^{VT}_N, U^N_{VT}-U^{VT}_T, U^N_{VT}-U^{VT}_N
	$\mathbf{R_yT_z(R_zT_xT_y)}$
	U^N_{VT}-U^T_{VT}, U^N_{VT}-U^{VT}
	$\mathbf{T_xT_z(R_xR_zT_y)}$
	U^T-U^T_N, U^T_N-U^T, U^T-U^T_{VT}, U^T_N-U^T_{VT}, U^T_{VT}-U^T, U^T_{VT}-U^T_N
	$\mathbf{T_xT_z(R_zT_y)}$
	U^{VT}-U^{VT}_T, U^{VT}-U^{VT}_N, U^{VT}_T-U^{VT}, U^{VT}_N-U^{VT}, U^{VT}_T-U^{VT}_N, U^{VT}_N-U^{VT}_T

Table A.10. Mobility properties of TNV Type PMs with 3-DoF with two parasitic mobility when $0° < \theta < 90°$

3-DoF	$\mathbf{T_z(R_xR_yR_zT_xT_y)(R_xR_zT_xT_y)}$
	U^T-U^N, U^T-U^N_T, U^N_T-U^N_T, U^T -U^N_{VT}, U^T_N-U^N_{VT}, U^T_{VT}-U^N, U^T_{VT}-U^N_T, U^T-U^{VT}, U^T-U^{VT}_T, U^T-U^{VT}_N, U^T_N-U^{VT}, U^T_N-U^{VT}_T, U^T_{VT}-U^{VT}_T, U^T_{VT}-U^{VT}_N, U^{VT}-U^T, U^{VT}-U^N, U^{VT}-U^T_N, U^{VT}-U^N_T, U^{VT}_T-U^T_{VT}, U^{VT}_T-U^N_{VT}, U^{VT}_N-U^T_{VT}, U^{VT}_N-U^N_{VT}, U^{VT}_T-U^T, U^{VT}_T-U^N, U^{VT}_T-U^T_N, U^{VT}_T-U^N_T, U^{VT}_N-U^T, U^{VT}_N-U^N_T
	$\mathbf{T_z(R_xR_yR_zT_xT_y)(R_yT_xT_y)}$
	U^T_N-U^N, U^T_N-U^{VT}_N, U^{VT}_N-U^N, U^{VT}_N-U^T_N
	$\mathbf{T_z(R_yR_zT_xT_y)(R_zT_xT_y)}$
	U^T_{VT}-U^N_{VT}, U^T_{VT}-U^{VT}
	$\mathbf{T_z(R_yR_zT_xT_y)(R_zT_y)}$
	U^{VT}-U^T_{VT}, U^{VT}-U^N_{VT}

Table A.11. Mobility properties of TNV Type PMs with 5-DoF when $\theta = 90°$

5-DoF	$\mathbf{R_xR_yT_xT_yT_z}$
	U^T-U^T, U^T-U^N, U^T-U^T_N, U^T-U^N_T, U^N-U^T, U^N-U^N, U^N-U^T_N, U^N-U^N_T, U^T_N-U^T, U^T_N-U^N, U^T_N-U^T_N, U^T_N-U^N_T, U^N_T-U^T, U^N_T-U^N, U^N_T-U^T_N, U^N_T-U^N_T

Table A.12. Mobility properties of TNV Type PMs with 4-DoF when θ = 90°

4-DoF	$\mathbf{R_xR_yR_zT_z}$
	U^T-U^{VN}, U^N-U^{VN}, U^T_N-U^{VN}, U^N_T-U^{VN}
	$\mathbf{R_xR_yT_xT_z}$
	U^T-U^T_{VT}, U^T-U^N_{VT}, U^N-U^T_{VT}, U^N-U^N_{VT}, U^T_N-U^T_{VT}, U^T_N-U^N_{VT}, U^N_T-U^T_{VT}, U^N_T-U^N_{VT}
	$\mathbf{R_xR_yT_yT_z}$
	U^T -U^T_{VN}, U^T -U^N_{VN}, U^N -U^T_{VN}, U^N -U^N_{VN}, U^T_N-U^T_{VN}, U^T_N-U^N_{VN}, U^N_T-U^T_{VN}, U^N_T-U^N_{VN}

Table A.13. Mobility properties of TNV Type PMs with 4-DoF with one parasitic mobility when θ = 90°

4-DoF	$\mathbf{R_xR_yT_z(R_zT_y)}$
	U^T-U^{VT}_{VN}, U^N-U^{VT}_{VN}, U^T_N-U^{VT}_{VN}, U^N_T-U^{VT}_{VN}
	$\mathbf{R_xT_yT_z(R_yT_x)}$
	U^T_{VN}- U^T, U^T_{VN}- U^N, U^T_{VN}-U^T_N, U^T_{VN}-U^N_T, U^T_{VN}-U^T_{VN}, U^T_{VN}-U^N_{VN}, U^N_{VN}-U^T, U^N_{VN}-U^N, U^N_{VN}-U^T_N, U^N_{VN}-U^N_T, U^N_{VN}-U^T_{VN}, U^N_{VN}-U^N_{VN}
	$\mathbf{R_yT_xT_z(R_xT_y)}$
	U^T_{VT}-U^T, U^T_{VT}-U^N, U^T_{VT}-U^T_N, U^T_{VT}-U^N_T, U^T_{VT}-U^T_{VT}, U^T_{VT}-U^N_{VT}, U^N_{VT}-U^T, U^N_{VT}-U^N, U^N_{VT}-U^T_N, U^N_{VT}-U^N_T, U^N_{VT}-U^T_{VT}, U^N_{VT}-U^N_{VT}

Table A.14. Mobility properties of TNV Type PMs with 4-DoF with two parasitic mobility when θ = 90°

4-DoF	$\mathbf{R_xT_z(R_yT_xT_y)(R_yT_x)}$
	U^T_{VN}-U^T_{VT}, U^T_{VN}-U^N_{VT}, U^N_{VN}-U^T_{VT}, U^N_{VN}-U^N_{VT}
	$\mathbf{R_yT_z(R_xT_xT_y)(R_xT_x)}$
	U^T_{VT}-U^T_{VN}, U^T_{VT}-U^N_{VN}, U^N_{VT}-U^T_{VN}, U^N_{VT}-U^N_{VN}
	$\mathbf{R_zT_z(R_xT_y)(R_yT_x)}$
	U^{VN}- U^{VN}

Table A.15. Mobility properties of TNV Type PMs with 3-DoF when θ = 90°

3-DoF	$\mathbf{R_xR_yT_z}$
	U^T-U^{VT}, U^T-U^{VT}_T, U^T-U^{VN}_T, U^T-U^{VT}_N, U^T-U^{VN}_N, U^T-U^{VN}_{VT}, U^N-U^{VT}, U^N-U^{VT}_T, U^N-U^{VN}_T, U^N-U^{VT}_N, U^N-U^{VN}_N, U^N-U^{VN}_{VT}, U^T_N-U^{VT}, U^T_N-U^{VT}_T, U^T_N-U^{VN}_T, U^T_N-U^{VT}_N, U^T_N-U^{VN}_N, U^T_N-U^{VN}_{VT}, U^N_T-U^{VT}, U^N_T-U^{VT}_T, U^N_T-U^{VN}_T, U^N_T-U^{VT}_N, U^N_T-U^{VN}_N, U^N_T-U^{VN}_{VT}
	$\mathbf{R_xR_zT_z}$
	U^T_{VN}- U^{VN}, U^T_{VN}-U^{VN}_T, U^T_{VN}-U^{VN}_N, U^N_{VN}-U^{VN}, U^N_{VN}-U^{VN}_T, U^N_{VN}-U^{VN}_N

Table A.16. Mobility properties of TNV Type PMs with 3-DoF with one parasitic mobility when $\theta = 90°$

3-DoF	**$R_xT_z(R_yR_z)$**
	U^{T}_{VN}-U^{VN}_{VT}, U^{N}_{VN}-U^{VN}_{VT}
	$R_xT_z(R_yR_zT_y)$
	U^{T}_{VN}-U^{VT}, U^{N}_{VN}- U^{VT}
	$R_xT_z(R_zT_y)$
	U^{T}_{VN}-U^{VT}_{T}, U^{T}_{VN}-U^{VT}_{VN}, U^{N}_{VN}-U^{VT}_{T}, U^{N}_{VN}-U^{VT}_{N}, U^{N}_{VN}-U^{VT}_{VN}, U^{T}_{VN}-U^{VT}_{N}
	$R_yT_z(R_xR_z)$
	U^{T}_{VT}-U^{VN}, U^{T}_{VT}-U^{VN}_{T}, U^{T}_{VT}-U^{VN}_{N}, U^{T}_{VT}-U^{VN}_{VT}, U^{N}_{VT}-U^{VN}, U^{N}_{VT}-U^{VN}_{T}, U^{N}_{VT}-U^{VN}_{N}, U^{N}_{VT}-U^{VN}_{VT}
	$R_yT_z(R_xR_zT_y)$
	U^{T}_{VT}-U^{VT}, U^{T}_{VT}-U^{VT}_{T}, U^{T}_{VT}-U^{VT}_{N}, U^{T}_{VT}-U^{VT}_{VN}, U^{N}_{VT}-U^{VT}, U^{N}_{VT}-U^{VT}_{T}, U^{N}_{VT}-U^{VT}_{N}, U^{N}_{VT}-U^{VT}_{VN}
	$R_zT_z(R_xR_yT_xT_y)$
	U^{VN}-U^{T}, U^{VN}-U^{N}, U^{VN}-U^{T}_{N}, U^{VN}-U^{N}_{T}, U^{VN}-U^{T}_{VN}, U^{VN}-U^{N}_{VN}
	$R_zT_z(R_xR_yT_y)$
	U^{VN}_{T}-U^{T}_{VN}, U^{VN}_{T}-U^{N}_{VN}, U^{VN}_{N}-U^{T}_{VN}, U^{VN}_{N}-U^{N}_{VN}
	$R_zT_z(R_xT_y)$
	U^{VN}-U^{VN}_{T}, U^{VN}-U^{VN}_{N}, U^{VN}_{T}-U^{VN}, U^{VN}_{N}-U^{VN}

Table A.17. Mobility properties of TNV Type PMs with 3-DoF with two parasitic mobility when $\theta = 90°$

3-DoF	**$T_z(R_xR_yR_zT_xT_y)(R_xR_zT_xT_y)$**
	U^{VT}- U^{T}, U^{VT}-U^{N}, U^{VT}-U^{VN}, U^{VT}-U^{T}_{N}, U^{VT}-U^{N}_{T}, U^{VT}-U^{VN}_{T}, U^{VT}-U^{VN}_{N}, U^{VT}-U^{T}_{VT}, U^{VT}-U^{T}_{VN}, U^{VT}-U^{N}_{VT}, U^{VT}-U^{N}_{VN}, U^{VT}-U^{VN}_{VT}, U^{VN}-U^{VT}, U^{VN}-U^{T}_{VT}, U^{VN}-U^{N}_{VT}, U^{VT}_{T}-U^{T}_{VT}, U^{VT}_{T}-U^{N}_{VT}, U^{VT}_{T}-U^{VN}_{VT}, U^{VN}_{T}-U^{VT}, U^{VN}_{T}-U^{T}_{VT}, U^{VN}_{T}-U^{N}_{VT}, U^{VT}_{N}-U^{T}_{VT}, U^{VT}_{N}-U^{N}_{VT}, U^{VT}_{N}-U^{VN}_{VT}, U^{VN}_{N}-U^{VT}, U^{VN}_{N}-U^{T}_{VT}, U^{VN}_{N}-U^{N}_{VT}, U^{VT}_{VN}-U^{T}_{VT}, U^{VT}_{VN}-U^{N}_{VT}, U^{VT}_{VN}-U^{VN}_{VT}, U^{VN}_{VT}- U^{T}, U^{VN}_{VT}- U^{N}, U^{VN}_{VT}-U^{VT}, U^{VN}_{VT}-U^{T}_{N}, U^{VN}_{VT}-U^{N}_{T}, U^{VN}_{VT}-U^{VT}_{T}, U^{VN}_{VT}-U^{VT}_{N}, U^{VN}_{VT}-U^{T}_{VT}, U^{VN}_{VT}-U^{T}_{VN}, U^{VN}_{VT}-U^{N}_{VT}, U^{VN}_{VT}-U^{N}_{VN}, U^{VN}_{VT}-U^{VT}_{VN}
	$T_z(R_xR_yR_zT_xT_y)(R_xR_zT_y)$
	U^{VT}-U^{VT}_{VN}, U^{VN}-U^{VT}_{T}, U^{VN}-U^{VT}_{N}, U^{VN}-U^{VT}_{VN}, U^{VN}-U^{VN}_{VT}, U^{VT}_{T}-U^{VN}, U^{VN}_{T}-U^{VT}_{VN}, U^{VT}_{N}- U^{VN}, U^{VN}_{N}-U^{VT}_{VN}, U^{VT}_{VN}-U^{VT}, U^{VT}_{VN}-U^{VN}, U^{VT}_{VN}-U^{VN}_{T}, U^{VT}_{VN}-U^{VN}_{N}, U^{VN}_{VT}-U^{VN}
	$T_z(R_xR_yR_zT_xT_y)(R_yT_xT_y)$
	U^{VT}_{T}-U^{T}, U^{VT}_{T}-U^{N}, U^{VT}_{T}-U^{T}_{N}, U^{VT}_{T}-U^{N}_{T}, U^{VT}_{T}-U^{VN}_{T}, U^{VT}_{T}-U^{VN}_{N}
	$T_z(R_xR_yR_zT_xT_y)(R_zT_y)$
	U^{VT}_{VN}-U^{T}, U^{VT}_{VN}-U^{N}, U^{VT}_{VN}-U^{T}_{N}, U^{VT}_{VN}-U^{N}_{T}, U^{VT}_{VN}-U^{T}_{VN}, U^{VT}_{VN}-U^{N}_{VN}
	$T_z(R_xR_yR_zT_y)(R_zT_y)$
	U^{VT}_{T}-U^{T}_{VN}, U^{VT}_{T}-U^{N}_{VN}, U^{VT}_{N}-U^{T}_{VN}, U^{VT}_{N}-U^{N}_{VN}
	$T_z(R_xR_yT_xT_y)(R_yT_xT_y)$
	U^{VN}_{T}-U^{T}, U^{VN}_{T}-U^{N}, U^{VN}_{T}-U^{T}_{N}, U^{VN}_{T}-U^{N}_{T}, U^{VN}_{T}-U^{VT}_{T}, U^{VN}_{T}-U^{VT}_{N}, U^{VT}_{N}-U^{T}, U^{VT}_{N}-U^{N}, U^{VT}_{N}-U^{T}_{N}, U^{VT}_{N}-U^{N}_{T}, U^{VT}_{N}-U^{VN}_{T}, U^{VT}_{N}-U^{VN}_{N}, U^{VN}_{N}-U^{T}, U^{VN}_{N}-U^{N}, U^{VN}_{N}-U^{T}_{N}, U^{VN}_{N}-U^{N}_{T}, U^{VN}_{N}-U^{VT}_{T}, U^{VN}_{N}-U^{VT}_{N}
	$T_z(R_xR_zT_y)(R_yT_x)$
	U^{VT}-U^{VT}_{T}, U^{VT}-U^{VT}_{N}, U^{VT}_{T}-U^{VT}, U^{VN}_{T}-U^{VN}_{VT}, U^{VT}_{N}-U^{VT}, U^{VN}_{N}-U^{VN}_{VT}, U^{VN}_{VT}-U^{VN}_{T}, U^{VN}_{VT}-U^{VN}_{N}, U^{VN}_{VT}-U^{VN}_{VT}
	$T_z(R_xR_zT_y)(R_zT_y)$
	U^{VT}_{T}-U^{VT}_{VN}, U^{VT}_{N}-U^{VT}_{VN}, U^{VT}_{VN}-U^{VT}_{T}, U^{VT}_{VN}-U^{VT}_{N}, U^{VT}_{VN}-U^{VT}_{VN}
	$T_z(R_xT_y)(R_yT_x)$
	U^{VT}_{T}-U^{VT}_{T}, U^{VT}_{T}-U^{VT}_{N}, U^{VN}_{T}-U^{VN}_{T}, U^{VN}_{T}-U^{VN}_{N}, U^{VT}_{N}-U^{VT}_{T}, U^{VT}_{N}-U^{VT}_{N}, U^{VN}_{N}-U^{VN}_{T}, U^{VN}_{N}-U^{VN}_{N}
	$T_z(R_yT_x)(R_xT_y)$
	U^{VT}-U^{VT}

Table A.18. Mobility properties of XYV Type PMs with 5-DoF

5-DoF	$\mathbf{R_xR_yT_xT_yT_z}$
	U^X-U^X, U^X-U^Y, U^X-U^X_Y, U^X-U^Y_X, U^Y-U^X, U^Y-U^Y, U^Y-U^X_Y, U^Y-U^Y_X, U^X_Y-U^X, U^X_Y-U^Y, U^X_Y-U^X_Y, U^X_Y-U^Y_X, U^Y_X-U^X, U^Y_X-U^Y, U^Y_X-U^X_Y, U^Y_X-U^Y_X

Table A.19. Mobility properties of XYV Type PMs with 4-DoF

4-DoF	$\mathbf{R_xR_yT_xT_z}$
	U^X-U^{VY}, U^X-U^{VY}_X, U^X-U^X_{VY}, U^X-U^Y_{VY}, U^X-U^{VY}_Y, U^Y-U^{VY}, U^Y-U^{VY}_X, U^Y-U^X_{VY}, U^Y-U^Y_{VY}, U^Y-U^{VY}_Y, U^X_Y-U^{VY}, U^X_Y-U^{VY}_X, U^X_Y-U^X_{VY}, U^X_Y-U^Y_{VY}, U^X_Y-U^{VY}_Y, U^Y_X-U^{VY}, U^Y_X-U^{VY}_X, U^Y_X-U^X_{VY}, U^Y_X-U^Y_{VY}, U^Y_X-U^{VY}_Y
	$\mathbf{R_xR_yT_yT_z}$
	U^X-U^{VX}, U^X-U^{VX}_X, U^X-U^X_{VX}, U^X-U^Y_{VX}, U^X-U^{VX}_Y, U^Y-U^{VX}, U^Y-U^{VX}_X, U^Y-U^X_{VX}, U^Y-U^Y_{VX}, U^Y-U^{VX}_Y, U^X_Y-U^{VX}, U^X_Y-U^{VX}_X, U^X_Y-U^X_{VX}, U^X_Y-U^Y_{VX}, U^X_Y-U^{VX}_Y, U^Y_X-U^{VX}, U^Y_X-U^{VX}_X, U^Y_X-U^X_{VX}, U^Y_X-U^Y_{VX}, U^Y_X-U^{VX}_Y

Table A.20. Mobility properties of XYV Type PMs with 4-DoF with one parasitic mobility

4-DoF	$\mathbf{R_xR_yT_z(R_zT_y)}$
	U^X-U^{VY}_{VX}, U^Y-U^{VY}_{VX}, U^X_Y-U^{VY}_{VX}, U^Y_X-U^{VY}_{VX}
	$\mathbf{R_xT_yT_z(R_yT_x)}$
	U^{VX}-U^{VX}, U^{VX}_X-U^{VX}_X, U^{VX}_X-U^{VX}_Y, U^X_{VX}-U^X, U^X_{VX}-U^Y, U^X_{VX}-U^X_Y, U^X_{VX}-U^Y_X, U^X_{VX}-U^X_{VX}, U^X_{VX}-U^Y_{VX}, U^Y_{VX}-U^X, U^Y_{VX}-U^Y, U^Y_{VX}-U^X_Y, U^Y_{VX}-U^Y_X, U^Y_{VX}-U^X_{VX} U^Y_{VX}-U^Y_{VX}, U^{VX}_Y-U^{VX}_X, U^{VX}_Y-U^{VX}_Y
	$\mathbf{R_yT_xT_z(R_xT_y)}$
	U^{VY}-U^{VY}, U^{VY}_X-U^{VY}_X, U^{VY}_X-U^{VY}_Y, U^X_{VY}-U^X, U^X_{VY}-U^Y, U^X_{VY}-U^X_Y, U^X_{VY}-U^Y_X, U^X_{VY}-U^X_{VY}, U^X_{VY}-U^Y_{VY}, U^Y_{VY}-U^X, U^Y_{VY}-U^Y, U^Y_{VY}-U^X_Y, U^Y_{VY}-U^Y_X, U^Y_{VY}-U^X_{VY}, U^Y_{VY}-U^Y_{VY}, U^{VY}_Y-U^{VY}_X, U^{VY}_Y-U^{VY}_Y
	$\mathbf{R_yT_xT_z(R_xR_zT_y)}$
	U^{VY}-U^{VY}_X, U^{VY}-U^{VY}_Y, U^{VY}_X-U^{VY}, U^X_{VY}-U^{VY}, U^X_{VY}-U^{VY}_X, U^X_{VY}-U^{VY}_Y, U^Y_{VY}-U^{VY}, U^Y_{VY}-U^{VY}_X, U^Y_{VY}-U^{VY}_Y, U^{VY}_Y-U^{VY},

Table A.21. Mobility properties of XYV Type PMs with 4-DoF with two parasitic mobility

4-DoF	$\mathbf{R_xT_z(R_yR_zT_xT_y)(R_zT_xT_y)}$
	U^{X}_{VX}-U^{VY}, U^{Y}_{VX}-U^{VY}
	$\mathbf{R_xT_z(R_yT_x)(R_zT_y)}$
	U^{X}_{VX}-U^{VY}_{Y}, U^{X}_{VX}-U^{Y}_{VY}, U^{X}_{VX}-U^{VY}_{Y}, U^{X}_{VX}-U^{VY}_{VX}, U^{Y}_{VX}-U^{VY}_{X}, U^{Y}_{VX}-U^{VY}_{Y}, U^{Y}_{VX}-U^{VY}_{VX}
	$\mathbf{R_xT_z(R_yT_xT_y)(R_yT_xT_y)}$
	U^{X}_{VX}-U^{X}_{VY}, U^{Y}_{VX}-U^{X}_{VY}, U^{Y}_{VX}-U^{Y}_{VY}
	$\mathbf{R_yT_z(R_xR_zT_xT_y)(R_zT_xT_y)}$
	U^{VY}-U^{VY}_{VX}, U^{X}_{VY}-U^{VY}_{VX}, U^{Y}_{VY}-U^{VY}_{VX}
	$\mathbf{R_yT_z(R_xR_zT_y)(R_zT_y)}$
	U^{VY}_{X}-U^{VY}_{VX}, U^{X}_{VY}-U^{X}_{VX}, U^{X}_{VY}-U^{Y}_{VX}, U^{Y}_{VY}-U^{X}_{VX}, U^{Y}_{VY}-U^{Y}_{VX}, U^{VY}_{Y}-U^{VY}_{VX}

Table A.22. Mobility properties of XYV Type PMs with 4-DoF with three parasitic mobility

4-DoF	$\mathbf{T_z(R_xR_yR_zT_xT_y)(R_yR_zT_xT_y)(R_zT_xT_y)}$
	U^{VY}_{VX}-U^{VY}
	$\mathbf{T_z(R_xR_zT_y)(R_yT_x)(R_zT_y)}$
	U^{VY}_{VX}-U^{VY}_{X}, U^{VY}_{VX}-U^{VY}_{Y}, U^{VY}_{VX}-U^{VY}_{VX}

Table A.23. Mobility properties of XYV Type PMs with 3-DoF

3-DoF	$\mathbf{R_xR_yT_z}$
	U^{X}-U^{VX}_{VY}, U^{Y}-U^{VX}_{VY}, U^{X}_{Y}-U^{VX}_{VY}, U^{Y}_{X}-U^{VX}_{VY}
	$\mathbf{R_xT_yT_z}$
	U^{VX}-U^{X}, U^{VX}-U^{Y}, U^{VX}-U^{X}_{Y}, U^{VX}-U^{Y}_{X}, U^{VX}-U^{VX}_{X}, U^{VX}-U^{X}_{VX}, U^{VX}-U^{Y}_{VX}, U^{VX}-U^{VX}_{Y}, U^{VX}_{X}-U^{X}, U^{VX}_{X}-U^{Y}, U^{VX}_{X}-U^{VX}, U^{VX}_{X}-U^{X}_{Y}, U^{VX}_{X}-U^{Y}_{X}, U^{VX}_{X}-U^{X}_{VX}, U^{VX}_{X}-U^{Y}_{VX}, U^{X}_{VX}-U^{VX}, U^{X}_{VX}-U^{X}_{X}, U^{X}_{VX}-U^{Y}_{X}, U^{Y}_{VX}-U^{VX}, U^{Y}_{VX}-U^{X}_{X}, U^{Y}_{VX}-U^{Y}_{X}, U^{VX}_{Y}-U^{X}, U^{VX}_{Y}-U^{Y}, U^{VX}_{Y}-U^{VX}, U^{VX}_{Y}-U^{X}_{Y}, U^{VX}_{Y}-U^{Y}_{X}, U^{VX}_{Y}-U^{X}_{VX}, U^{VX}_{Y}-U^{Y}_{VX}
	$\mathbf{R_yT_xT_z}$
	U^{VY}-U^{X}, U^{VY}-U^{Y}, U^{VY}-U^{X}_{Y}, U^{VY}-U^{Y}_{X}, U^{VY}-U^{X}_{VY}, U^{VY}-U^{Y}_{VY}, U^{VY}_{X}-U^{X}, U^{VY}_{X}-U^{Y}, U^{VY}_{X}-U^{X}_{Y}, U^{VY}_{X}-U^{Y}_{X}, U^{VY}_{X}-U^{X}_{VY}, U^{VY}_{X}-U^{Y}_{VY}, U^{VY}_{Y}-U^{X}, U^{VY}_{Y}-U^{Y}, U^{VY}_{Y}-U^{X}_{Y}, U^{VY}_{Y}-U^{Y}_{X}, U^{VY}_{Y}-U^{X}_{VY}, U^{VY}_{Y}-U^{Y}_{VY}

Table A.24. Mobility properties of XYV Type PMs with 3-DoF with one parasitic mobility

3-DoF	**$R_xT_z(T_xT_y)$**
	U^{VX}-U^{VY}, U_X^{VX}-U_X^{VY}, U_X^{VX}-U_Y^{VY}, U_Y^{VX}-U_X^{VY}, U_Y^{VX}-U_Y^{VY}
	$R_xT_z(R_yR_zT_xT_y)$
	U^{VX}-U_X^{VY}, U^{VX}-U_{VY}^{X}, U^{VX}-U_{VY}^{Y}, U^{VX}-U_Y^{VY}, U^{VX}-U_{VX}^{VY}, U_X^{VX}-U^{VY}, U_X^{VX}-U_{VY}^{X}, U_X^{VX}-U_{VY}^{Y}, U_Y^{VX}-U^{VY}, U_Y^{VX}-U_{VY}^{X}, U_Y^{VX}-U_{VY}^{Y},
	$R_xT_z(R_yT_xT_y)$
	U^{VX}-U_{VY}^{VX},
	$R_xT_z(R_yT_x)$
	U_X^{VX}-U_{VY}^{VX}, U_Y^{VX}-U_{VY}^{VX},
	$R_xT_z(R_yR_zT_y)$
	U_X^{VX}-U_{VX}^{VY}, U_Y^{VX}-U_{VX}^{VY}
	$R_xT_z(R_yT_y)$
	U_{VX}^{X}-U_{VY}^{VX}, U_{VX}^{Y}-U_{VY}^{VX},
	$R_yT_z(TxTy)$
	U^{VY}-U^{VX}, U_X^{VY}-U_X^{VX}, U_X^{VY}-U_Y^{VX}, U_Y^{VY}-U_X^{VX}, U_Y^{VY}-U_Y^{VX},
	$R_yT_z(R_xR_zT_xT_y)$
	U^{VY}-U_X^{VX}, U^{VY}-U_Y^{VX}, U^{VY}-U_{VY}^{VX}, U_X^{VY}-U_{VY}^{VX}, U_Y^{VY}-U_{VY}^{VX}
	$R_yT_z(R_zT_xT_y)$
	U^{VY}-U_{VX}^{X}, U^{VY}-U_{VX}^{Y},
	$R_yT_z(R_xR_zT_y)$
	U_X^{VY}-U^{VX}, U_Y^{VY}-U^{VX},
	$R_yT_z(R_zT_y)$
	U_X^{VY}-U_{VX}^{X}, U_X^{VY}-U_{VX}^{Y}, U_Y^{VY}-U_{VX}^{X}, U_Y^{VY}-U_{VX}^{Y},
	$R_yT_z(R_xT_y)$
	U_{VY}^{X}-U^{VX}, U_{VY}^{X}-U_X^{VX}, U_{VY}^{X}-U_Y^{VX}, U_{VY}^{X}-U_{VY}^{VX}, U_{VY}^{Y}-U^{VX}, U_{VY}^{Y}-U_X^{VX}, U_{VY}^{Y}-U_Y^{VX}, U_{VY}^{Y}-U_{VY}^{VX},

Table A.25. Mobility properties of XYV Type PMs with 3-DoF with two parasitic mobility

3-DoF	$\mathbf{T_z(R_xR_yR_zT_xT_y)(R_xR_zT_xT_y)}$
	U_{VX}^{VY}-U_{VY}^{VX}
	$\mathbf{T_z(R_xR_yR_zT_xT_y)(R_xR_zT_y)}$
	U_{VX}^{VY}-U^{VX}, U_{VX}^{VY}-U_{X}^{VX}, U_{VX}^{VY}-U_{Y}^{VX}
	$\mathbf{T_z(R_xR_yR_zT_xT_y)(R_yR_zT_xT_y)}$
	U_{VY}^{VX}-U^{X}, U_{VY}^{VX}-U^{Y}, U_{VY}^{VX}-U^{VY}, U_{VY}^{VX}-U_{Y}^{X}, U_{VY}^{VX}-U_{X}^{Y}, U_{VY}^{VX}-U_{X}^{VY}, U_{VY}^{VX}-U_{VX}^{X}, U_{VY}^{VX}-U_{VY}^{X}, U_{VY}^{VX}-U_{VX}^{Y}, U_{VY}^{VX}-U_{VY}^{Y}, U_{VY}^{VX}-U_{Y}^{VY}, U_{VY}^{VX}-U_{VX}^{VY}
	$\mathbf{T_z(R_xR_yT_xT_y)(R_yT_xT_y)}$
	U_{VY}^{VX}-U^{VX}
	$\mathbf{T_z(R_xT_y)(R_yT_x)}$
	U_{VY}^{VX}-U_{X}^{VX}, U_{VY}^{VX}-U_{Y}^{VX}, U_{VY}^{VX}-U_{VY}^{VX}
	$\mathbf{T_z(R_yR_zT_xT_y)(R_zT_xT_y)}$
	U_{VX}^{VY}-U_{VY}^{X}, U_{VX}^{VY}-U_{VY}^{Y}
	$\mathbf{T_z(R_yT_x)(R_zT_y)}$
	U_{VX}^{VY}-U^{X}, U_{VX}^{VY}-U^{Y}, U_{VX}^{VY}-U_{Y}^{X}, U_{VX}^{VY}-U_{X}^{Y}, U_{VX}^{VY}-U_{VX}^{X}, , U_{VX}^{VY}-U_{VX}^{Y}